Synthesis of Waste Derived CaO Promoted Hydrotalcite Based Catalyst for Sorption Enhanced Steam Reforming of Methane

By

Mariam Ayesha

School of Chemical and Materials Engineering

National University of Sciences and Technology

2021

Synthesis of Waste Derived CaO Promoted Hydrotalcite Based Catalyst for Sorption Enhanced Steam Reforming of Methane

MARIAM AYESHA

Registration number: 00000277674

This thesis is submitted in partial fulfilment of the requirements for Degree of

MS Chemical Engineering

Supervised by: Dr. Umair Sikandar (SCME)

Co-supervised by: Dr. Asif Hussain Khoja (USPCAS-E)

School of Chemical and Materials Engineering (SCME)

National University of Sciences and Technology (NUST)

H-12 Islamabad, Pakistan

May,2021

Dedication

I am grateful to Allah Almighty who gifted me a life and guided me in every stage of life. Secondly, I want to dedicate this work to my supervisor Dr. Umair Sikandar who always supported me and co supervisor Dr. Asif Hussain Khoja, who mentored me, helped me for the work I have done. This devotion is not completed without my parents, who have been a constant source of strength throughout this program and always encouraged me to accomplish my dreams.

Acknowledgments

In the name of Allah, The beneficent and the most Merciful. It's esteem to Allah Almighty, who gave me a supremacy and guidance for this work. Indeed, without His priceless help and blessings, I could have done nothing.

"My parents are my strength" and obviously it is not completed without them. I am thankful to my parents for their moral and financial support for fulfilling my dreams by distinguishing my potentials.

I am indebted to my supervisor **Dr. Umair Sikandar** for his moral support and sympathetic behaviour. This was his courage and strong words which became the reason of my survival during my struggling phase of this period. It is an admiration to my co-supervisor and my mentor **Dr. Asif Hussain Khoja** for his prodigious support. His critical and vigilant scrutiny with instructive interpretations, assisted me to assemble my work in a very short time. It was not possible for me to complete my work without his supervision and involvement. I am beholden to my research fellows in Fossil Fuel lab (USPCAS-E) for their guidance.

I would acknowledge **Dr. Sarah Farrukh** and **Dr. Bilal Khan Niazi** for being on my guidance and evaluation committee. Finally, I want to convey my gratefulness to all the friends who have provided valuable support to my study.

May Allah bless all.

Abstract

The waste derived CaO promoted Mg-Ni-Al based hydrotalcites hybrid catalyst was produced by co-precipitation and wetness impregnation method. The hybrid material was tested for sorption enhanced steam methane reforming (SESMR) for hydrogen (H_2) production. The catalyst samples were characterized using X-ray diffraction (XRD), field emission scanning electron microscope (FESEM), scanning electron microscopy (SEM) with energy dispersive X-ray (EDX) analysis, Brunauer Emmett Teller (BET), temperature programmed reduction (TPR), thermogravimetric analysis (TGA) and Fourier transform infrared spectroscopy (FTIR). Various sequences of CaO loadings from 0-15 % into the Mg-Ni-Al based hydrotalcites (MNA HTc) were assessed for SESMR in a fixed bed reactor. The results showed that 10% CaO@MNA exhibited best performance in terms of longer pre-breakthrough period with respect to other sequences. The CH_4 conversion, H_2 purity, and CO_2 production in the absence of CaO was marked at 60%, 55%, and 14% respectively. However, the CH_4 conversion and H_2 purity improved to 84% and 80%, while CO_2 decreased to 3% in the pre-breakthrough period for 10% CaO @ MNA, respectively at 650 ° C and S/C of 2. The hybrid catalyst was also tested at various temperatures from 650-850 °C to investigate the effect of CaO sorbent. It was found that elevated temperatures >750 °C reduced the carbonation reaction and shifted the technique to SMR. The spent catalyst exhibited negligible carbon formation on the catalyst. The performance of the reported catalyst-sorbent system is encouraging for further regeneration studies for SMR.

Keywords: *Hydrotalcites, Mg-Ni-Al, CaO, H_2 production, CO_2 reduction, Sorption enhanced steam reforming of methane*

Table of Contents

Table of Figures

List of Tables

List of Abbreviations

SMR	Steam methane reforming
H_2	Hydrogen
CH_4	Methane
WSGR	Water shift gas reaction
SESMR	Sorption enhanced steam reforming of methane
LDH	Layered double hydroxides
HTc	Hydrotalcites
SGR	Steam reforming of glycerol
SAR	Steam reforming of acetone
SRE	Steam reforming of ethanol
DMR	Dry reforming of methane
3DOM	Three dimensionally ordered macroporous
MgO	Magnesium oxide
CaO	Calcium oxide
LOS	Lithium orthosilicate

Chapter 1

Introduction

1.1 Research Background

Environmental complications of fossil fuels in the energy systems are encouraging research in the production of hydrogen (H_2) using clean and economical routes. H_2 is excessively needed for the ammonia and methanol production, and processing of fossil fuels in various chemical and petroleum industries [1]. Furthermore, H_2 has a higher heating value (140 MJ/kg) as compared to other common fuels, thus being an ideal energy carrier and constantly increasing the demand of H_2 production [2]. Approximately 70 Mt of H_2 was produced in 2019, globally, 76% of which was generated from natural gas, 23% from coal and remaining 1% from oil and electricity, which lead to the emission of 2.6% of CO_2 emissions [3].

The existing technologies for H_2 production include coal gasification [4, 5], chemical looping technology [6, 7], steam methane reforming (SMR) [8, 9], thermochemical water splitting [10, 11]. Among these methodologies, SMR has been applied industrially, despite its drawbacks such as energy consumption and complexity [12]. The main reactions in SMR include an endothermic methane (CH_4) reforming (Eq. (1)) followed by an exothermic water gas shift reaction (WSGR) (Eq. (2)), making an overall endothermic process is described as follows:

$$CH_4 + H_2O \leftrightarrow CO + 3H_2 \quad \Delta H_{298K} = +206.3\ kJ/mol \tag{1}$$

$$CO + H_2O \leftrightarrow CO_2 + H_2 \quad \Delta H_{298K} = -41.1\ kJ/mol \tag{2}$$

Typically, H_2 purity around 70% was exhibited in the product, because of the equilibrium SMR reaction [13]. Also the process gives at least a net 3 kg CO_2 per kg of consumed CH_4 [14]. Recently, a process known as Sorption Enhanced Steam Methane Reforming (SESMR) has attracted consideration as a green method in recent studies [15-17]. The process is the coupling of the conventional SMR and CO_2 capture via solid sorbent, that pushes the equilibrium rate of reactions towards the H_2

formation and reducing CO_2 from the product phase, based on Le Chatelier's principle [18, 19]. Saturated sorbent can be regenerated at conditions different than SESMR, resulting in concentrated CO_2 production for disposal [20] or for use as feedstock [21].

Various catalysts for SMR have been reported in literature including Ni based [22, 23], Co based [24] and noble metals (Ru [25], Pt [13] and Rh [26]). Despite the better performance of Ni catalysts, a decline in activity is observed with time because of carbon formation. Catalytic activity is significantly affected by the support used and preparation method, as the electronic configuration and structure of catalysts are dependent on its interaction with the support [27]. With regard to the aforementioned points, double layered hydroxides (LDH) like hydrotalcites (HTc) have proven limited sintering and uniform dispersion of Ni particles with large surface area [18]. These materials belong to the family of anionic clays comprising of aluminium (Al) and magnesium (Mg) layers with water and carbonate ions as inter-layers represented by the general formula of $Mg_6Al_2(OH)_{16}.CO_3.4H_2O$. Al and Mg are trivalent and divalent metal cations that are accommodated in the brucite like layers into octahedral holes, which can be substituted by any different active metals [28]. Furthermore, it is necessary to calcine the HTc based structure to form pre-spinel oxides that enhances the specific surface area [29]. Ruthenium (Ru) supported on Ni-Mg-Al mixed oxides were prepared via HTc route for testing in SMR for H_2 production. Ru impregnation in HTc resulted in Ru-Ni interaction which promotes higher catalytic activity due to the formation of easily reducible oxides [30]. Similarly, catalytic activity and reaction studies were performed for SMR over Ni catalysts from HTc precursors. Results indicated that a higher surface area, better Ni dispersion and enhanced surface area were highly reliant on the Mg/Al molar ratios. It was found that higher Mg content in the HTc structure improved the catalytic activity [31]. Various HTc derived catalysts have been reported for other reforming techniques. For example, Lanthanum (La) promoted Ni/Mg-Al was synthesized for steam reforming of glycerol (SGR) [32], Cobalt (Co) promoted mixed oxides from HTc precursors tested for steam reforming od acetone (SAR) [33], Co and La impregnated Zn based HTc tested for steam reforming of ethanol (SRE) [34].

Various high temperature sorbents have been studied, including Li_2O_3Zr [35], Na_2O_3Zr [36], $Li_4O_4Si_4$ [37], CaO [38] and MgO based [39]. Among them, CaO based sorbents are highly considered owing to the following reasons: (i) carbonation (Eq. (3)) occurs at atmospheric pressure and 600-700 °C, conditions lower than conventional SMR, (ii) adequate CO_2 sorption capacity and strong affinity for CO_2 at temperatures higher than 500 °C [40].

$$CaO + CO_2 \leftrightarrow CaCO_3 \quad \Delta H^\circ_{298K} = -178.2\ kJ/mol \tag{3}$$

Considering the stability of CaO based sorbents, their sorption capacity undergoes reduction with the increase in cycle number [41, 42]. This decrease is due to sintering, which can be improved by integrating a support with the porous solid structure [43]. To ensure better sorption and reforming characteristics, hybrid materials consisting of reforming catalyst and sorbent enhanced the access to the metal active sites and high rates of diffusion. Various hybrid materials have been stated in literature in the recent past. For instance, CaO based Ni-Al_2O_3 HTc was synthesized for H_2 production of purity around 90% [44]. Kim et al. [45] synthesized CaO based $Ca_{12}Al_{14}O_{33}$-Ni to produce 95% pure H_2. Ghungrud et al. [16] prepared Ce-promoted hybrid materials of Co, Ni and HTc for SESMR. Ce promotion resulted in providing basic sites for CO_2 adsorption resulting in improved H_2 production (>90 mol%) at 500 °C and S/C of 6. Radfarnia et al. [46] developed CaO based Al stabilized-Ni hybrid for SESMR. The catalyst exhibited 96% H_2 efficiency while 99% CH_4 conversion. Various metal ions laden on CaO for SESMR were also examined such as Ce^{4+} [47], Zr^{4+} [48]. For example, Ni/CaO-Zr was synthesized using wet mixing technique. A 91% H_2 purity was obtained using an optimum 20.5% NiO loading in the CSCM

.

1.2 Problem statement

Although, SMR is the most established path for H_2 production over various catalysts but the process has some limitations as well. Rapid sintering of catalyst and high energy requirements are the most concerning issues in SMR. Moreover, it is challenging to reduce the CO_2 production in the reaction without any purification, before venting it to the environment. It is important to consider a waste derived sorbent with HTc based catalyst to test for SESMR while maintaining high purity H_2 and higher CH_4 conversion in the reaction. Effect of temperature on the SESMR reaction and influence on CH_4 conversion, H_2 yield and CO_2 concentration in the outlet stream is to be studied.

1.3 Research hypothesis

It is desired to have sorbent addition in catalyst to form a combined sorbent catalyst material (CSCM) for the SESMR process. CO_2 adsorbent should have high cyclic stability, suitable adsorption kinetics and characteristics, enhanced cyclic stability and good mechanical strength [49]. Among various sorbents as mentioned above, commercial CaO based catalysts have been highly considered. Commercial CaO based hybrid materials have been reported in literature [44, 50, 51]. Waste derived CaO is known to have smaller particle size and higher exposed surface for the carbonation reaction [52, 53]. It seems to be a more economical and a green source for the enhanced H_2 purity as a raw material. Thus, to consider the SESMR application, it is appropriate to synthesize waste eggshell derived CaO sorbents and examine its activity in Mg, Ni, and Al based HTc in a fixed bed reactor. To the best of our knowledge, such comparison with unpromoted HTc and waste derived CaO promoted HTc for the application of SMR and SESMR has been done for the first time.

1.4 Research objectives

To produce H_2 through a cleaner energy source, SMR is considered the most mature technology. Considering the disadvantages of SMR, SESMR have proven to overcome its limitations. The main objective of this work is to synthesize and

characterize HTc, CaO and hybrid of both. To study the effect of waste derived CaO incorporation into the Mg-Ni-Al HTc to test for SESMR at lower temperature. To evaluate the activity of the waste derived CaO based HTc with varying quantities of CaO is compared in terms of CH_4 conversion, H_2 purity and CO_2 produced. To characterize the spent catalyst from reaction.

1.5 Scope and limitations

The scope of this work is to develop a promising catalyst for the sorption enhanced steam methane reforming (SESMR) process. SMR have already been applied at industrial scale to produce H_2 gas. Although SMR is a mature technology, sill, it suffers from drawbacks such as GHG production and catalyst sintering during the reaction. For 1 mole of CH_4 reformed, 1 mole of CO_2 is produced as a by-product and must be disposed. This is a major issue as it results in the production of large amount of GHG going into the atmosphere. Process purifications are required to make H_2 pure. SESMR process allows the pure H_2 production with reduction in CO_2 content in a single step. This process may allow less coking and sintering of catalyst, which can enable the use of economical wall materials at industrial scale. Also, the process produces 4 moles of pure H_2 with each mole of CH_4 reformed and the process operates at lower temperature (500-700 °C). Therefore, the focus of this study is to synthesize a hybrid catalyst suitable for the process and testing at lower temperature and Steam to carbon (S/C) ratio.

Chapter 2

Literature Review

2.1 Basics of Steam methane reforming (SMR)

2.1.1 Basic Chemistry and kinetics of SMR

SMR is a catalytic process that comprises a reaction between steam and light hydrocarbons or natural gas that gives major quantity of H_2 and CO_2. At present, SMR of natural gas is carried out in tubular packed-bed reactors via Ni-based catalysts, supported on ceramic oxides, due to high efficiency of Ni and low cost. Though, sintering and coking are major problems for Ni-based catalysts, that usually occurs from side reactions, mainly during CH_4 cracking [54-57].

During the process, desulfurized natural gas is mixed with steam, generally at S/C ratio in a range of 2.5-3.0 to lower coke formation and fed to the reactor where H_2 and CO are produced as in equation (Eq. (1)). As a result, highly endothermic reaction occurs, and significant amount of energy is necessary to attain the reaction temperature and to overcome the heat of reaction. The reaction occurs on catalyst bed inside furnace tubes, where the additional energy is provided by the burning of purge gas from product purification. Optimum temperature and pressure ranges in commercial technology for H_2 production are 800-1000 °C, 1.5-3.0 MPa [30, 58, 59].

The WSGR then occurs to convert CO and H_2O and unconverted CH_4 into CO_2 and H_2O as presented in equation (Eq. (2)) [60]. Additional steam may be added to allow more H_2 production. A high temperature (HT) shift reactor operating at 350-400 °C having chromium iron oxide catalyst, and a low temperature (LT) shift at 200 °C having copper or zinc catalyst, have been used to achieve enhance equilibrium conversion of CO. The gas composition on dry basis from LT shift reactor is about 76% H_2, 3% CO, 17% CO_2, and unconverted CH_4 [61, 62]. Pressure swing adsorption (PSA) has become a dominant technique for H_2 purification. Multiple activated carbon or silica gel packed beds provide constant off-gas and product composition. The adsorbent removes the impurities at high pressure and ambient

temperature, whereas H_2 stays unchanged as it passes through the bed. H_2 purity of greater than 99% may be achieved through this process. The purge gas, with feed impurities and unconverted H_2, is sent to the reformer to supply a part of energy to the unit [63]. A schematic view of the process is exemplified in Figure 2.1.

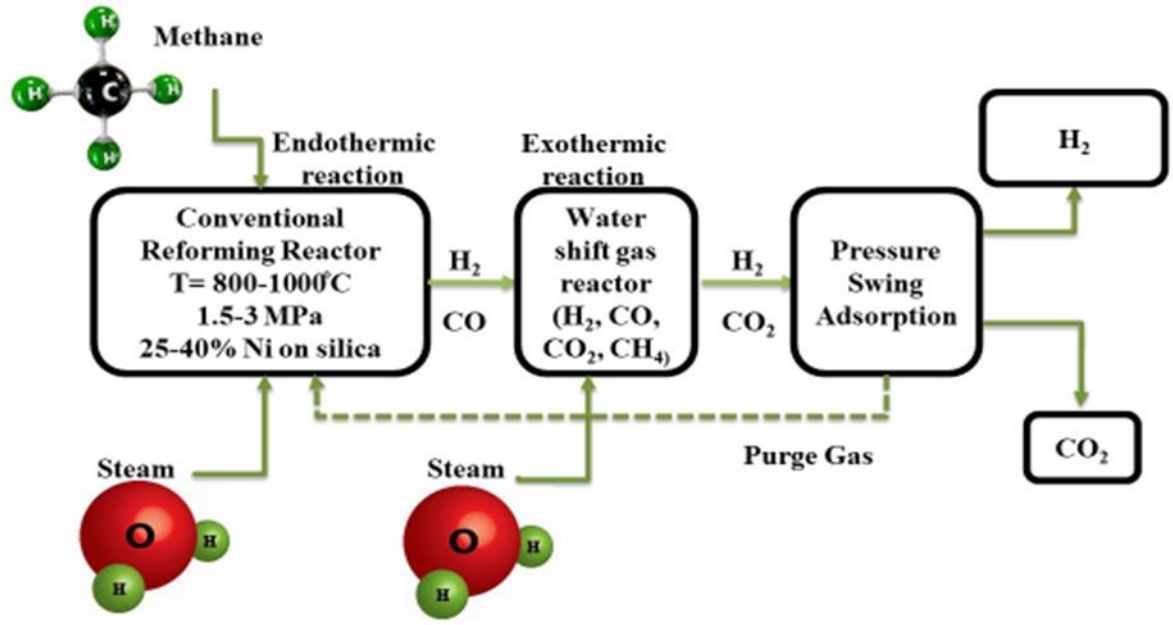

Figure 2.1 Conventional multi-stages for H_2 production via SMR

Different models were proposed by researchers to understand the reaction kinetics and basic understanding of CH_4 dissociation and product formation.[64-66]. Initially, the proposed reaction mechanism of SMR used $Ni/MgAl_2O_4$ as a catalyst, which studied the extensive mechanism indicating that the carbon intermediates reactions with adsorbed oxygen as rate determining, as shown in Figure 2.2. It is suggested that the oxygen concentration determine the reaction kinetics to a large extent [67].

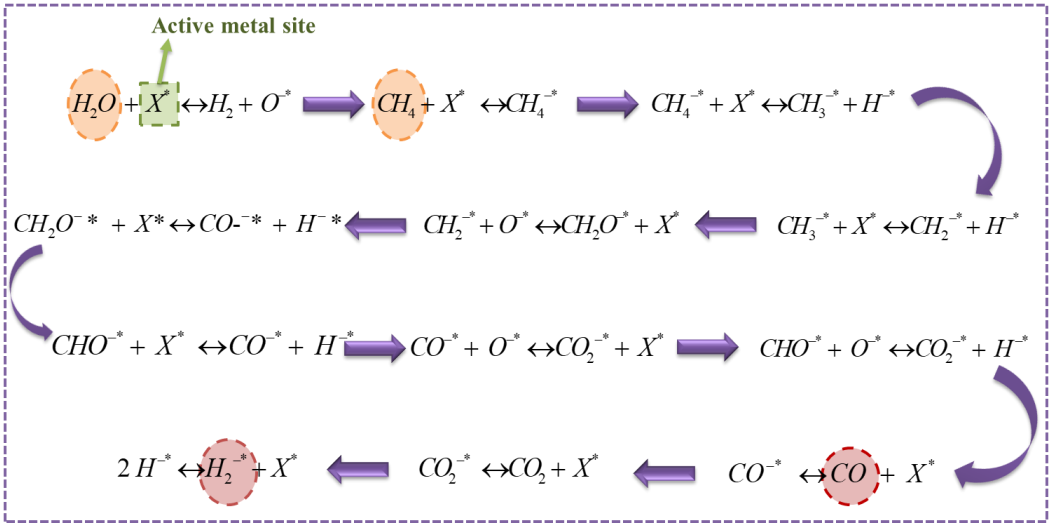

Figure 2.2 Detailed mechanism of SMR over active metal catalyst

In most cases, surface active sites encourage cracking and subsequent polymerization of hydrocarbons, leading to carbon formations on the surface of catalyst during CH_4 cracking (Eq. (4)) and Boudouard reaction (Eq. (5)). Alkali metal addition can suppress carbonaceous deposition, but they can decrease the catalytic activity [68]. Proper acid-base properties and metal-support interaction should be considered to hinder carbon formation [65].

$$CH_4 \rightarrow C + 2H_2 \ [(\Delta H^{\circ}_{298}) = +75\ kJ/mol] \quad (4)$$

$$2CO \rightarrow C + CO_2 \ [(\Delta H^{\circ}_{298}) = -172\ kJ/mol] \quad (5)$$

Figure 2.3 illustrates the mechanism of CH_4 being converted into CO and H_2, followed by WSGR, that converts CO to CO_2, with steam on active metal catalyst on support. The reaction occurs in a way that CH_4 is dissociated on adsorption onto active metal site, while water is dissociated on adsorption onto the interface of metal and support to produce CO and H_2 [69]. For the complete conversion of CH_4 and steam into syngas, requires minimum formation of C and CO_2. Important factors to reduce the carbon build-up are the size of metal particles and the interaction between support and metal particles. Ni decorated on α-alumina is the most promising for industrial sector [70-73]. Usually, if Ni is deposited in a well-defined structure, the resulting reduction temperature is more than alone NiO, implying the confirmation of metal-support interactions. Various structures having Ni in the form of both oxide

state into the perovskite and metallic state (e.g. LaNi-Fe, $NiAlO_3$, LaNi-Co…) were investigated for SMR [70, 74-77].

Another aspect to consider, while selecting catalyst for SMR is the particle sintering, as it can cause deactivation of catalyst. The extent of particle sintering depends on reaction conditions, metal loading, and crystallite size. The understood mechanism for particle sintering is coalescence and migration [78]. For instance, to prevent the particle migration on the surface of support, the metal-support interaction must be chosen properly. Ru supported on Ni-Mg-Al from hydrotalcite (HTc) precursors with 2,4 and, 6 molar ratios were synthesized to study the catalytic performances and reduction in secondary reactions. It was found that even with a low Ru content, the oxide particles were highly dispersed, showed better catalytic activity, and less subjected to secondary reactions during the process [30].

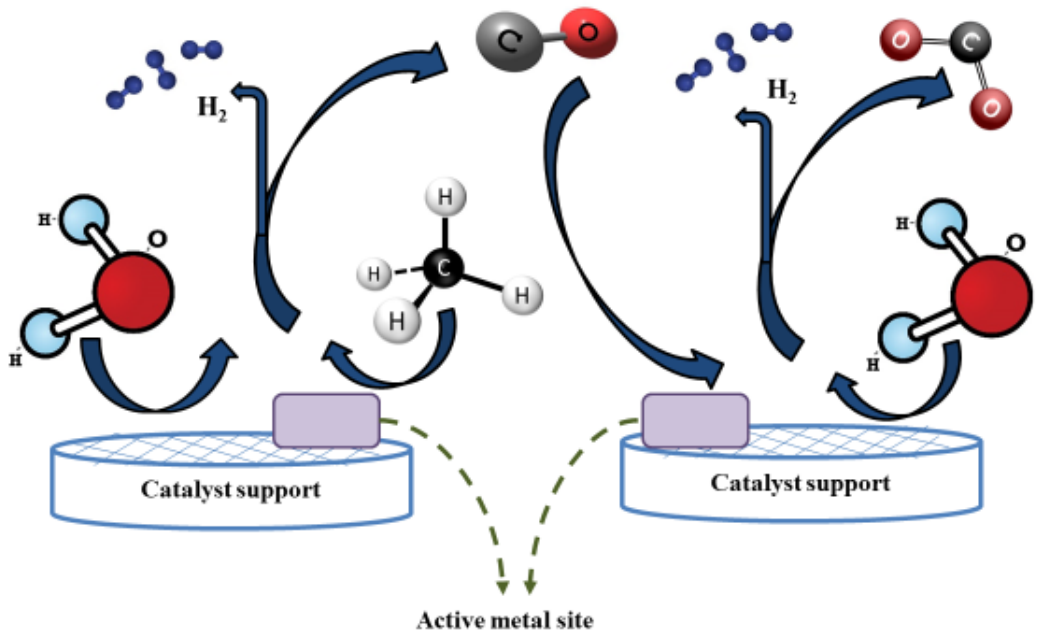

Figure 2.3 Mechanism of SMR on active metal catalyst and support

The spinel $MgAl_2O_4$ has been studied as a support in different chemical reactions due to its surface basicity, and high chemical, thermal and mechanical strength [79]. In comparison with generally used Al_2O_3 or SiO_2-based catalysts, Ni-loaded $MgAl_2O_4$ exhibited high coke resistance in DMR [80, 81], SMR [82], and SESMR reactions [83]. $MgAl_2O_4$ have been proven tricky to form highly defined mesopores with high

thermal stability, due to the sintering deformation initiating at around 700 °C, whereas the optimum SMR temperature range is 750-800 °C [72]. It was analysed that $MgAl_2O_4$ having higher sintering resistance could be prepared from defect spinel structure [84]. It was observed that on increasing the Mg content, catalytic activity increases, however carbon deposition and reducibility decreases due to the strong bonding of Ni ions with the surface of catalyst [85]. Similarly, the effect of Mg loading on the crystal size of Ni was studied to investigate the resulting catalytic performance and coke resistance of the $Ni/MgAl_2O_4$ in SMR reaction. It was found that catalyst with higher Mg content showed greater resistance against coke deposition [72]

Similarly, Fonseca et al. [86] prepared HTc precursors to form Ni-based catalyst at 750 °C for 8 hours in a quartz tube reactor for SMR. It was analysed that uniform active sites distribution in HTc structure reduced the carbonaceous deposit formation. In addition, Ni chelates have resulted in higher CH_4 conversion in comparison with other catalysts due to better active sites dispersion.

2.2 Recent progress in catalysts for SMR

2.2.1 Supported Ni-based Catalyst

Supported noble-metal catalysts such as Pt and Pd have shown superb stability for SMR, while Ni based supported catalysts present comparable reactivity towards SMR [87-89]. In comparison to the noble metal catalysts in SMR, supported Ni-based are less active and undergo deactivation by oxidation of the active metal phase Ni^0 and by carbon formation [90]. To enhance the performance of catalyst and minimize catalyst coking, various modifications in metal content, support and preparation method can be done [91]. According to the mechanism of SMR, carbon species are formed on the active site after the decomposition of CH_4. The catalyst support improves the steam adsorption [92]. Several researchers reported that reducible oxides such as ZrO_2 or CeO_2, promotes stability during SMR and improves the catalytic performance of metals. Supports with mixed oxides promoted the catalytic activity and stability in CH_4 reforming reactions. $Ni/Ce\text{-}ZrO_2$ catalyst containing ZrO_2 initially showed 2-3 times more catalytic activity as compared to

catalyst without ZrO_2, but they deactivated, retaining almost 70% of their initial activity at the end of test. Nevertheless, they were more active than the fresh catalyst [93].

Table 2.1 shows a compilation of investigations for the previous works and advancements for supported Ni based catalysts SMR along with the operating conditions and CH_4 conversions. The activity of Ni-supported catalysts synthesized via wetness impregnation and co-precipitation technique was examined at temperature less than 600 °C for SMR. Ni/Zn-Al and Ni/Mg-Al catalysts synthesized using co-precipitation method exhibited higher catalytic activity and stability compared to Ni/Al_2O_3 and Ni/SiO_2 (prepared via wetness impregnation) owing to the enhanced metal-support interactions of the catalysts. The higher catalytic activity was ascribed to small particle size for Ni based Zn-Al and Mg/Al as compared to the others. Thus, smaller particle size and better metal-support interaction prevented the carbon dissolution [94]. Various papers have described the enhanced characteristics of catalyst synthesized via sol-gel method, for instance Rodemerck and Linke [95] reported mesoporous silica with hexagonal pores as a promising Ni-based candidate in SMR. Ni/SiO_2 was synthesized via sol-gel method to reduce the particle size of Ni and comparison done via conventional preparation techniques. It was observed that sol-gel method produces smaller and finely dispersed Ni particles. Similarly, Ni was introduced into Al_2O_3, SiO_2 and SBA-15 supports using wetness impregnation technique. Catalysts with 10% Ni on SBA -15 proved highest coking resistance and catalytic activity. The catalyst Ni/SBA was promoted with cerium that resulted in improving the reaction rate of CH_4 and better catalytic stability [96]. An attempt to synthesize Ni nanoparticles to impregnate Ni on SiO_2 surface modified with alumina support was reported. The prepared nanoparticles revealed exceptionally better stability and catalytic activity compared to the catalysts formed via conventional impregnation technique due to the smaller particle size (6 nm in comparison to 19 nm for the later), higher dispersion, and high reducibility [22].

The calcination temperature of a catalyst directly impacts on the crystal surface area and metallic particle size and hence the catalytic activity, thus, offering a need to always optimize the calcination temperature of the catalysts. In this respect, Bej et

al. [97] examined the impact of Ni loading and calcination temperature to improve the crystallite size of NiO on a Ni/SiO_2 catalyst synthesized via sol-gel method. It was found that lower calcination temperatures around 400 °C produced smaller Ni particles resulting in 96% CH_4 conversion at 700 °C operating temperature and S/C of 3.5.

Table 2.1 Nickel based catalysts for SMR

Catalyst	**Metal loading**	**Process conditions**	**CH_4 conversion**	**H_2 yield**	**CO selectivity**	**H_2/CO ratio**	**Ref**
Ni/α-Al_2O_3 Ni/SiO_2 Ni/Zn/Al	7-9wt% Ni	500 °C 600 °C	-		0.1- 0.3	-	[94]
Ni/Ce-zZrO_2/θ-Al_2O_3	12 wt% Ni	700 °C GHSV=10,000 ml/g_{cat}	97%		-	-	[98]
Ni/MgO-Al_2O_3	12 wt% Ni	600 °C	30%	-	-	-	[99]
Ni/ZrO_2	9 wt% Ni	700 °C S/C =4	65%	68%	-	-	[100]
Ni/Al_2O_3 Ni/MgO-Al-$_2O_3$ Ni/CeO_2 Ni/$Ce_{0.4}Zr_{0.6}O_2$	10 wt% Ni	750 °C 100 mg	97%	73.5% 71.5% 70.5% 70.3%	8.2% 8.8% 10.9% 11.2%	6.5 5.0 6.0 10	[101]
Ni/CaO-ZrO_2/γ-Al_2O_3	10 wt% Ni, 5wt%CaO-ZrO_2	650 °C 100 mg	60%	35%	-	-	[102]
Ni/SiO_2	10% wt% Ni	500 °C S/C = 1	60%	-	40%	-	[103]
Paper-like Ni/MgO	NA	800 °C Gas velocity=	90%	-	-	-	[104]

		18,000 h^{-1}					
NiO/SiO_2	10 wt% Ni	700 °C S/C = 3.5	95.7%	3.8 mol H_2/mol of CH_4 reacted	20%	-	[97]
Ni/TiO_2	10 wt% Ni	700 °C S/C =1.2	45%	-	77%	1.0	[105]
$Ni/Mg\text{-}Al_2O_4$	15 wt% Ni	800 °C S/C =3	75%	-	-	3.6	[72]
$Ni/MgAl_2O_4$	15 wt% Ni	600 °C S/C =5	45%	-	-	4.5	[82]
Ni/Ce-Gd	30 wt% Ni	700 °C S/C =3	73%	-	-	11	[106]
$Ni/Ce_{01.5}\text{-}Zr_{0.85}O_2$	10 wt% Ni	800 °C	66.6%	-	52.9%	7.0	[107]
Ni/SiO_2 Ni/TiO_2	10 wt% Ni 10 wt%Ni	500 °C S/C = 1	32% 28%	- -	- 26%	- -	[108]
Ni/SiO_2	10 wt% Ni	800 °C S/C =0.5	45%	-	-	-	[109]
$Ni/SiO_2/ZrO_2$	Varying quantity of Ni	750 °C S/C = 2.5	95%	-	70%	-	[110]
$Ni/Al_2O_3\text{-}Y_2O_3\text{-}ZrO_2$	5 wt% Ni	850 °C S/C = 1.5	95.6%	67%	87%	5.0	[111]

2.2.2 Perovskites for SMR

Recently, perovskites-based catalysts have been explored and achieved much attention. This type of material has shown promising results in emerging applications, such as ceramic membranes [112, 113], heterogeneous catalysis [114, 115], and solar cells [116, 117]. Initially, oxides like $LaFeO_3$ and $NaNbO_3$ were reported to catalyse CO oxidation [118]. Since then, investigations on perovskite-based catalysts to reforming of CH_4, ethanol, and tar etc. have been studied in literature [115, 119-121]. Perovskites are the mixed metal oxides that can hold 90% of the metal element at A or B active sites, without damaging crystal structure. For example, A sites could be occupied with Sr, La and Ce etc, while B site could be solely or partially occupied by Co and Ni [122, 123]. This perovskite structure improves thermal stability, avoids carbon formation, and reduces sintering making them suitable candidates for gaseous reactions at elevated temperatures [90, 124]. Therefore, perovskites may not be used as a catalyst but as catalyst precursors. As Ni metal can catalyse SMR process, therefore, perovskite oxides containing Ni cations can act as precursors for the reforming reaction. After the reduction of H_2, Ni cations are reduced to real metal active sites for reforming [125]. Its extensive application in CH_4 reforming could be credited to the point that catalysts with segregated active phases are attached uniformly onto unreduced oxides matrix after reduction [126]. Figure 2.4 explains a generalized illustration for the migration of Ni metal. The scheme clearly shows that after reduction, the surface becomes enriched with Ni metal in perovskites [127].

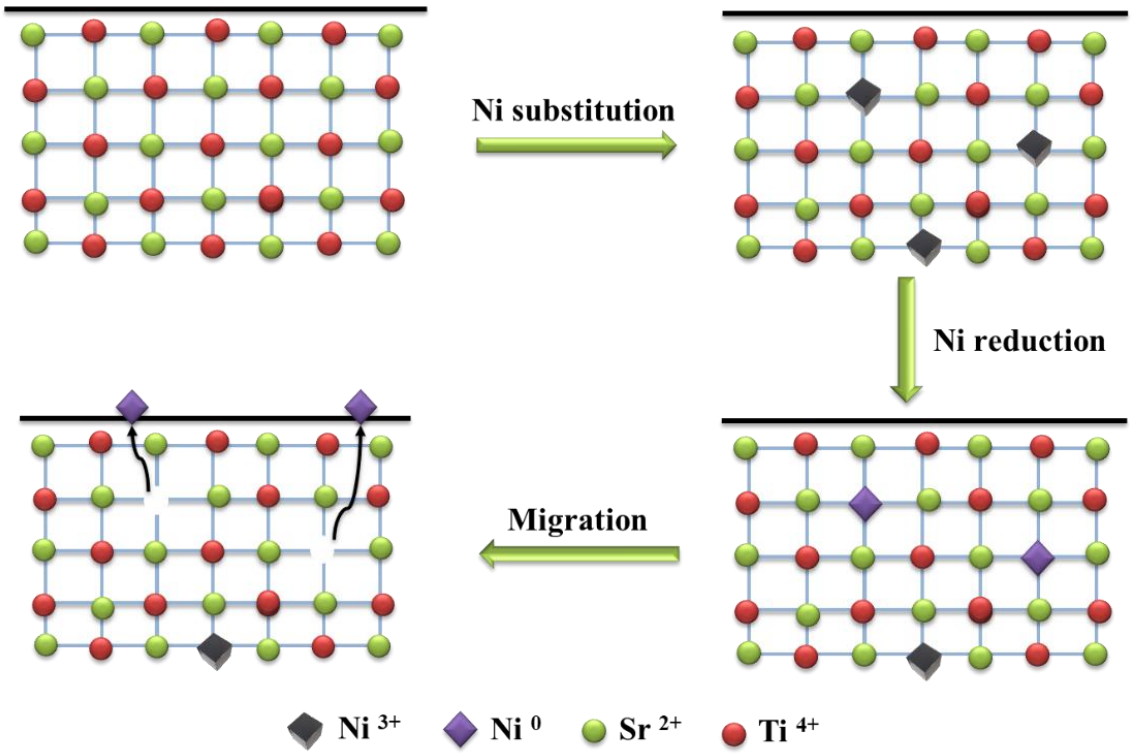

Figure 2.4 Proposed mechanism of Ni metal migration in perovskites (recreated from [127])

Three-dimensionally ordered macroporous $LaFeO_3$ (3DOM-$LaFeO_3$) and nano-$LaFeO_3$ perovskites were produced via impregnation technique to test for chemical looping SMR (CL-SMR). The process is based on CH_4 being partially oxidized by the oxygen carrier in the reactor to syngas, followed by the oxidation of the reduced oxygen carrier by steam to produce H_2 in the reactor. The success of the process is dependent on appropriate oxygen carriers capable of producing H_2 with a better activity for H_2O splitting, high CH_4 conversion and resistance to agglomeration. In this respect, perovskites metal oxides are gaining more attentions as oxygen carriers [128]. The synthesized three-dimensional catalyst resulted in a surface area of 8.08 m^2/g, more than the nano-$LaFeO_3$ (4.32 m^2/g). In case of nano-$LaFeO_3$, a high CO selectivity of 67.3% was stabilized to 100% after 4 minutes. While for 3DOM-$LaFeO_3$, a gradual increase in the CO selectivity in the initial 8 minutes was observed. Similar trend for H_2 selectivity was observed with final H_2 selectivity of 85%. CH_4 conversion obtained was 85.3% and 69.9% for nano type and 3DOM-

$LaFeO_3$, respectively. A higher stable reactivity of CH_4 oxidation and improved endurance to carbon deposition was ascribed to the greater surface area of 3DOM perovskites. Figure 2.5 (a-b) presents the SEM images of freshly prepared and spent (after 10 cycles) 3DOM-$LaFeO_3$ perovskite oxides. After 10 redox cycles, the structure and skeleton of 3DOM perovskite totally collapsed due to the long thermal and chemical stresses during the reforming reactions, however, no agglomeration and sintering appeared on the sample surface. It was also validated by XRD as the grain size and crystallinity of the spent catalyst were reduced. Figure 2.5 (c-d) shows the difference in the granular structure of nano-$LaFeO_3$ after 10 redox cycles. The particles after a series of cycles were combined to a stratiform morphology with slight sintering on the surface [129].

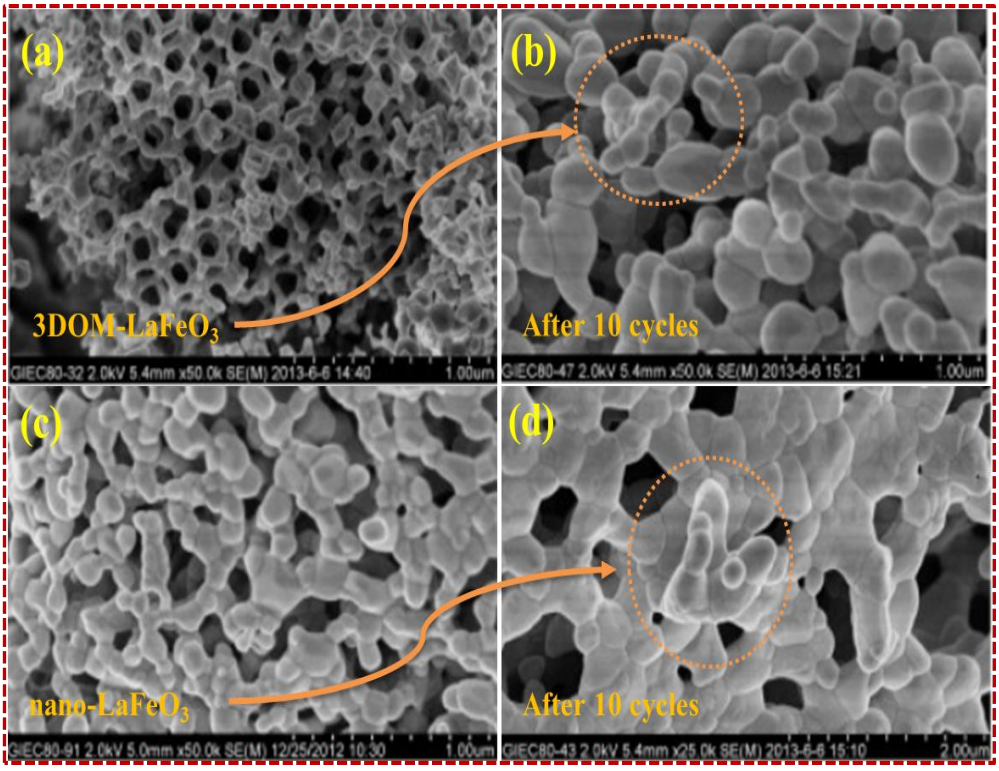

Figure 2.5 SEM images of freshly prepared and spent 3DOM-$LaFeO_3$ and nano-$LaFeO_3$. Recreated from [129]

The Cu^{2+} and Ca^{2+} substitutions are reported to improve the reactivity in the perovskite structure. Carrasco et al. [130] proved that the presence of Cu^{2+} at $LaCu_1$-

$_xM_xO_3$ (M = Ti, Mn) surface was advantageous for the reactivity. In this manner, Jiang and Jin [131] prepared a novel hybrid with Cu^{2+} and Ca^{2+} substitutions in La perovskite structure for H_2 production. The results presented an increase in the reactivity of $La_{0.1}Ca_{0.9}Ni_{0.9}Cu_{0.1}O_3$ on increasing Ca^{2+} in the perovskite. Among different compositions prepared, $La_{0.1}Ca_{0.9}Ni_{0.9}Cu_{0.1}O_3$ showed high resistance to carbon deposition, best reactivity and renderability. CH_4 conversion and CO selectivity of the catalyst reached 52% and 60%, respectively. Similarly, Moradi et al. [132] proved that the combination of Cu^{2+} and Ni^{2+} in $LaCu_xNi_{1-x}O_3$ improved the CH_4 conversion in CH_4 reforming.

Redox nature of perovskites performs major role in reforming reactions as carbon species produced on the surface of perovskites are detached on reaction with the surface reaction. Table 2.2 summarizes various perovskites used in SMR and CL-SMR. Layered $Sr_{n+1}Ti_{n-x}Ni_xO_{3n+1}$ was observed to enhance the activity in syngas production at 20,000 h^{-1} GHSV, and S/C of 3. In a range of 600-750 °C, CH_4 conversion increased from 60% to 89% for $Sr_4Ti_{2.3}Ni_{0.7}O_{10}$, while a higher conversion was observed for $SrTi_{0.3}Ni_{0.2}O_3$ from 84% to 97%. Lower conversions of CH_4 observed for lower values of n in layered perovskite could be due to the variation in the surface area of oxides [127]. Zhang et al. [133] performed CL-SMR over cerium doped perovskites ($La_{1-x}Ce_xFeO_3$) prepared via sol-gel method. For all samples prepared, CH_4 conversion and H_2 selectivity increased, while CO_2 selectivity decreased with the appearance of Fe^0 and consumption of lattice oxygen. $La_{0.5}Ce_{0.5}FeO_3$ resulted in maximum 90% CH_4 conversion and CO selectivity, and minimum coke formation.

Ordered double perovskites differ in properties and structure from simple perovskites, with rare earth metal and transition metal as A and B sites, respectively. Tuza and Souza [134] studied SMR over catalysts derived from double perovskites (La_6NiTiO_6) in a temperature ranging from 550 °C to 950 °C, resulting in 95% CH_4 conversion at 950 °C [135]. Huang et al. [136] used double perovskites Sr_2CoMoO_6 and Sr_2NiMoO_6 for SMR as catalysts. Sr_2CoMoO_6 performed better reaction activity as compared to the other. These catalysts have been hardly used for SMR but have

great potential in enhancing coking resistance because the perovskite structure supplies oxygen lattice to the metallic surface, converting carbon deposits to gaseous compounds.

Table 2.2 Perovskites for SMR and CL-SMR

Catalyst	**Application**	**Process conditions**	**CH_4 conversion**	**H_2 yield**	**CO selectivity**	**H_2/CO ratio**	**Ref**
$Ni_{0.5}Mg_{2.5}AlO_9$ $Ni/ZrO_2/Al_2O_3$	SMR	S/C = 3:1 Residence time= 20ms	100% 86%	-	-	-	[137]
$LaNiO_3$	SMR	850 °C S/C = 2	86%	88.15%	-	-	[138]
$La_{1-x}Sr_xFeO_3$	CL-SMR	850 °C	80%	-	-	2.0	[139]
$Ba_{1-x}Sr_xCoO_{3-\delta}/CeO_2$	CL-SMR	850 °C 1g loading	-	-	95%	1.8	[140]
$Sr_{n+1}Ti_{n-x}Ni_xO_{3n+1}$	SMR	750 °C S/C =3 GHSV = 20,000 h^{-1}	97%	-	-	-	[127]
$BaCoO_{3-\delta}/CeO_2$	CL-SMR	860 °C 0.5 g loading	-	-	6.0	2.0	[141]

2.2.3 Catalyst with promoters and noble metals for SMR

Studies revealed that the incorporation of metal additives to the reforming catalyst can overcome the shortcomings of Ni-based catalysts and improves the catalytic stability. These additives helped improving the reaction activity, and reduction in coke deactivation, thus increasing the yield of H_2 [96]. Table 2.3 presents a summary of works reported on catalysts with promoters and noble metals for SMR. A sequence of noble metal catalysts supported on Al_2O_3 and $MgAl_2O_4$ prepared via impregnation route were investigated for SMR process. Rh and Ir recorded exceptionally higher metal dispersions around 50% and 100%, respectively. Particle size less than 2 nm were observed, which indicated five times greater stability than the $Ni/MgAl_2O_4$. The SEM images validated the small particle size production of $MgAl_2O_4$ as compared to Al_2O_3 that justified the reduction noticed in CH_4 conversion for 5 wt% Rh/Al_2O_3 from 90% to 78%, whereas 5 wt% $Rh/MgAl_2O_4$ maintained 95% initial conversion [142].

Lee and Hong [143] enhanced the carbon resistance of catalytic porous membrane by adding Pd as a promoter for low temperature SMR. It was noticed that the incorporation of Pd upgraded the catalytic stability and activity of the Ni-YSZ membrane, thus, increasing the H_2 yield and CH_4 conversion because of the equilibrium shift due to the difference in permeation rates between H_2 and other product gases as per Le Chatelier's principle. Pd clusters played major part in reducing the carbon formation on the catalyst surface during the process.

CeO_2 have better characteristics to use as a support for Ni impregnation, but due to its beneficial impact, CeO_2 gives pronounced results when used as a promoter. CeO_2 support provides the role of oxygen vacancies for the catalyst. In this respect, Castro et al. [13] added CeO_2 to Pt/Al_2O_3 for the steam reforming of toluene and CH_4 to explore the impact of CeO_2. It was found that CeO_2 provided the source of oxygen to control the redox property of the synthesized catalyst during the reforming reaction. However, a slight deactivation of catalysts was noted due to the adsorption of both CH_4 and toluene in the same active sites causing the build-up of carbon on the surface. Similarly, Duarte et al. [144] promoted CeO_2 and Sm_2O_3-CeO_2 with

Al_2O_3 support and dispersed Rh to investigate the stability and activity in SMR at 500 °C. The CeO_2-Al_2O_3 support contributes to the partial stability of Rh, leading to the formation of nanosized and atomically dispersed particles of Rh. This was due to the reason that CeO_2 favours the stabilization of atomically distributed small metal particles because of durable metal-support interaction [145].

Table 2.3 Promoters and noble metals for SMR

Promoter/ Noble metal	**Catalyst composition**	**Catalyst/ Promoter loading**	**Process conditions**	**CH_4 conversion**	**H_2 yield**	**Ref**
Alkali promoter (K_2O)	$NiO-Al_2O_3$	1-4 wt% K_2O in K/Al_2O_3	450-500 °C S/C =1.4-6	65%	-	[146]
Ce-based	Ni-Ce/Al	13 wt% Ni 1.02 wt% Ce	S/C =3	75%	-	[96]
CeO_2-based	$Pt/CeO_2/Al_2O_3$	1.4 wt% Pt	700 °C S/C = 4	74%	-	[13]
Mo-based	$Mo-NiO/Al_2O_3$	0.05 wt% Mo	700 °C S/C = 2	85%	55%	[147]
B-based	$B-Ni/\gamma Al_2O_3$	15 wt% Ni 1 wt% B	800 °C	61%	-	[148]
Ag-based	$Ag-Ni/CeZrO_2$	10 wt% Ni 1 wt% Ag	850 °C	57%	-	[149]
Pd-based	Pd-Ni-YSZ	0.5 wt% Pd	650 °C S/C = 3 GHSC= $3800h^{-1}$	94.6%	>3.9	[150]
Rh-based	$Rh/MgAl_2O_4$	5 wt% Rh	850 °C S/C = 3	41%	-	[142]
Rh-based	$Rh/Ce_{0.15}Zr_{0.85}O_2$	3 wt% Rh	500 °C	28.1%	-	[107]

Co-based	Co-MgAl-CO_3	NA	750 °C 100 mg of catalyst	80%	-	[151]
Pd-based	Pd/CeO_2/γAl_2O_3	10% CeO_2	550 °C S/C =3	-	-	[152]
Pd-based	Pd/CeO_2/Al_2O_3	CeO_2 >12wt%	650 °C	-	-	[153]
Ru-based	Ru/Al_2O_3	8 wt % Rh	800 °C S/C = 1.5	88.7%	-	[154]
Ir-based	Ir/$MgAl_2O_4$	5 wt%	850 °C S/C =3	55%	-	[142]
Pt-based	Pt/Al_2O_3	1 wt%	700 °C S/C =4	70%	-	[13]

2.2.4 Bi-metallic catalysts

Noble metals supported on different oxides have been significantly investigated to overcome the drawbacks of reforming catalysts. Yet, noble metals are quite expansive which limits its utilization as promoters for SMR. Therefore, bimetallic catalysts were introduced where noble metals were added to the transition metals as Ni and Co to develop transition-noble metal alloys with improved and ultimate properties due to higher catalytic performance and reduced cost [155, 156]. A series of supported bimetallic catalysts with 12% Ni loading but varying Co loading was investigated for SMR by You et al. [157]. The addition of Co in Ni/γ Al_2O_3 improved the reaction stability and coke tolerance by alloy formation on the surface of Ni-Co, which reduced the metal dispersion and blocked the part of low coordinated active Ni sites. Recently, the addition of varying quantities of Pt into Ni/$MgAl_2O_4$ was synthesized and studied for SMR by Jaiswar et al. [158]. With 0.1% optimum Pt loading, Pt-Ni alloy formation on the catalyst surface increased the metal surface area and hence higher catalytic activity was observed. However, Pt loading beyond 0.1 wt% resulted in lowering the catalyst stability, agglomeration, and activity of the active metals in the catalyst.

Bimetallic catalysts have been observed to increase the reaction stability and performances in comparison to the monometallic catalysts [157]. Table 2.4 summarizes the bimetal catalysts with CH_4 conversions for SMR. Formation of Ni-Co alloy for CH_4 reforming have been investigated by several groups, that resulted in improving the coke resistance of the catalysts [159-161]. Yu et al. [162] and Zhang et al. [163] also noticed the promotional effects to the higher metal dispersion on Co addition. Wang et al. [164] determined the reactions occurring in bimetallic Ni based catalytic systems modified with Au, Ah, and Cu to investigate the catalyst producing least carbon quantity. The results suggested Ni-Cu catalyst as a promising bimetallic material with higher active carbon tolerance for SMR. Homsi et al. [165] prepared highly stable and reactive Co/Ru based catalyst for H_2 production. It was found that an interaction between Co and Ru favoured the formation of finely dispersed Co/Ru

oxide species. The catalyst resulted in higher catalytic stability up to 100 hours on stream and trace level formation of coke on the surface.

Table 2.4 Bimetallic catalysts for SMR

Catalyst/ sorbent composition	**Optimum loading**	**Process conditions**	**CH_4 conversion**	**H_2 yield**	**CO selectivity**	**H_2/CO ratio**	**Ref**
Ni-La/α-Al_2O_3	7 wt% Ni 3 wt% La	800 °C 0.15g loaded GHSV=32,000 ml/g_{cat}/hr	97%	94%	-	-	[23]
Pt/La_2O_3-Al_2O_3	12 wt% La 0.5 wt% Pt	650 °C	84%	-	95%	-	[166]
Co-Pt/Al_2O_3-ZrO_2-CeO_2	5wt% Co-Pt	750 °C GHSV= 1000 hr^{-1}	95.4%	95%	-	3.6-4.0	[167]
Ru/La-Al_2O_3	1.5 wt% Ru/ 3 wt% La 100 mg	800 °C S/C =3	97.3%	78.3%	50%	5.0	[168]
Ni/La-Ca/Al_2O_3	21.6 wt% Ni	GHSV= $1.2*10^5$ h^{-1} S/C = 3	98%	-	-	-	[137]

$Ni/Ag/Al_2O_3$ **$Ni-Au/Al_2O_3$**	1 wt% Ag 1 wt% Au 8 wt% Ni	700 °C S/C =4	49% 96%	-	-	-	[169]
$Co-Ni/CeO_2$	1.6-3.2 wt% Ni 12 wt% Co	750 °C	76.1%	44.5%	-	-	[170]
$Ru/Co_{6-x}Mg_xAl_2$	1 wt% Ru 0-6 wt% Co 200 mg	600 °C S/C =3	93%	-	-	-	[165]
(Pd/Rh)/Ce ZrO_2-Al_2O_3	0.09 wt%	800 °C S/C =1.5	92.7%	-	-	4.2	[154]

2.3 Sorption enhanced steam methane reforming (SESMR)

For the past few years, focus on H_2 production is shifted towards the technologies that support the reduction of GHG emissions. Yet fossil fuels as a feedstock for H_2 will remain for the foreseeable future, various investigations have reported advanced technologies in the process that use modified catalysts to overcome the limitations in SMR [171-173]. One way is to remove either CO_2 or H_2 continuously, therefore, shifting the thermodynamic equilibrium towards H_2 production. As shown in the previous studies, there is a possibility to replace the complex multi-step reactions by single-step reaction which utilizes a mixed bed of catalyst matrix and solid sorbent operating in an intermediate range of temperature [174]. The process known as SESMR, is an intensification of reaction (Eq. (1)) and (Eq. (2)) via a high temperature solid-sorbent, hence, coupling the commercial SMR with in-situ CO_2 capture [15]. Using this technique, equilibrium of reforming and shift reactions is shifted towards H_2 production from 80% to 95%, as per Le Chatelier's principle [2]. The concept behind SESMR process is centred around utilization of a reforming catalyst and a solid regenerable sorbent to capture in-situ CO_2 from the reformer [175].

Sorption enhanced process enables reaction at lower temperatures, reduce coking and sintering of catalyst. In addition, the heat essential for the endothermic reforming reactions is provided by the heat released from exothermic carbonation reaction. Hence, approximately 15-20% CO_2 in the outlet gases can be captured from SMR. The yield of H_2 produced is dependent on the properties of reforming catalyst and the sorbing agent used for CO_2 capture, leading to a product yield more than 97% H_2 [176].

However, the process requires a sorbent regeneration stage to reuse the sorbent once it is saturated with CO_2. After saturation, sorbent can be regenerated at higher temperature conditions that depends on the partial pressure of CO_2, producing pure CO_2, ready for storing as chemical feedstock [21]. Reaction temperature and pressure in SESMR are in a range of 400-600 °C and 0.1-0.3 MPa, respectively, much lower than the conventional

SMR. The lower operating temperatures suggest the need of very active reforming catalyst [94]. Accordingly, the process has been investigated in various configurations including fluidized bed, bubbling bed and fixed bed under atmospheric or high pressure [43, 177-183]. Extensive studies on the low-cost H_2 production systems have been carried out including SESMR [44, 184-188].

The configuration of reactor consists of a reforming catalyst and sorbent that mitigates CO_2 as soon as it is produced by reforming and WSGR. An ideal CO_2 sorbent should have a high cyclic stability, adequate adsorption characteristics, satisfactory adsorption/ desorption kinetics, and high mechanical strength. In recent years, numerous sorbents have been stated in the literature, e.g., mixed oxides such as magnesium oxide (MgO) [41, 189] and calcium oxide (CaO) [94, 190], HTc based materials [16, 28], lithium orthosilicate (LOS) [191], and multifunctional sorbent-catalyst materials[182, 192]. Table 2.5 presents different sorbent-catalyst systems for SESMR process. Among these, CaO-based sorbents have a strong chemical interaction with CO_2 to form $CaCO_3$, resulting in the highest adsorption capacity, fast calcination/carbonation cycles, and adequate reversibility [38, 193, 194]. Figure 2.6 demonstrates the mechanism of CaO-based sorbents and catalyst for SESMR. CaO particle helps to react with the CO_2 produced during the reforming reaction over an active metal site, depositing $CaCO_3$ on the surface of catalyst.

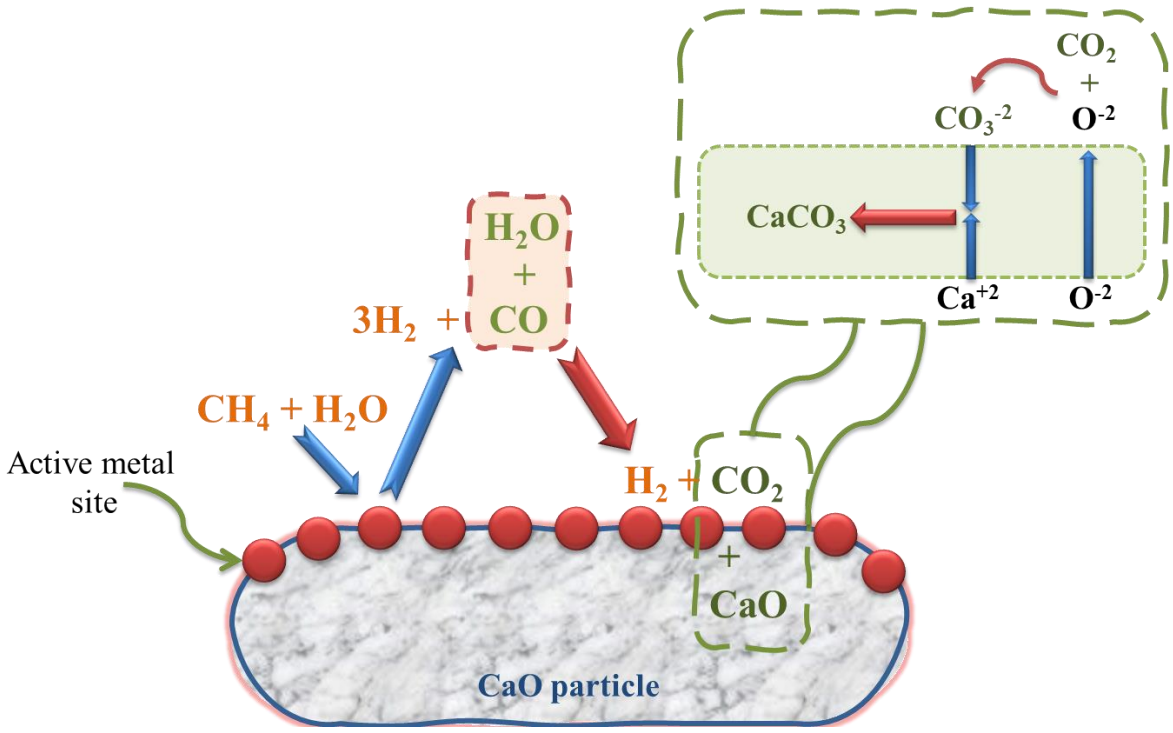

Figure 2.6 Mechanism of CaO-based catalyst for SESMR ($CaCO_3$ deposition on the catalyst surface on reaction of CO_2 released with CaO particle)

However, the major drawback of CaO sorbents are the decay in the adsorption capacity throughout the multicycle operation, low conversions (54% after reaction of 10% CO_2 with $CaCO_3$ at 650 °C) due to the formation of $CaCO_3$ layer that covers and fills the pores of CaO, thus hindering the CO_2 diffusion to the reaction interface [195]. For this reason, attention have been paid to modify CaO-based sorbents either by changing the calcium precursors, steam reactivation, modification of pore structure, or by incorporating a variety of metal oxides like ZrO_2, MgO, Al_2O_3 and La_2O_3 into CaO system [196-199]. This group of synthetic CaO-based modified sorbents have shown a decrease in sintering phenomena because the metal oxides may behave as spacer between CaO particles, protecting them from accumulation of sintered grains during

multiple cycles. Resultingly, a noticeable improvement of active surface area, mechanical and thermal stability, may be observed [200].

CaO dispersion on a high surface area γ-Al_2O_3 was investigated to study the effect on stability and kinetics in comparison with bulk CaO as a sorbent. The synthesized catalyst/sorbent was tested for 84 cycles at 650 °C and showed long term stability as compared to bulk CaO as sorbent. This sorbent was a candidate for SESMR with CO_2 uptake efficiency up to 15% [201]. CaO based $CaTiO_3$ coated adsorbents were analysed for the improvement in sorption of CO_2 during SMR. Durability in the sorption capacity up to 5.3 mol/kg after 40 cycles of carbonation/calcination reaction was observed due to $CaTiO_3$ coating, while capacity up to 3.7 mol/kg without coating was observed [202]. CO_2 sorbents derived from Al and Ca precursors are expected to be applied in SESMR process. Among various precursors, CaO-$Ca_9Al_6O_{18}$ with 80 wt% CaO content showed best performance for sorption and stability over multiple cycles [203]. Similarly, a bifunctional catalyst from HTc precursor containing calcium as sorbent and Ni as reforming catalyst. CO_2 sorption capacity observed over 10 cycles was 0.074 g CO_2/g sorbent and stabilized over 7 cycles with 0.3% average decay rate per cycle. The material with Ca developed a larger quantity of high-purity H_2 than with Ni-SiO_2 [204]

HTc are encouraging sorbents for CO_2 capture, distinguished as layered double hydroxides (LDH) from a family of anionic clays, with general chemical formula $[M^{II}_{1-x}M^{III}_x(OH)_2]^{x+}[A^{n-}_{x/n}.yH_2O]^{x-}$, where A^{n-} represents n-valent anions, M^{II} and M^{III} are the divalent cations (e.g., Cu^{+2}, Mg^{+2}, Zn^{+2}, Mn^{+2}) and trivalent metal cations (e.g., Fe^{+3}, Co^{+3}, Al^{+3}, Cr^{+3}) [205]. For example, they consist of layers of aluminium and magnesium with exchangeable interlayers of carbonate ions and H_2O molecules. The layers present a brucite-like structure, i.e. Mg $(OH)_2$, in which Mg accelerates the selective adsorption of CO_2. The cations Mg^{+2}, are octahedrally linked with OH^- and arranged in sheets held together by H-bonds. The Mg^{+2} cations in this structure are partially substituted by Al^{+3}, resulting in a positive charge, compensated due to the

presence of CO_3^{-2} ions that can exist in conjunction with H_2O molecules between two brucite-type sheets [206]. Calcination of such LDH gives a homogenous mixture of M^{II} and M^{III} oxides that are finely dispersed, associated with a high thermal stability and surface area. HTc based catalysts have shown promising results owing to the uniform dispersion of active metal on the catalyst surface, large surface area, and memory effect which enables HTc to its original form after contact with aqueous solution [72]. Lately, Ni-loaded calcined HTs have been promising for the catalytic reforming of different hydrocarbons.

At elevated temperature of 400-450 °C, HTc have an acceptable CO_2 capture capacity of 0.45-1 mol/kg. Dewoolkar et al. [207] prepared Ni based HTc for SESMR and produced 98.5% H_2 rich gas. Prepared HTc adsorbed almost 1.1 mol CO_2/kg of sorbent and showed stability up to 16 cycles. Similarly, cerium promoted HTc for SESMR, improved the H_2 production and offered strong basic sites for the adsorption of CO_2. Adsorption capacity up to 1.74 mol/kg sorbent was observed at a S/C of 6. Thus, improved adsorption characteristics and catalytic activity made the material regenerable and stable [16]

Table 2.5 Catalyst-sorbent system for SESMR

Sorbent	**Catalyst/ sorbent composition**	**Optimum loading**	**Process conditions**	**CH_4 conversion**	**H_2 yield**	**Ref**
CaO-based	Ni/CaO Ni/Al_2O_3	12.5wt% Ni/CaO	600 °C S/C =3	10% 80%	-	[208]
CaO-based	$Ni\text{-}Al_2O_3$ $Ni\text{-}CaO/Al_2O_3$	10wt% Ni 1.5g catalyst loading	500 °C S/C =9	90%	20.1%	[207]
CaO-based	$Ni_{0.5}/Mg_{2.5}Al$ $CaO\text{-}Ca_9Al_6O_{18}$	Ni:Mg:Al= 0.5:2.5:1	650 °C	83%	-	[43]
CaO-based	$CaO\text{-}Ca_9Al_{16}O_{18}$	80 wt% CaO 10 mg loading	650 °C	-	-	[203]
CaO-based	CaO/NiO	18.5 wt% NiO	650 °C S/C = 3	98%	93%	[209]
CaO-based	Al-stabilized CaO-NiO	25 wt% NiO	650 °C S/C = 5	99.1%	97.3%	[46]
CaO-based	$CaO\text{-}NiO/NiAl_2O_4$	10 wt% NiO	650 °C S/C =1.6	94%	2.6%	[210]

CaO-based	Ni/CaO-Zr	20.5 wt% NiO	650 °C S/C =4	99%	92%	[48]
MgO-based	Ni/MgO	NA	700 °C S/C =1.5	90%	-	[211]
MgO-based	Ni/MgO-Al_2O_3	12wt% Ni 10 mg	800 °C	90%	-	[212]
ZrO_3 based	Ni/Li_2ZrO_3	40wt% Ni 20 mg	550 °C	-	-	[213]
ZrO_3 based	Ni/Na_2ZrO_3	NA	500 °C S/C = 3	95%	-	[214]

Chapter 3

Research Methodology

3.1 Synthesis and experimental section

3.1.1 Preparation of Mg-Ni-Al (MNA), CaO and CaO @ MNA

Mg-Ni-Al (MNA-121) was synthesized by the co-precipitation procedure presented in Figure 3.1(a). All materials were sourced from Sigma Aldrich ® Ltd. 0.25M solution of [$Ni(NO_3)_2.6H_2O$] (99%) and 0.75M solutions of [$Mg(NO_3)_2.6H_2O$] (99%) and [$Al(NO_3)_3.9H_2O$] (98.5%) were prepared. 1M solution of NaOH, to maintain the Ph, and 0.5M solution of Na_2CO_3 (CO_3^{-2} to act as cation exchange reagent), were added into mixing solution. Afterwards, Na_2CO_3 solution was vigorously stirred at 70˚C and solution of metal nitrates was continuously titrated dropwise. Constant pH of 10 was maintained by dropwise NaOH solution addition. Resulting precipitates were filtered and washed with deionized water several times. Vacuum filtration was carried out 5 times till the precipitates are free from sodium ions. After filtration, the precipitates thus produced were dried in air drier at 90˚C for 18 hours and then calcined at 850˚C for 6 hours in a muffle furnace.

Waste eggshells were collected and washed with purified water numerous times until properly cleaned. The eggshells were crushed and dried in an oven for 24 hours at 100˚C. The shells were then pulverized by a grinder, smaller enough to slip through a sieve of 0.25mm. The powdered eggshell was calcined at 900˚C for 3 hours in muffle furnace and stored in a desiccator for future utilization. The CaO preparation scheme from waste chicken eggshells is presented in Figure 3.1(b)

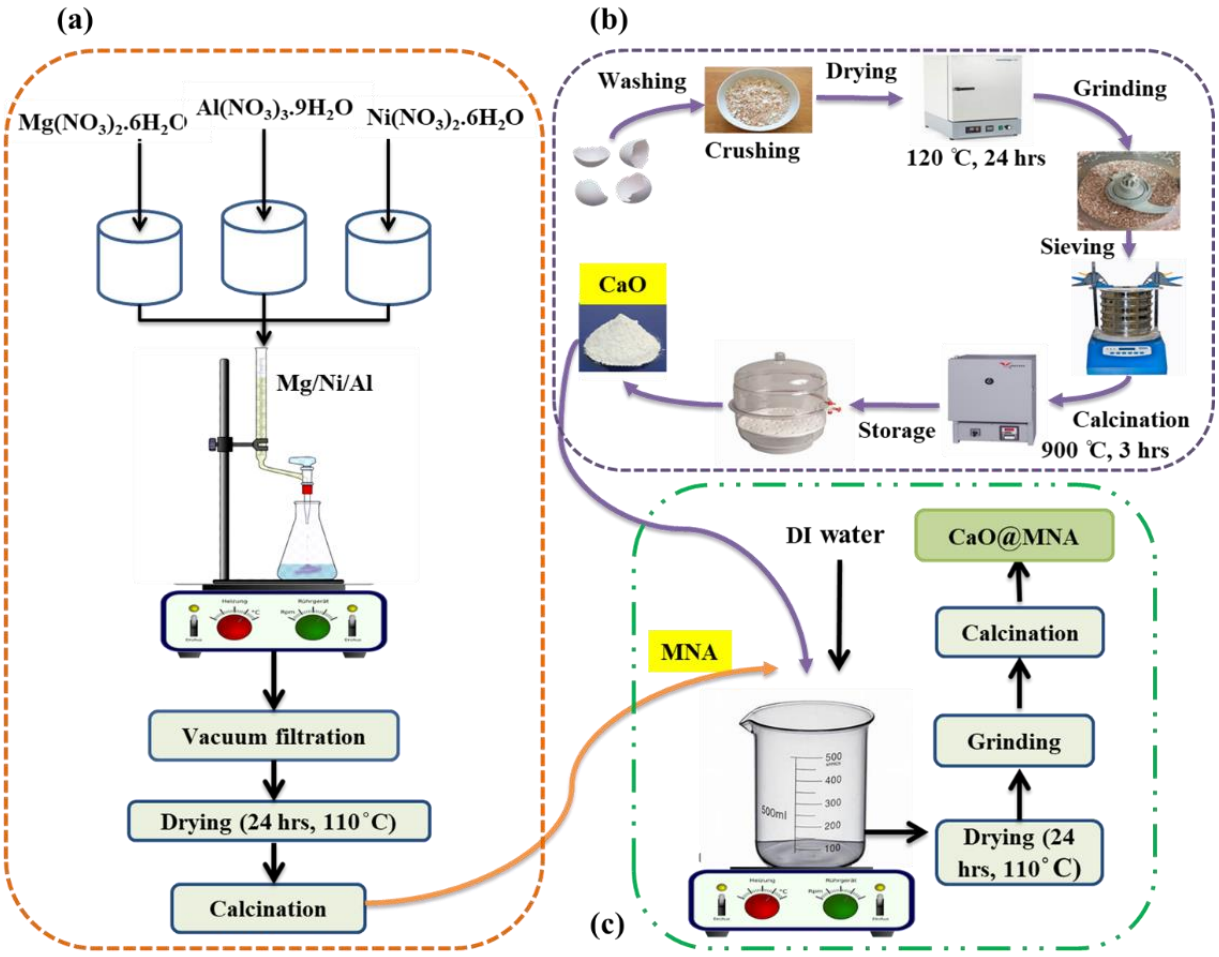

Figure 3.1 Schematic diagram of synthesis of (a) MNA (b) CaO (c) CaO @ MNA

CaO @ MNA catalyst was made by the wet-impregnation technique as illustrated in Figure 3.1(c). Different loadings of the waste derived CaO, 5%, 10%, and 15% were decorated on MNA in the same manner to estimate the effect of enhancement of CO_2 capture in the product gas of SESMR process. After the vigorous mixing of catalyst and CaO, that acted as a sorbing agent, mixtures were dried overnight at 110˚C. Prepared samples were crushed, followed by calcination for 6 hours at 850˚C.

3.1.2 Experimental setup for SMR

The schematic diagram of the fixed bed set-up (Parr instrument, 5401, USA) for the experimentation of SMR and SESMR is shown in Figure 3.2. The unit is distributed into three segments relevant to feed, reactor for reforming and analysis of product, respectively. The feed section has gas cylinders for H_2, and CH_4. Flow rate of CH_4

(99.9%) and H_2 was controlled by mass flow controller (Brooke instruments, USA). The H_2 gas was used for the reduction of catalyst while CH_4 and steam are feed gases. Controlled amount of these gases flow into the preheater. Deionized water was fed directly into the preheater to get vaporized and to attain a given steam to carbon ratio (S/C) in the reactor. Temperature of the reforming reactor was controlled by a process controller (4871, Parr instruments), which may vary slightly (5-10 °C more) from temperature of catalyst. Temperature of preheater was controlled by a thermocouple. The flow and temperature were monitored via online SCADA system. The thermal reactor included a stainless steel (SS 316) vertical fixed bed reactor having a length of 300 mm and an inner diameter ID= 12 mm. The condenser was used to eliminate any moisture and liquid product formed. The analyser section consisted of a gas chromatograph (GC-TCD) (GC-2010 Plus by Shimadzu Japan) and thermal conductivity detector, equipped with a capillary column (RT-MS5A, 30m x 0.32mm, 30 µm) for the detection of CH_4, H_2, CO_2, and CO.

The catalyst was loaded in a known amount using quartz wool sandwiched in the middle of SS reactor and reduced for 1 hour in the presence of H_2 gas at constant flow of 20 ml/min at 750 °. After reduction, H_2 gas was switched to CH_4 gas and steam at the required operating temperature. The product gas, after the reaction entered the condenser where it was collected in the water condensate collector. The composition of product gas was analysed, and results were recorded every 20 minutes.

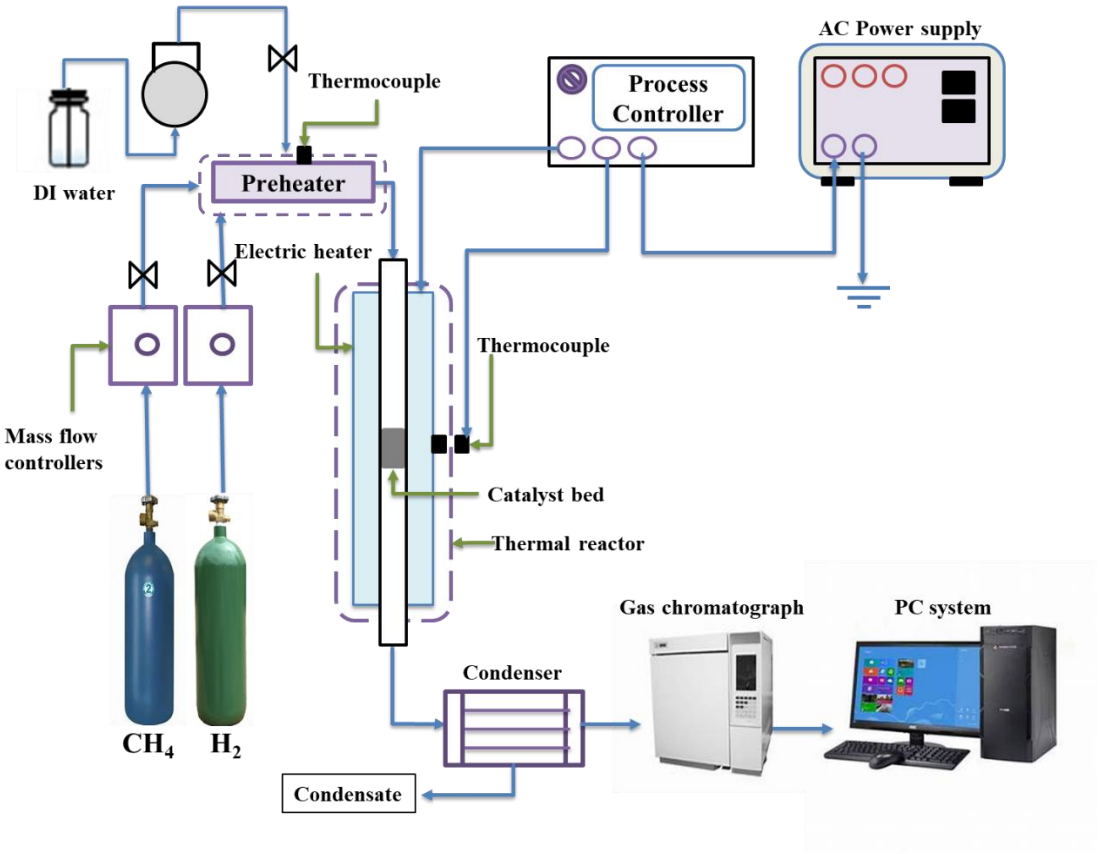

Figure 3.2 Schematic diagram of the experimental setup for SMR

3.1.3 Catalytic performance

The catalytic activity of SMR was analysed for CH_4 conversion and H_2 yield presented in Eq. (6-8). The CH_4 conversion was defined as follows:

$$CH_4\,\text{conversion}\left(X_{CH_4}\right)\% = \left[\frac{(n\,CH_4)_{\text{converted}}}{(n\,CH_4)_{\text{feed}}} \times 100\right] \tag{6}$$

Where, $(CH_4)_{feed}$ and $(CH_4)_{converted}$ are the inlet and outlet flowrates of CH_4, respectively. The H_2 yield was defined as follows:

$$H_2\ \text{yield}\left(Y_{H_2}\right)\% = \left[\frac{(nH_2)_{\text{produced}}}{4\times(nCH_4)_{\text{feed}}} \times 100\right] \tag{7}$$

Where, $(H_2)_{produced}$ are the molar percentages of H_2 produced in the product stream. In this study, enhancement factor was calculated by the differences in CH_4 conversions in the pre-breakthrough stage (SESR, where CaO sorbent was active) and the post-

breakthrough stage (SR, where CaO sorbent was saturated). The EF values were calculated as follows:

$$EF\ (\%) = \left(\frac{(CH_4)_{SESR} - (CH_4)_{SR}}{(CH_4)_{SR}} \right) \times 100 \quad (8)$$

Where, $(CH_4)_{SESR}$ is the CH_4 conversion in the pre-breakthrough time and $(CH_4)_{SR}$ is the conversion in post-breakthrough time.

3.2 Catalyst characterisation

3.2.1 X-ray diffractometer (XRD)

It is a non-destructive technique to evaluate the molecular or atomic structure of different materials. This technique works effectively with the materials that are fully or partially crystalline [215]. The crystallinity analysis and structure of the prepared and spent catalysts were evaluated using XRD technique in instrument as shown in Figure 3.3. The XRD patterns were conducted with X-ray diffractometer D8 Advance (Bruker Advanced) furnished with scintillation detector having a radiation wavelength of 1.5418 Å.

This analysis can characterize catalyst particles based on their diffraction pattern and determines the orientation of single grains or crystals. This technique compares the data with known standards, which are for the random orientations known as JCPDS file. All catalyst samples were scanned in a range from 5-80˚ of 2θ with step rate of 0.02 per second.

Figure 3.3 X-ray diffractometer (XRD)

3.2.2 Field Emission Scanning Electron Microscope (FESEM)

It is a non-destructive technique which provides morphological and topographical information within magnifications of 10x to 300,000x. It works by providing probing beams with the help of a field emission cathode present in the electron gun. This results in improved resolution of the images that require highest possible magnification. The morphology of the synthesized catalyst powder was analysed using the instrument Zeiss Supra 55VP (Figure 3.4) for scanning with a 30 Kx magnification.

Figure 3.4 Field emission scanning electron microscope (FESEM)

3.2.3 Scanning Electron Microscopy (SEM)-Energy dispersive X-ray spectroscopy (EDX)

SEM-EDX is an analytical technique for the elemental analysis of various samples. Using EDX technique, the chemical composition including the elements of the samples are determined with their concentration and distribution. When combined with SEM, variety of signals offer information about the sample, while EDX uses secondary electrons and produce topographic information regarding the sample [216].

The elemental distribution of the particles and the morphological structures of the synthesized catalysts of various compositions were analysed using SEM-EDX analyser (Model JSM-6490A of JEOL, Japan) as shown in Figure 3.5. 20 kV voltage was used to record various magnifications.

Figure 3.5 Scanning electron microscopy (SEM)- Energy dispersive X-ray spectroscopy (EDX)

3.2.4 Brunauer Emmett Teller (BET)

The specific surface area and pore size distribution of catalyst is measured using Brunauer Emmett Teller (BET). Samples are dried under purging N_2 at increasing temperatures. At the boiling point of N_2, the volume of adsorbed gas to the particle surface is measured. The measurements are based on thr BET theory. N_2 adsorption-desorption isotherms at -150 °C is used to analyse the BET surface area, pore volume and diameter using surface area analyser (ASAP 2020) (Figure 3.6) of the samples.

Figure 3.6 Brunauer Emmett Teller (BET)

3.2.5 H_2-Temperature-Programmed Reduction (H_2-TPR)

H_2-Temperature-Programmed Reduction (H_2-TPR) is a technique that relates the thermal conductivities of two gases. One of the gas is H_2 while the other is the carrier gas. H_2-TPR was carried out to determine the reduction temperature of species. Analysis was carried out in a tubular reactor containing 100 mg of catalyst. The catalyst was reduced in a mixture gas of 5% H_2/N_2 from 100 °C to 800 °C at a rate of 10 °C/min. The decrease in H_2 amount at the outlet was studied by QWE Gas Chromatograph with Thermal Conductivity Detector (TCD) as in Figure 3.7.

Figure 3.7 Thermal Conductivity Detector (TCD).

3.2.6 Thermal Gravimetric Analysis (TGA)

TGA is an evaluation technique that evaluates the masses of different substances as temperature is increased over a certain time and rate. In this technique, samples are weighted continually while heating with an inert gas passing over it. The samples undergo certain reactions and variations in the remaining mass of the substances are recorded in instrument as shown in Figure 3.8.

Thermal analysis of the synthesized and spent catalyst was performed by using Thermal Gravimetric Analyser TGA 5500 (TA instruments, USA) with N_2 as reference gas to evaluate the percentage loss and derivative thermal analysis. Samples were heated at a rate of 10˚ C/min from 25˚-900˚ C. The flow rate of N_2 was fixed to 35 ml/min to investigate the thermal stability of catalyst.

Figure 3.8 Thermal Gravimetric Analyser (TGA)

3.2.7 Fourier transform infrared spectroscopy (FTIR)

FTIR is a characterization technique used to detect various materials including organic, polymers and inorganic materials. The method uses infrared light for scanning of test samples and give detailed information about the functional groups and elemental chains in the sample.

Fourier transform infrared spectroscopy (Model: FTIR spectrum 100 PerkinElmer, MID-IR) (Figure 3.9) was used to investigate the functional groups, absorption bands and the appearance of bonding formed after the synthesis of catalysts. Prior to the analysis, the catalyst samples were blended with KBr powder and compressed under pressure to form a small pallet. The pallet was placed in disc holder to measure the peaks in a frequency range of 650-4000 cm^{-1}.

Figure 3.9 Fourier transform infrared spectroscopy (FTIR)

Chapter 4

Results and Discussion

4.1 Physicochemical properties of catalyst

The XRD analysis of the as-prepared MNA HTc and 10 wt% CaO @ MNA calcined at 850 °C is shown in Figure 4.1(a-c). The diffraction patterns of the catalyst and composite could be indexed to double layered HTc. The diffraction peaks reveal the presence of $MgAl_2O_4$, NiO, $MgNiO_2$, $NiAl_2O_4$, MgO and CaO in agreement with the corresponding JCPDS files .The $MgAl_2O_4$ (JCPDS# 47-0254) peaks are detected with a 2θ value at 36.02˚(040) and 64.7˚(360), respectively [30]. The spinal $MgAl_2O_4$ indexed to the orthorhombic phase demonstrates the space group (227: $Fd\bar{3}m$). The existence of a strong diffraction peak at 37.3˚(111), 43.2˚(200), 63.0˚(220) is attributed to the pure cubic structured NiO (JCPDS# 47-1049) with the space group (225: $Fm\bar{3}m$). A sharp peak of NiO is observed in the synthesized composite as compared to the broad peak of the synthesized MNA. The diffraction peaks of NiO are in agreement with the literature reported [217]. The cubic $MgNiO_2$ (JCPDS# 24-0712) having a space group (225: $Fm\bar{3}m$) has been detected at 2θ = 37.1˚, 43.1˚and 62.5˚with hkl indices (111), (200) and (220) respectively, with a negligible peak shift in the synthesized composite [218]. The peak at 2θ (hkl) = 36.9˚(111), 42.9˚(200) and 62.3˚(220) indicates the presence of cubic structured MgO (JCPDS# 45-0946) [219]. The calcination of CaO from the calcination of grounded eggshells revealed strong and sharp peaks of CaO (JCPDS# 37-1479) [220] at 2θ (hkl) = 32.3˚(111), 37.3˚(200), 53.8˚(220), 64.1˚(311), and 67.3˚(222) as demonstrated in Figure 4.1(b). The appearance of peak at 2θ = 32.2˚reveals the presence of CaO in the hybrid material as in Figure 4.1(a). Furthermore, the $NiAl_2O_4$ (JCPDS# 10-0339) has been detected in the composite at 2θ = 19.07˚, 31.4˚, 37.0˚, 44.9˚, 59.6˚and 65.5˚with (hkl) = (111), (220), (311), (400), (511) and (440), respectively [30]. A cubic structure of $NiAl_2O_4$ is observed with a space group of (227: $Fd\bar{3}m$).

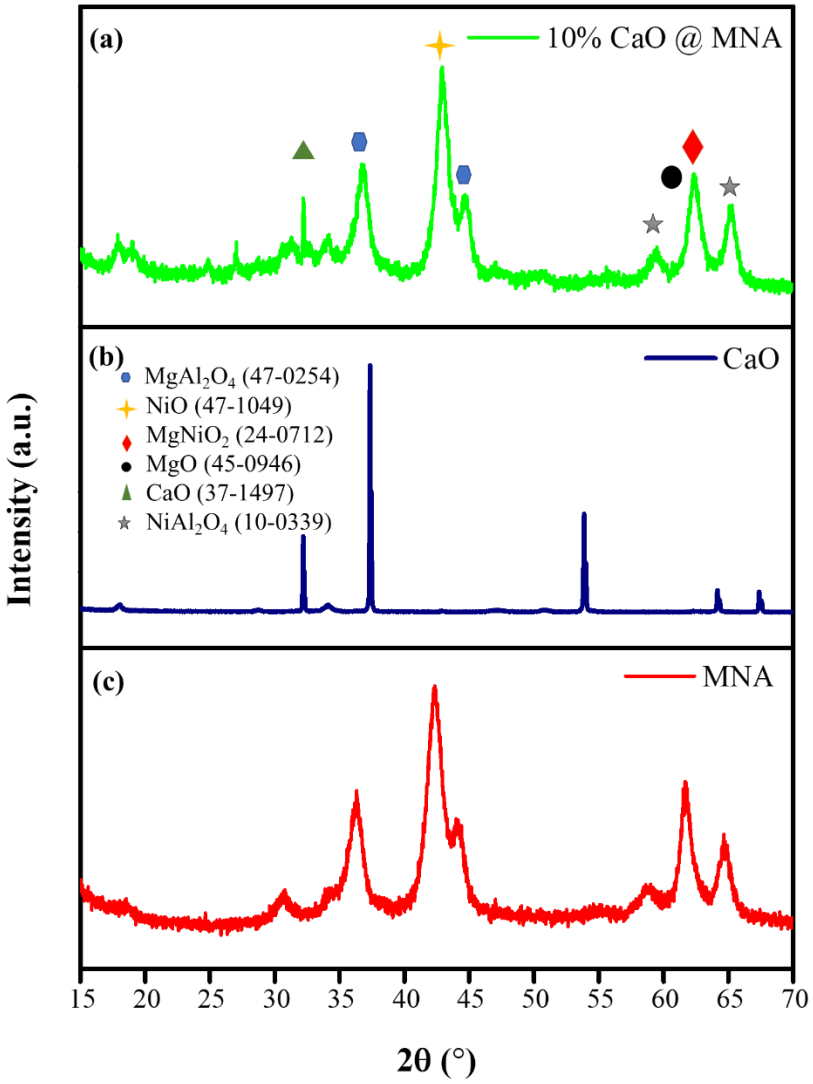

Figure 4.1 Schematic diagram of the experimental setup for SMR (a) 10% CaO @ MNA (b) CaO (c) MNA

The FESEM micrographs of the synthesized MNA HTc at 2 µm, 1 µm, and 200 nm are shown in Figure 4.2(a-c). The micrograph in Figure 4.2(a) clearly presents a coral-like structure [221]. The mixed oxides usually show a coral-like structure when the pH of metal nitrates solution is 10 [222]. Figure 4.2(b- c) shows the highly porous plate morphology which is due to the occurrence of divalent and trivalent cations in the structure of HTc. Moreover, the incorporation of Ni can be clearly seen as bright particles in the structure that results in the reduction of porosity, as the pore surfaces are covered by the Ni active sites [223]. The formation of nano crystalline structure of HTc

could be due to the Ni influence in the crystal growth and nucleation process during synthesis via co-precipitation method [222].

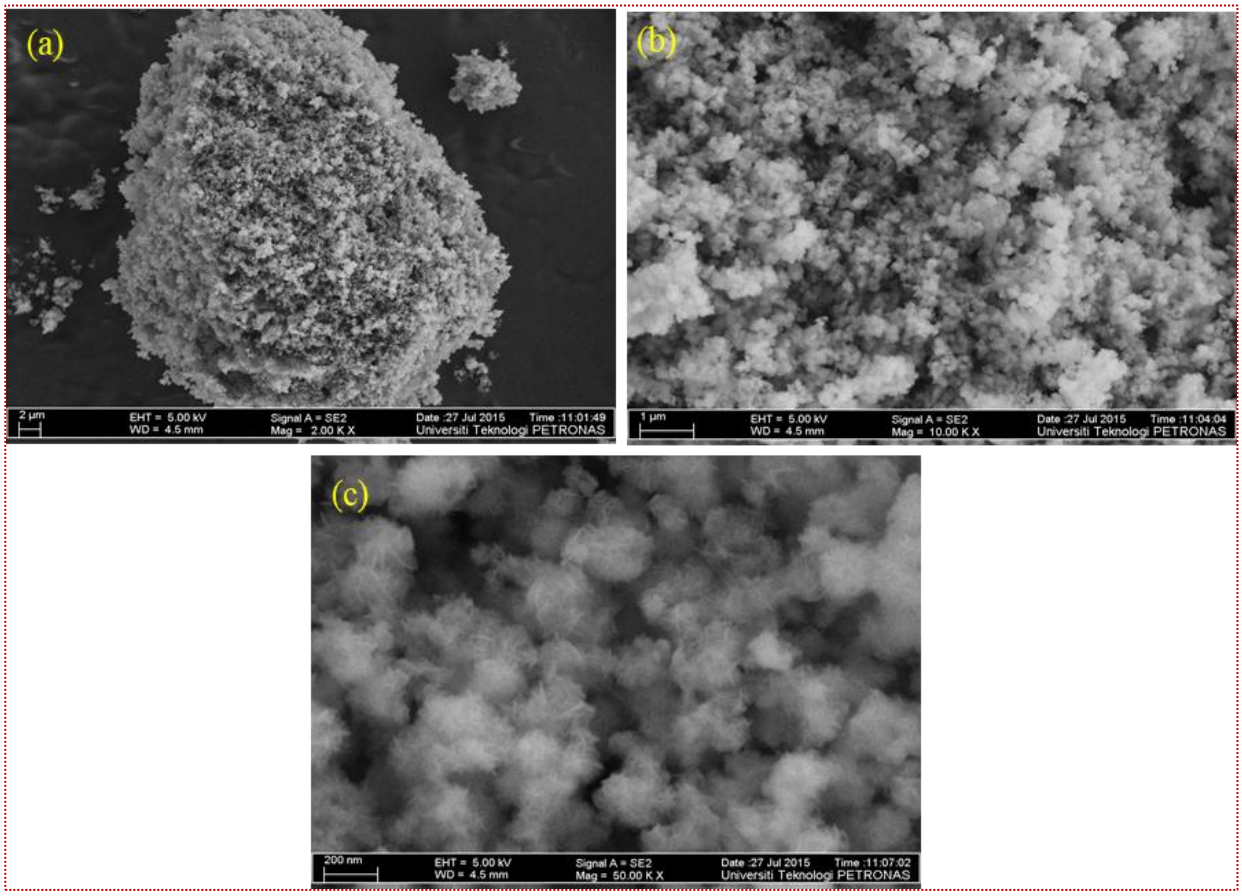

Figure 4.2 FESEM micrographs of MNA HTc at various field magnification (a) 2 µm (b) 1 µm (c) 200 nm

The SEM micrographs of calcine MNA HTc, CaO and 10% CaO @ MNA are presented in Figure 4.3. The SEM images of fresh MNA HTc prepared via co-precipitation method is presented in Figure 4.3(a-b). The dried sample exhibited relative dense particles formed by the aggregation of small and irregular but highly porous particles as typically observed [221, 224]. Calcination of MNA precursors at 850 °C made changes in the morphology by forming a spinel structure by crystallization of the oxide phases. The catalyst developed a porous sponge/coral-like structure due to the trivalent (Al^{3+}) and divalent (Mg^{2+}, Ni^{2+}) cations in the outer layer of HTc. The uniform distribution of small brighter particles in the image indicates the presence of Ni active sites. This indication of Ni particles have also been reported in literature [225]. Figure 4.3(c-d) shows the waste

derived CaO synthesized which formed an interconnected skeleton structure with large sized voids. CaO has been reported to contain amorphous web-like structure [50]. Incorporation of CaO in MNA reduced the crystallinity of the composite, suggesting the smaller particle size as compared to MNA as illustrated in Figure 4.3(e-f) and observed in the XRD of hybrid material. However, a stable hybrid catalyst was obtained after 650 °C with reduced weight loss compared to MNA which was also confirmed by thermal stability analysis. The hybrid material exhibited same sponge-like structure with layered platelets of CaO stacked on each other [44]. The microporous structure facilitates the diffusion of gas to the active sites and various platelets. The presence of $NiAl_2O_4$ and NiO in the composite can be seen as smooth and granular surfaces on top of each other. Similar type of well-defined spinel structures was also confirmed by XRD and have been reported in other HTc based catalysts [70, 74, 226] .

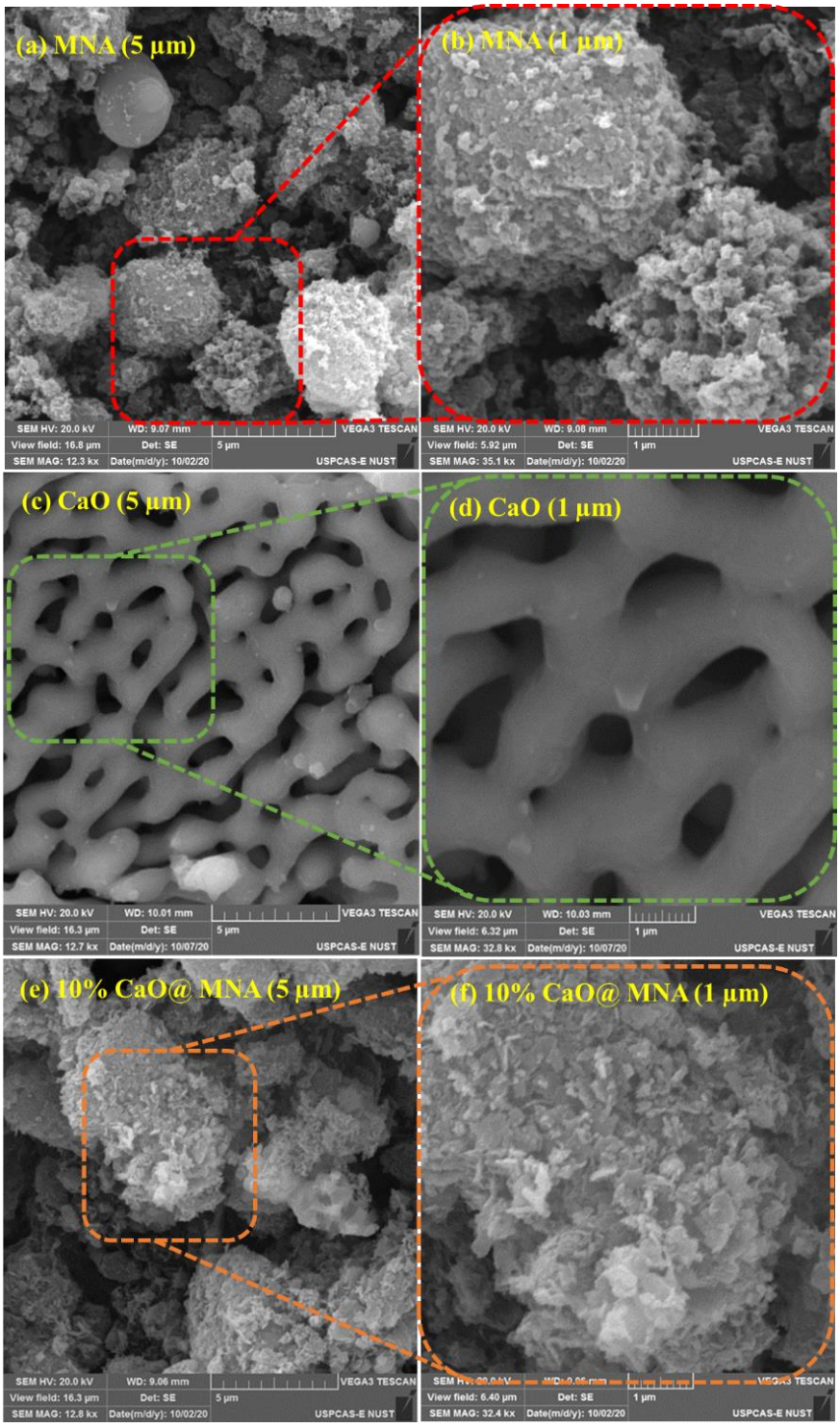

Figure 4.3 SEM micrographs of synthesized catalyst with 5 µm and 1 µm (a-b) MNA (c-d) CaO (e-f) CaO @ MNA

Presence of CaO in hybrid was further confirmed by EDX analysis. Figure 4.4 illustrates the presence of various elements compositions detected in the synthesized catalysts.

Figure 4.4(a) (left) shows a SEM spectrum of MNA HTc, identifying the existence of Mg, Ni, Al, and O with approximately same ratio of Mg and Al (for reference) compared to the theoretical value. Figure 4.4(b) identifies the presence of Ca particles in MNA because of CaO addition by wet impregnation method.

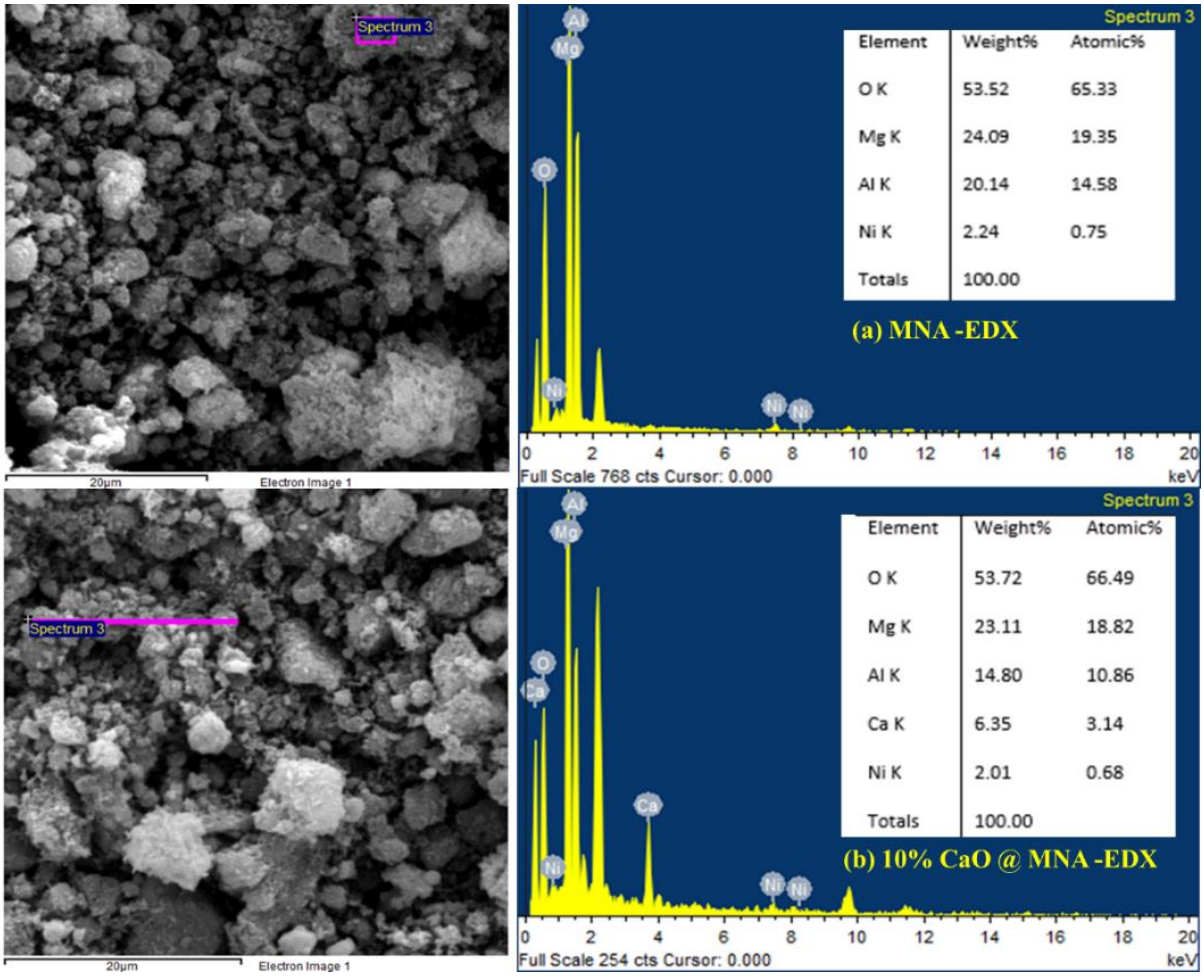

Figure 4.4 EDX analysis of fresh (a) MNA (b) 10% CaO @ MNA

N_2 adsorption-desorption isotherm of the synthesized MNA HTc is shown in Figure 4.5(a). H-3 type hysteresis is displayed for the synthesized catalyst at high relative pressure. The presence of hysteresis loop and sharp N_2 uptake at high relative pressure is depicting highly mesoporous structure that is generated owing to the agglomeration of the nanoparticles. It is reported that mixed oxides containing Mg^{2+} show hysteresis loop with high relative pressure close to unity [222]. Pore size distribution (PSD) is illustrated inset Figure 4.5(a). The synthesized MNA HTc generated a high PSD of 30-40 Å , which ascribes to contain large open and well dispersed pores on the catalyst surface due

to high concentration of Mg^{2+} in the brucite layer of MNA [38]. Table 4.1 exhibits the surface area, pore volume and radius of the MNA HTc. MNA catalysts possess a high surface area of 295.2 m^2/gm, pore volume of 0.67 cm^3/gm and a pore radius of 90.6 Å which is highly feasible for CaO integration for SESMR. CaO exhibited a surface area, pore volume and pore radius of 4.005 m^2/gm, 0.014 cm^3/gm and 21.3 Å, respectively exhibited in Table 4.1.

The H_2-TPR analysis of the MNA HTc presented in Figure 4.5(b) was investigated to check the reducibility of the synthesized catalyst under H_2 atmosphere from 100 °C to 1000 °C. At 350 °C, a visible peak splitting was identified, which relates with the reduction of surface NiO crystals [32]. The catalyst exhibited high NiO concentration in the calcined catalyst structure. The peak around 500 °C is due to the weaker interactions between metal and support [227]. Moreover, a broad peak around 700 °C is ascribed to the reduction of NiO strongly interacting with MgO and Al_2O_3 [228].

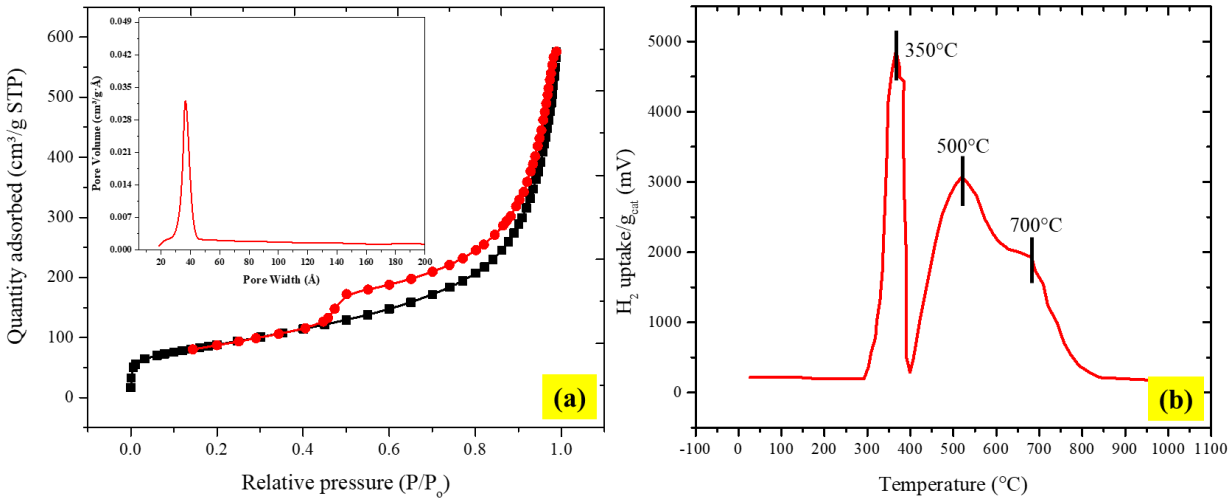

Figure 4.5 Physicochemical analysis of the synthesized MNA (a) N_2 adsorption-desorption isotherm with PSD (b) H_2-TPR profile

Table 4.1 Surface properties of the synthesized MNA

Sample name	S_{BET} (m^2/gm)	V_P (cm^3/gm)	r_p (Å)
MNA	295.2	0.67	90.6
CaO	4.005	0.014	21.3

The weight loss and thermal stability of the synthesized catalysts were analysed by TGA presented in Figure 4.6(a-c). The thermograph of MNA illustrated in Figure 4.6(a) exhibited two weight loss stages. First decomposition elbow (6.3% weight loss) in MNA ranging from 30-250 °C is credited to the loss of interlayer and physically adsorbed water. Second decomposition elbow (9% weight loss) in a range of 300-650 °C is attributed to the simultaneous dehydroxylation and expulsion of intercalated carbonate anions in the form of CO_2 [229, 230]. During calcination, the release of CO_2 hinders the sintering of oxide elements according to the literature [231]. A slight weight loss in MNA HTc after 500 °C indicates that HTc precursor was changed into mixed metallic oxides and that the decomposition process was completed. This confirms the formation of stable and porous oxide composite with a high surface area. Waste derived CaO exhibited a total weight loss of 2.4% in two steps in range of 350–650 °C as shown in Figure 4.6(b). First step is attributed to the loss of organic matter in the material. The second step may be ascribed to the conversion of unreacted $CaCO_3$ to CaO and CO_2 phase at higher temperatures [232, 233], presence of which is also confirmed by FTIR and XRD. Figure 4.6(c) indicates the weight loss curve of the hybrid 10% CaO @ MNA. Weight loss (5%) in a range of 150-350°C may be ascribed to the loss of interlayer hydroxyl groups and the step around 400 °C is due to the removal of organic components in the hybrid as in CaO. However, a weight loss (7.5%) before 630 °C is due to the exclusion of carbonate ions and dihydroxylation in the interlayers. Moreover, CaO incorporation in the MNA catalyst increased the stability and reduce the weight loss to some extent as compared to MNA.

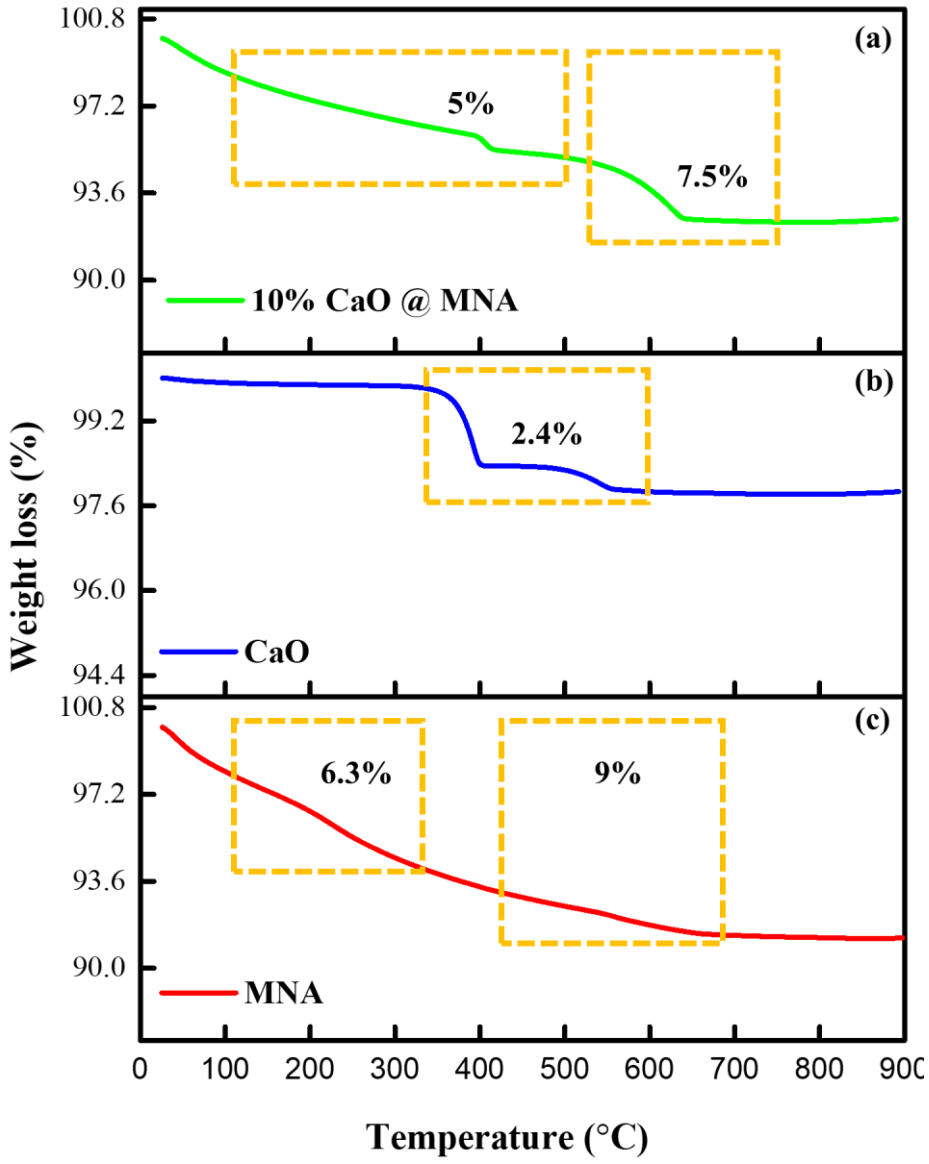

Figure 4.6 TGA profile of fresh (a) 10% CaO @ MNA (b) CaO (c) MNA

The FTIR spectroscopy can be used to identify the structure of the compounds. Figure 4.7 presents the FTIR analysis of the catalyst samples. In MNA and 10%CaO @ MNA, the broad and strong band with wavenumber around 3470-3440 cm^{-1} represents the O-H stretching vibrations in the metal hydroxyl layer [234], which occur at lower frequency in the LDHs compared with the stretching mode of O-H group at 3600 cm^{-1} in free water [235]. This corresponds to the hydrogen bonding of water (interlayer) with the O-H groups of layers of LDHs and with the guest anions [236, 237]. Presence of a second type of O-H vibration at 2900 cm^{-1} is possibly due to the formation of hydrogen

bonding with carbonate in the interlayer spacing. A shoulder in a range of 1630-1640 cm^{-1} is due to the stretching absorption of C—O and C==O in CO_3^{2-}, which is slightly reduced due to the addition of CaO. An intense band at 1409 cm^{-1} is ascribed as the absorption equivalent to the υ_3 mode of interlayer carbonate with a shoulder around 1480 cm^{-1} [238], which is increased and broadened on the addition of CaO . Bands observed around 1380 cm^{-1} and 830 cm^{-1} are due to the NO_3^-/CO_3^{-2} vibrations [239]. The peaks observed in the low frequency region are attributed to the metal-oxygen (Ni-O, Mg-O and/or Al-O) from 850-600 cm^{-1} and interpreted as the lattice vibration modes [240]. A sharp peak at 3640 cm^{-1} is found in samples containing CaO corresponds to OH in $Ca(OH)_2$ occurred during water adsorption by CaO [53]. A peak in a range of 500-580 cm^{-1} 10% CaO @ MNA is due to Ca—O [241].

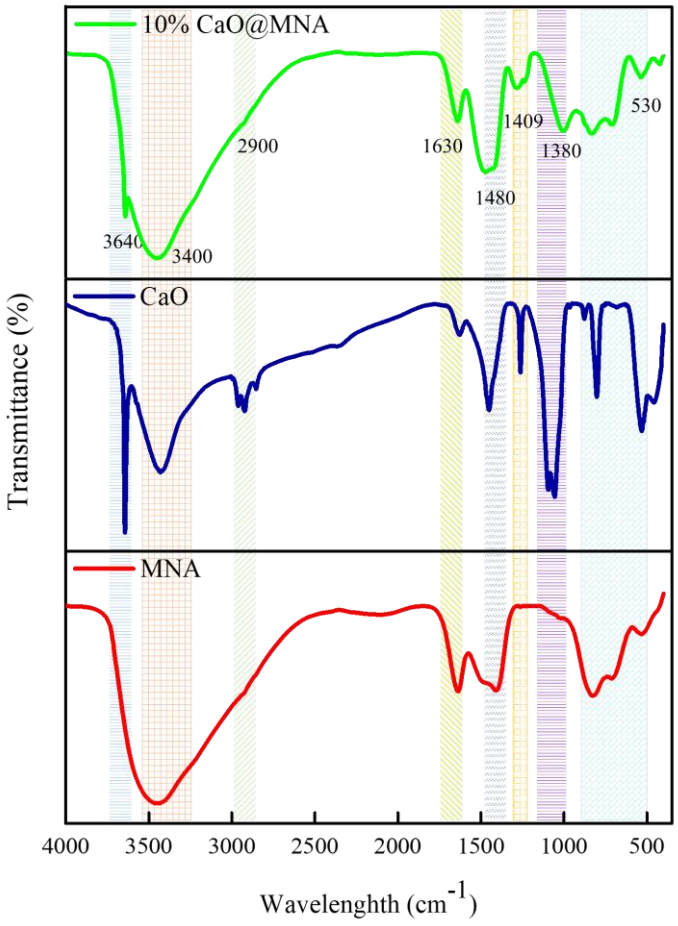

Figure 4.7 FTIR spectroscopy of fresh (a) MNA (b) CaO (c) 10% CaO @ MNA

4.2 Catalyst activity test

4.2.1 SMR using MNA as a catalyst

SMR was investigated using powder MNA catalyst. The impact of temperature on H_2 yield and CH_4 conversion was considered in a range of 650-850 °C, and S/C = 2. As expected, enhancing the reaction temperature aided the production of H_2. The H_2 yield was maximized at 43% at 850 °C, while CH_4 conversion was 86%, as demonstrated in Figure 4.8 However, it is worth mentioning that the H_2 purity is low owing to the large quantity of CO_2 in the product gas. Also, very high temperatures require higher energy costs [207]. Thus, high H_2 purity and CH_4 conversion cannot be achieved by SMR in a single step as the reaction is limited by equilibrium [242]. To overcome this limitation, the synthesized catalyst was combined with a sorbent and tested for SESMR [207, 243].

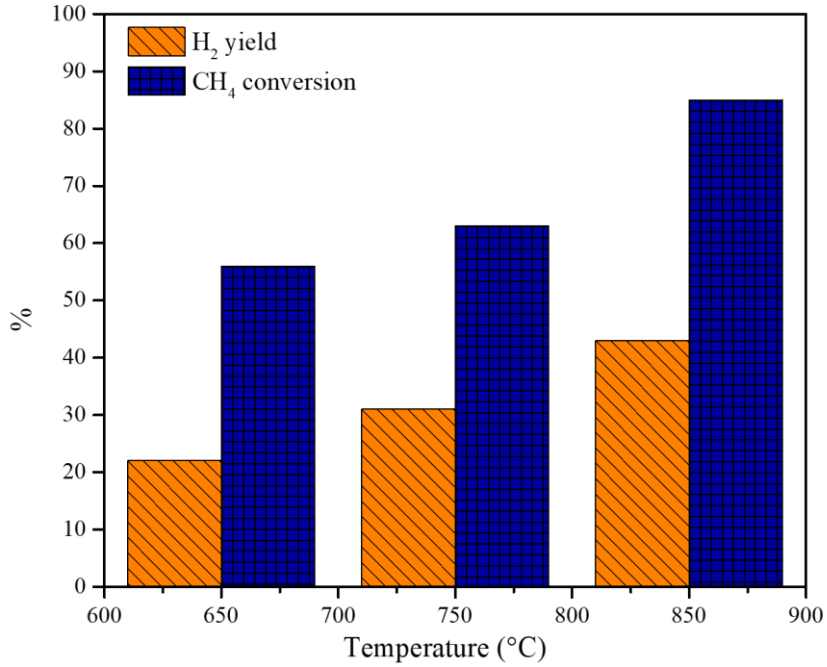

Figure 4.8 Impact of temperature on CH_4 conversion and H_2 yield tested for SMR over MNA catalyst at S/C = 2

4.2.1 SESMR catalytic performance analysis

A series of experiments were done at different temperatures ranging from 650-850 °C and S/C=2. Hybrid materials synthesized with CaO and MNA at varying concentrations

were tested for SESMR and results were compared with MNA at same conditions. Figure 4.9 illustrates the experimental results at 650 °C in fixed-bed reactor for 10% CaO @ MNA, in terms of product composition (H_2, unconverted CH_4, CO and CO_2) with respect to time on stream (TOS). The results exhibited three stages, widely reported in literature for SESMR [51, 244, 245]. Initial stage where reforming, carbonation and shift reaction take place simultaneously is known as pre-breakthrough period [217]. For this stage, H_2 concentration up to 80% was obtained, while the concentrations of CO and CO_2 decreased below 4%. In this phase, CaO reacts with the produced CO_2 and shifts the equilibrium towards H_2 production. CH_4 conversion is greater than 70% with a H_2 selectivity around 51%. Stage II is the breakthrough stage, occurs when the sorbent starts to saturate as the adsorbent sites are increasingly occupied, thus leaving fewer sites for new CO_2 molecules, resulting in decrease in the sorption capacity of sorbent [28]. As obvious from Figure 4.9, the product compositions were observed in a sequence of breakthrough. Stage III is the post-breakthrough stage, where CaO is completely saturated, thus no CO_2 sorption occurs and only SMR takes place [246]. In stage I, WGS reaction was enhanced, followed by the reforming reaction. Then, the efficiency of WGS reaction began to decrease when most of the CaO is converted into $CaCO_3$. Hence, a reduction in CH_4 conversion (65%) and H_2 concentration (67%) were observed.

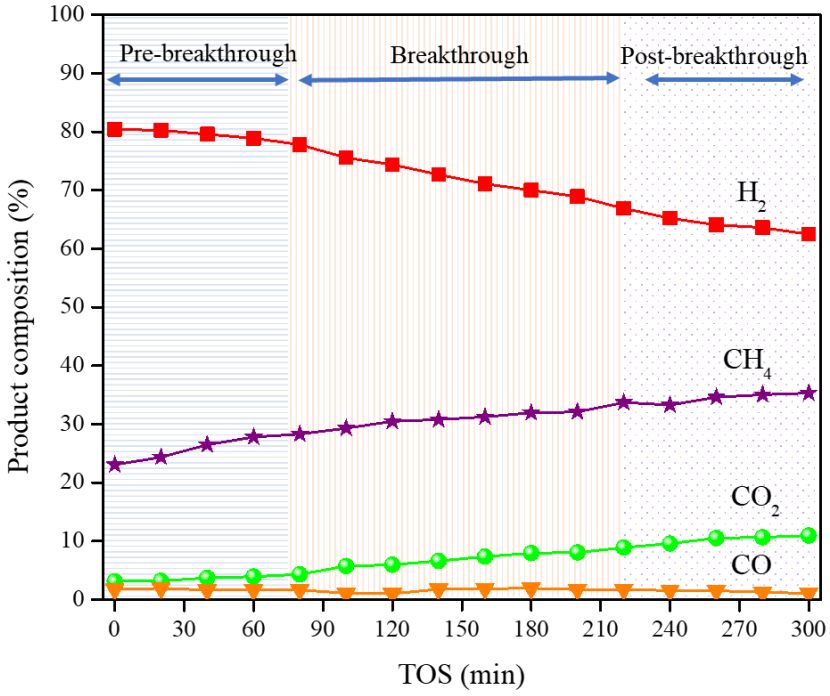

Figure 4.9 Product composition with reference to TOS for 10% CaO @ MNA at 650 ° C, S/C = 2 (with details of pre-breakthrough, breakthrough, and post-breakthrough periods).

Synthesized MNA HTc mixed with varying quantities of CaO and tested for SESMR at 650 °C and S/C of 2 are presented in Figure 4.10. From these findings, it is worth noting that H_2 yield and CH_4 conversions in all CaO composites were higher than those obtained from catalyst (MNA) as evident in Figure 4.10(a-d). Figure 4.10(a) reveals the performance of MNA at 650 °C with around 57% CH_4 conversion and 27% H_2 yield. Figure 4.10(b-d) exhibited higher conversion and yields due to higher purity of the product stream, thus shifting the equilibrium towards H_2 production due to sorption [16]. This occurs because the CO_2 formed is adsorbed by the sorbent following the (Eq. (3)) [207]. 5% CaO @ MNA presented lower breakthrough time as compared to 10% CaO and 15% CaO but higher CH_4 conversions in the pre-breakthrough period. This is because 5% CaO @ MNA has a greater content of MNA catalyst, which enhanced the conversion and yield owing to the combination of catalytic activity of MNA and carbonation reaction. Further, 10% CaO @ MNA and 15% CaO @ MNA exhibited longer breakthrough time as the CaO content increased which enhanced the adsorption capacity due to strong chemisorption. However, a reduction in CH_4 conversion and H_2

yield was observed due to the reduction of metal active sites with CaO addition as evident from Figure 4.10(c, d). This supports the research by Clough et al. [247], who reported that more Ni contribution and less CaO content to the hybrid material results in enhanced H_2 concentration. Though, CO_2 concentration increased to a certain Ni content followed by decreasing trend because of sintering of particles. Though in the present case, fixed amount of Ni content is used in the catalyst, still the number of Ni vary as CaO content is increased, while MNA is decreased from 100% MNA.

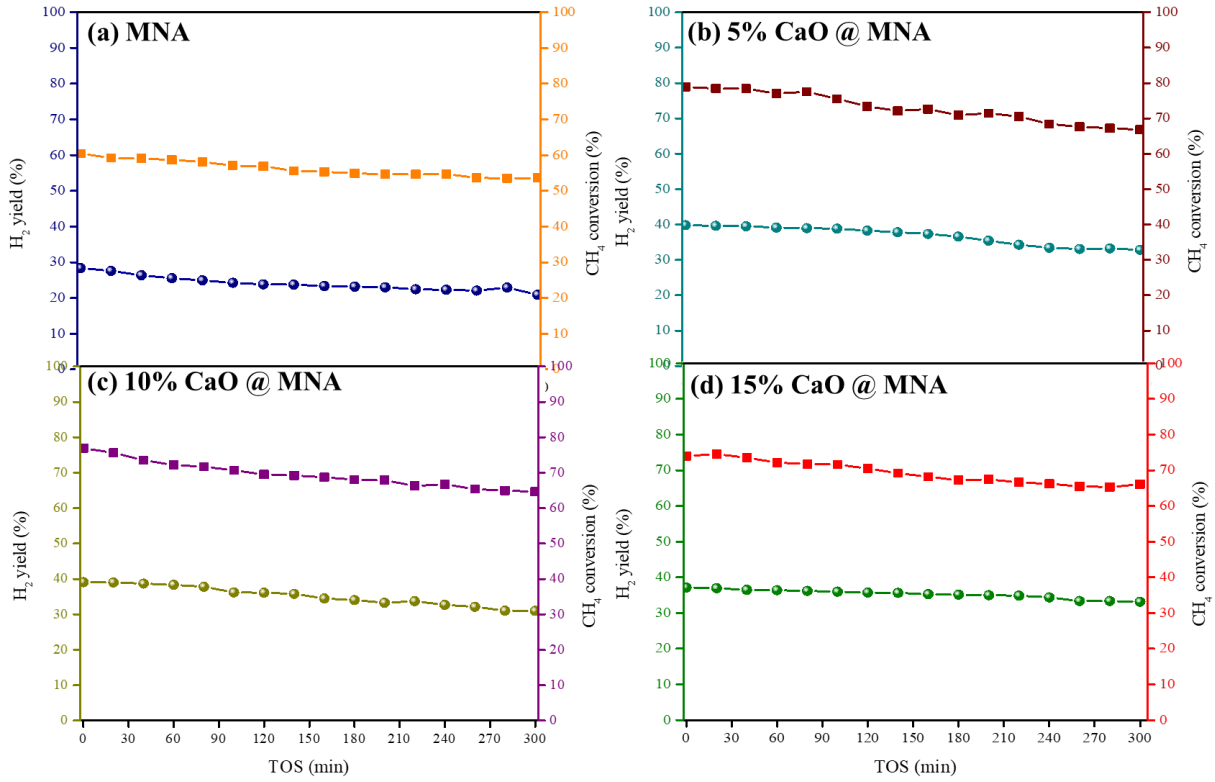

Figure 4.10 Effect of the CaO loading over MNA on CH_4 conversion and H_2 yield (a) MNA (b) 5% CaO@MNA (c) 10% CaO@MNA (d) 15% CaO@MNA for SESMR at 650 °C and S/C = 2

Figure 4.11(a-d) shows the H_2 and CO_2 percentage in the product stream in a TOS of 300 min at same conditions. MNA sample presented lower H_2 purity and higher concentration of CO_2 as compared to the samples containing various quantities of CaO with no pre-breakthrough period as shown in Figure 4.11(a). Samples with hybrid containing catalyst and sorbent exhibited extremely low CO_2 concentrations in the pre-breakthrough period. However, the CO_2 concentration increased as the sorbent began to saturate, which became constant as the post-breakthrough period started. This decreased

the CH_4 conversion and H_2 yield to a larger extent as the active sites are now covered with a layer of $CaCO_3$ on top of it as can be seen in the previous Figure 4.10. In case of 5% CaO@MNA, 50 min longer pre-breakthrough period was exhibited. However, the material was saturated after a TOS of 190 min as illustrated in Figure 4.11(b). For 10%CaO@MNA, longest pre-breakthrough time of 75 min was observed with CO_2 increasing and decreasing H_2 concentration in the breakthrough period. CO_2 adsorbed in 15% CaO@MNA was lesser as compared to 10% CaO@MNA possibly due to agglomeration of CaO particles. 15 and 25 min longer pre-breakthrough period was observed in 10% CaO@MNA as compared to 15% and 5% CaO@MNA. The results were consistent with the findings of Pecharaumporn et al. [248], reported that smaller pre-breakthrough period may occur due to particle agglomeration during the reaction.

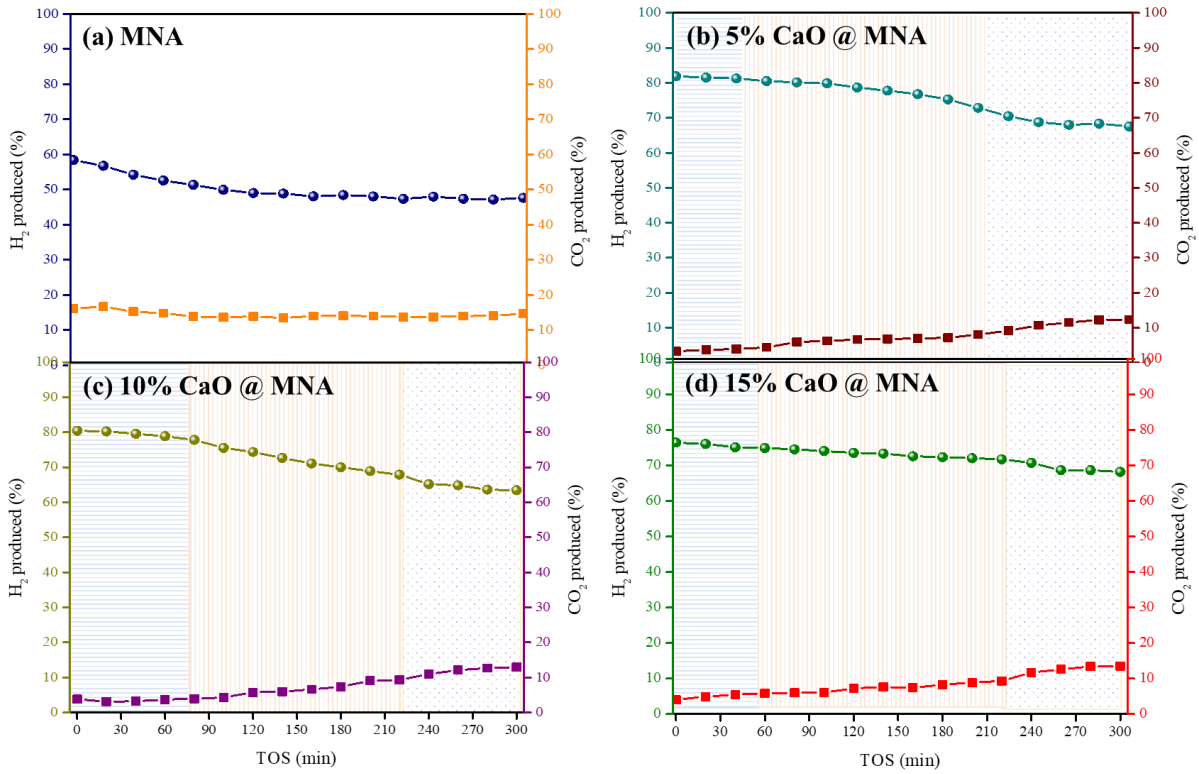

Figure 4.11 CO_2 and H_2 produced in (a) MNA (b) 5% CaO @ MNA (c) 10% CaO @ MNA (d) 15% CaO @ MNA for SESMR at 650 °C and S/C = 2

4.2.3 Effect of temperature on SESMR

The influence of temperature on SESMR on the activity of 10% CaO @ MNA in a range of 650-850 °C and S/C of 2. Concluding the findings of Figure 4.12(a, b), it is clear that increasing the temperature from 650 °C to 850 °C, H_2 yield and CH_4 are increased. This is assigned to the fact that with rise in temperature, the enhancement of endothermic reaction occurs [249]. However, the process shifts from SESMR to the conventional SMR, as CO_2 adsorption occurs at temperatures lower than 760 °C. At reaction temperature of 850 °C, SMR occurred which increased the CH_4 conversion and H_2 yield to maximum values but reduced the purity of product gas with no CO_2 adsorption. Also, it can be seen in Figure 4.12(c) that temperature rise results in lower adsorption capacity and breakthrough times owing to the reduced surface coverage [248]. Thus, it can be concluded that lower temperatures are the carbonation dominating SESMR processes as the product gas composition is mainly influenced by the WGS. Higher temperatures reduced the influence of carbonation reaction due to its endothermic nature and

promoted the SMR (Eq. (1)), but not the WGS (Eq. (2)), shifting the process to lower purity product gas. Reported literature revealed that the CaO conversion to $CaCO_3$ reduced at higher temperature. With the temperature rise from 500 °C to 800 °C, the sorbent capability to adsorb CO_2 decreased, resulting in reducing the purity of H_2 [250].

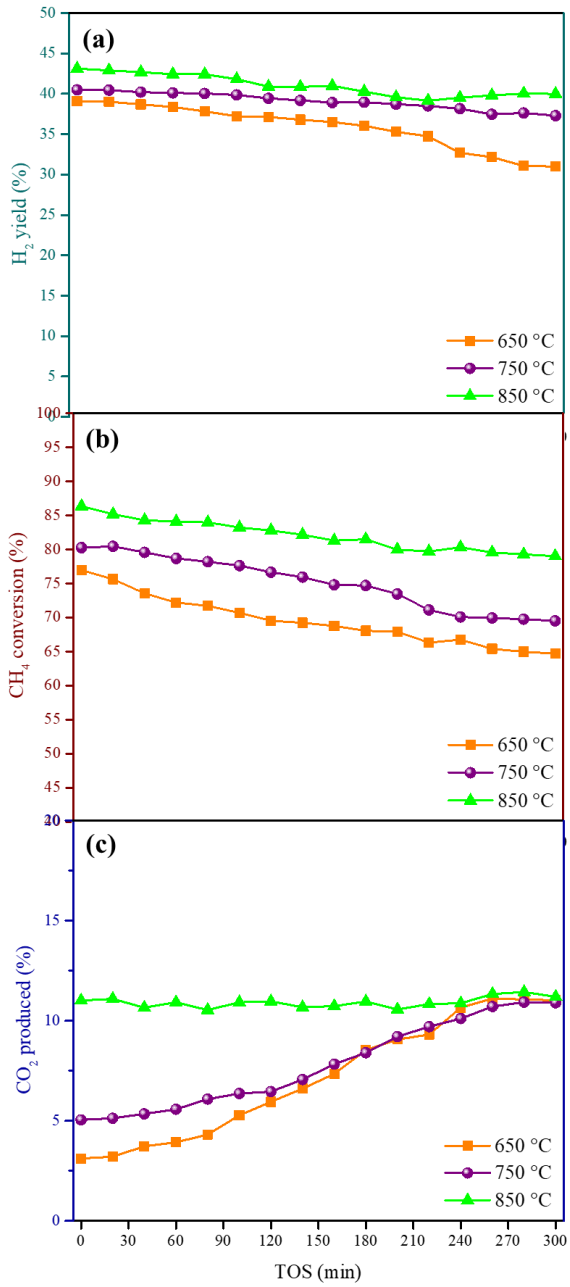

Figure 4.12 Impact of temperature on the performance of 10% CaO @ MNA (a) H_2 yield, (b) CH_4 conversion, (c) CO_2 produced at S/C = 2.

The CH_4 conversions over 10% CaO@MNA at the reaction stages in SESMR at increasing temperatures are presented in Figure 4.13. SESR (sorption enhanced steam reforming) is the pre-breakthrough period, with higher CH_4 conversions, while SR (steam reforming) is the post breakthrough period. As expected, the rise in reforming temperature resulted in increasing the CH_4 conversions in SR stage possibly because the performance of the endothermic reaction (Eq. (1)) was reduced at lower temperatures. Highest EF value (>20%) was observed at 650 °C, which decreased with increase in temperature. In literature, EF greater than 90% are also reported for temperatures lower than 600 °C [244], but with very lower CH_4 conversions. CH_4 conversions at SESR stage exhibited insignificant change with SR stage at 850 °C. This is due to the equilibrium of carbonation reaction of CaO [15], that higher temperatures become unfavourable for the exothermic carbonation reaction of CaO.

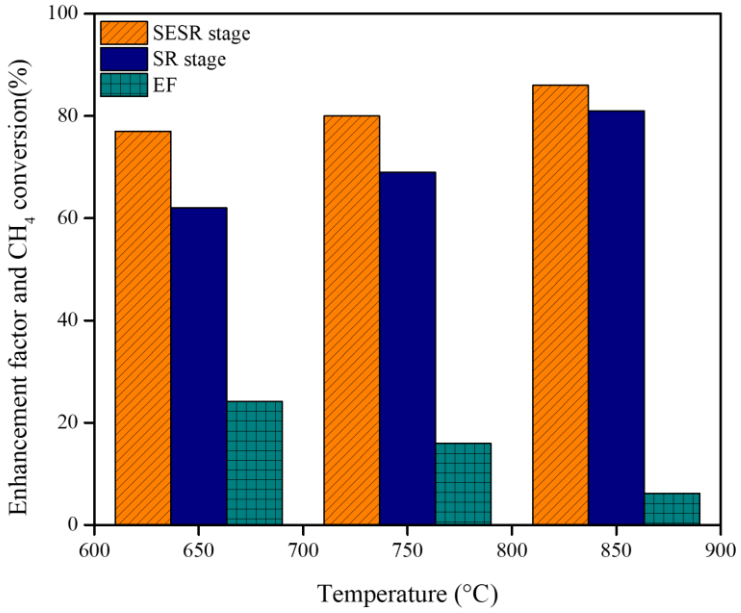

Figure 4.13 Effect of temperature on the enhancement factor (EF) values for SESMR experiments over 10% CaO@MNA at S/C ratio = 2

4.3 Characterization of spent catalyst

The morphology of the spent 10% CaO@MNA composites with EDX analysis is demonstrated in Figure 4.14(a-c). The surface of the spent catalyst has been modified possibly due to the formation of $CaCO_3$ Figure 4.14(a, b). Structure carbon is not seen in the SEM analysis. Some CaO pallets can also be seen in some dark sites, which reduce the carbon deposition possibly forming the carbonates. It also agrees with the statement that smaller Ni particles size and catalysts with certain composition of support containing CaO and Al particles reduce the carbon deposition and higher catalytic activity [251]. Figure 4.14(c) shows the EDX analysis of the spent composite. As can be observed, Mg, Ni, Al, O, Ca can be clearly seen from the spectrum with a tiny peak of carbon, indicating lower carbon formation on the catalyst surface.

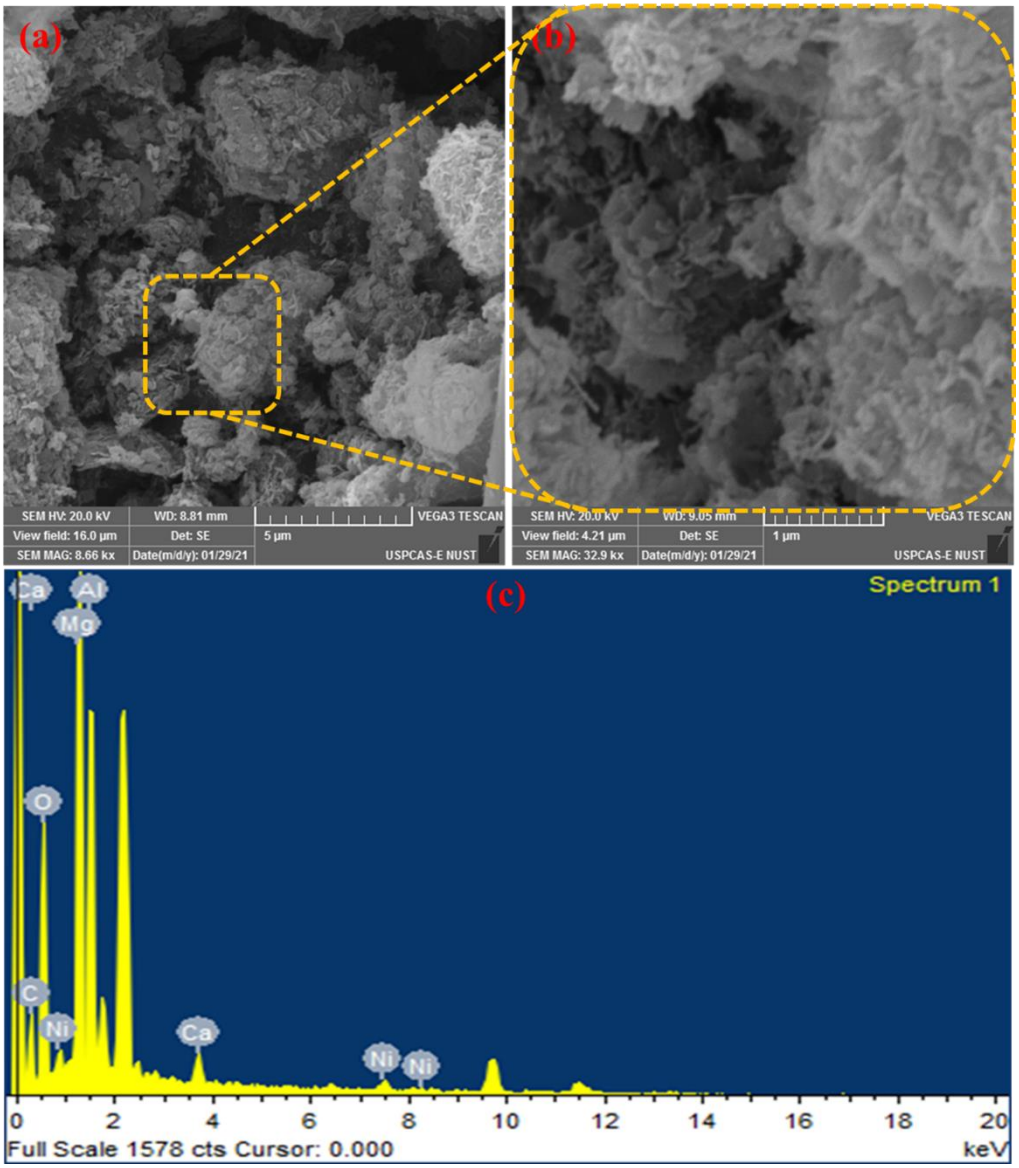

Figure 4.14 SEM images of spent 10% CaO @ MNA (a) 5 µm, (b) 1 µm, (c) EDX analysis.

TGA/DTG analysis was used to elucidate the thermal stabilities and the carbon deposition on the surface of the spent catalyst and composite. Figure 4.15(a) shows the TGA/DTG for spent MNA and 10% CaO@MNA. In case of MNA, initial weight loss is owing to the desorption of adsorbed water, while a weight loss (6%) from 250 - 450 °C is associated with the oxidation of amorphous carbon [228, 252]. Weight loss dip after 650 °C is ascribed to the oxidation of carbon species with a graphitization degree which occurs in case of various HTc materials [228, 243]. Weight loss before 130 °C is due to the adsorbed water while a very slight weight loss (4%) observed after 200 °C could be

due to the small number of carbonaceous species which is less as compared to MNA, suggesting a better resistance to carbon formation [253]. A 5% weight loss in a range of 600-700 °C in 10% CaO@MNA is due to the desorption of CO_2 from the decomposition of $CaCO_3$ formed during the SESMR reaction [243]. It can be seen that overall, 5% weight loss was observed in spent 10% CaO@MNA which is less as compared to MNA, which may be ascribed to the stability developed due to the formation of $CaCO_3$, resulting in very low carbon formation as observed in Figure 4.15(b). The carbon deposition during SESMR reaction is characterized via Raman spectroscopy as demonstrated in Figure 4.15(b). No distinct signals at 1000-1800 cm^{-1} representing the D and G band of carbonaceous species were exhibited by the spent hybrid catalyst indicating very little carbon formation [254]. The result also aligns with the EDX and TGA analysis.

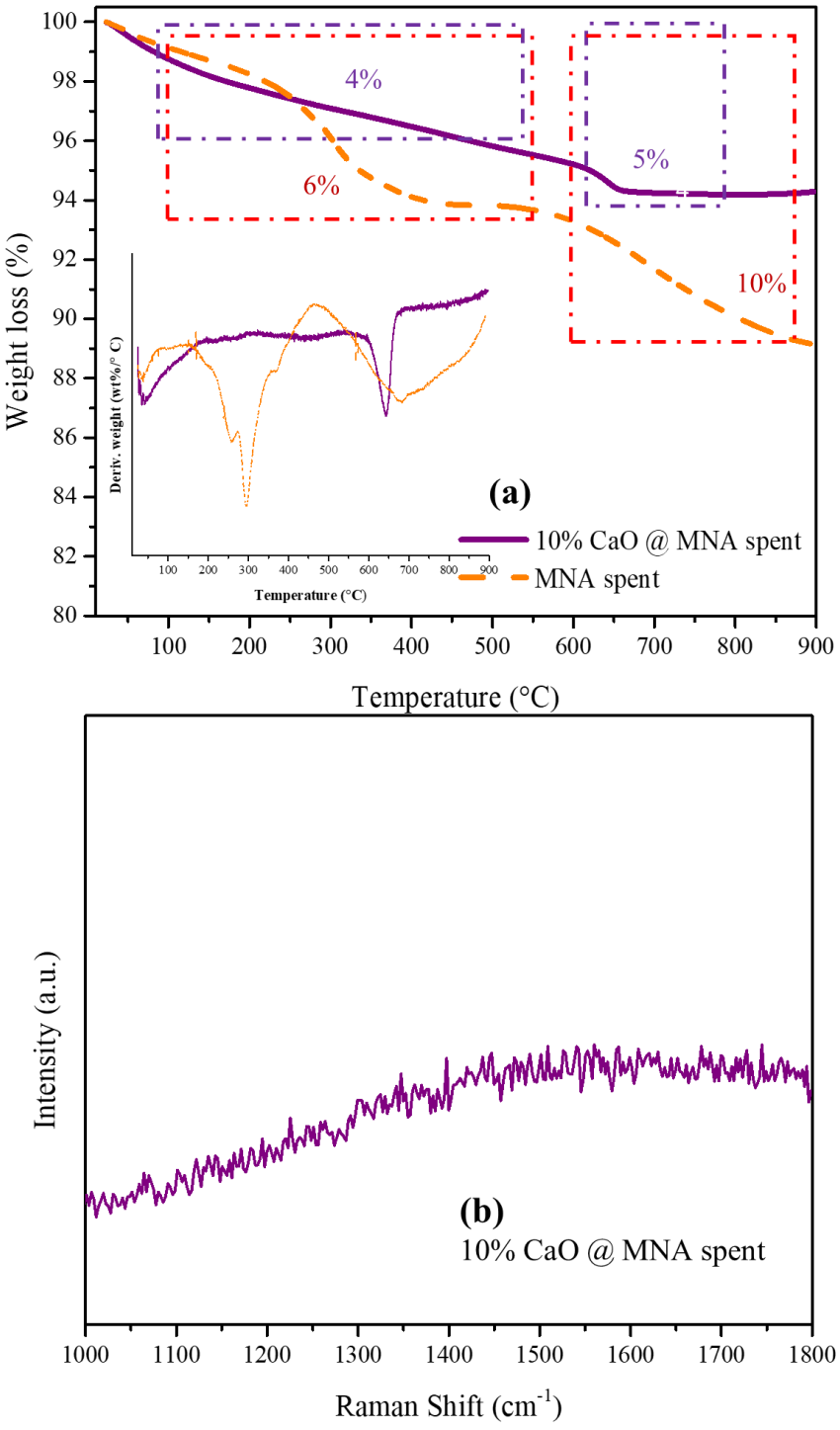

Figure 4.15 Analysis of spent catalysts (a) TGA/DTG (b) RAMAN analysis

Conclusions

The present work focused on the preparation of a hybrid material (waste-derived sorbent + catalyst) via wet impregnation method for testing in SESMR. The hybrid material (CaO @ MNA) was promising for high purity H_2 production. On testing varying concentrations of waste derived CaO with MNA in fixed bed reactor, it was found that 10% CaO @ MNA was the appropriate ratio, as it exhibited longer breakthrough time as compared to 5% and 15% CaO @ MNA and 80% H_2 concentration. However, higher CH_4 conversion was observed for 5% CaO @ MNA owing to the availability of more active sites to the feed gas as compared to 15% CaO @ MNA. Effect of increasing temperature was investigated to evaluate the catalyst for its reduction in CO_2 in the product gas. It was concluded that higher temperatures elevated the conversions but reduced the purity of product gas. Also, the sorbent was only efficient at lower temperatures, suggesting the process to run as SMR at temperatures greater than 750 °C as evident in results. Thus, employing the hybrid material (CaO @ MNA) is potentially attractive for SESMR at lower temperatures.

Future Outlook

In the present work, HTc based catalysts have been combined with CaO based sorbent. In future, different type of noble metals can be incorporated to evaluate the catalytic activities. Furthermore, regeneration studies can be performed on the present catalyst. Commercial CaO sorbent can be combined with HTc and compared with the present waste derived CaO sorbent combined with HTc.

References

[1] Y. Yan, V. Manovic, E.J. Anthony, P.T. Clough, Techno-economic analysis of low-carbon hydrogen production by sorption enhanced steam methane reforming (SE-SMR) processes, Energy Conversion and Management, 226 (2020) 113530.

[2] M. Shokrollahi Yancheshmeh, H.R. Radfarnia, M.C. Iliuta, High temperature CO2 sorbents and their application for hydrogen production by sorption enhanced steam reforming process, Chemical Engineering Journal, 283 (2016) 420-444.

[3] IEA (2019), The Future of Hydrogen, IEA, Paris https://www.iea.org/reports/the-future-of-hydrogen.

[4] H. Liu, S. Liu, Life cycle energy consumption and GHG emissions of hydrogen production from underground coal gasification in comparison with surface coal gasification, International Journal of Hydrogen Energy, 46 (2021) 9630-9643.

[5] M. Gür, E.D. Canbaz, Analysis of syngas production and reaction zones in hydrogen oriented underground coal gasification, Fuel, 269 (2020) 117331.

[6] Y. Feng, N. Wang, X. Guo, S. Zhang, Dopant screening of modified Fe_2O_3 oxygen carriers in chemical looping hydrogen production, Fuel, 262 (2020) 116489.

[7] M. Luo, Y. Yi, S. Wang, Z. Wang, M. Du, J. Pan, Q. Wang, Review of hydrogen production using chemical-looping technology, Renewable and Sustainable Energy Reviews, 81 (2018) 3186-3214.

[8] M. De Falco, G. Santoro, M. Capocelli, G. Caputo, A. Giaconia, Hydrogen production by solar steam methane reforming with molten salts as energy carriers: Experimental and modelling analysis, International Journal of Hydrogen Energy, 46 (2021) 10682-10696.

[9] z. ou, z. zhang, C. Qin, H. Xia, t. deng, j. niu, J. Ran, C. Wu, Highly Active and Stable Ni/perovskite Catalyst in Steam Methane Reforming for Hydrogen Production, Sustainable Energy & Fuels, (2021).

[10] R.R. Bhosale, A novel three-step GeO_2/GeO thermochemical water splitting cycle for solar hydrogen production, International Journal of Hydrogen Energy, 45 (2020) 5816-5828.

[11] R.R. Bhosale, F. AlMomani, Hydrogen production via solar driven thermochemical cerium oxide – cerium sulfate water splitting cycle, International Journal of Hydrogen Energy, 45 (2020) 10381-10390.
[12] R. Chaubey, S. Sahu, O.O. James, S. Maity, A review on development of industrial processes and emerging techniques for production of hydrogen from renewable and sustainable sources, Renewable and Sustainable Energy Reviews, 23 (2013) 443-462.
[13] T.P. de Castro, E.B. Silveira, R.C. Rabelo-Neto, L.E.P. Borges, F.B. Noronha, Study of the performance of Pt/Al_2O_3 and $Pt/CeO_2/Al_2O_3$ catalysts for steam reforming of toluene, methane and mixtures, Catalysis Today, 299 (2018) 251-262.
[14] M.R. Cesário, B.S. Barros, Y. Zimmermann, C. Courson, D. Melo, A. Kiennemann, CO_2 sorption enhanced steam reforming of methane using $Ni/CaO\cdot Ca_{12}Al_{14}O_{33}$ catalysts, Advanced Chemistry Letters, 1 (2013) 292-299.
[15] A. Di Giuliano, K. Gallucci, Sorption enhanced steam methane reforming based on nickel and calcium looping: a review, Chemical Engineering and Processing - Process Intensification, 130 (2018) 240-252.
[16] S.A. Ghungrud, K.D. Dewoolkar, P.D. Vaidya, Cerium-promoted bi-functional hybrid materials made of Ni, Co and hydrotalcite for sorption-enhanced steam methane reforming (SESMR), International Journal of Hydrogen Energy, 44 (2019) 694-706.
[17] A. Di Giuliano, J. Girr, R. Massacesi, K. Gallucci, C. Courson, Sorption enhanced steam methane reforming by Ni–CaO materials supported on mayenite, International Journal of Hydrogen Energy, 42 (2017) 13661-13680.
[18] U. Sikander, S. Sufian, M.A. Salam, A review of hydrotalcite based catalysts for hydrogen production systems, International Journal of Hydrogen Energy, 42 (2017) 19851-19868.
[19] Y. Wang, M.Z. Memon, M.A. Seelro, W. Fu, Y. Gao, Y. Dong, G. Ji, A review of CO_2 sorbents for promoting hydrogen production in the sorption-enhanced steam reforming process, International Journal of Hydrogen Energy, (2021).
[20] D.C. Miller, J.T. Litynski, L.A. Brickett, B.D. Morreale, Toward transformational carbon capture systems, AIChE Journal, 62 (2016) 2-10.

[21] I. Ganesh, Conversion of carbon dioxide into methanol – a potential liquid fuel: Fundamental challenges and opportunities (a review), Renewable and Sustainable Energy Reviews, 31 (2014) 221-257.
[22] S. Ali, M.J. Al-Marri, A.G. Abdelmoneim, A. Kumar, M.M. Khader, Catalytic evaluation of nickel nanoparticles in methane steam reforming, International Journal of Hydrogen Energy, 41 (2016) 22876-22885.
[23] M. Boudjeloud, A. Boulahouache, C. Rabia, N. Salhi, La-doped supported Ni catalysts for steam reforming of methane, International Journal of Hydrogen Energy, 44 (2019) 9906-9913.
[24] H. Wu, V. La Parola, G. Pantaleo, F. Puleo, A.M. Venezia, L.F. Liotta, Ni-Based Catalysts for Low Temperature Methane Steam Reforming: Recent Results on Ni-Au and Comparison with Other Bi-Metallic Systems, Catalysts, 3 (2013).
[25] F. Watanabe, I. Kaburaki, N. Shimoda, S. Satokawa, Influence of nitrogen impurity for steam methane reforming over noble metal catalysts, Fuel Processing Technology, 152 (2016) 15-21.
[26] H. Song, X. Meng, Z.-j. Wang, Z. Wang, H. Chen, Y. Weng, F. Ichihara, M. Oshikiri, T. Kako, J. Ye, Visible-Light-Mediated Methane Activation for Steam Methane Reforming under Mild Conditions: A Case Study of Rh/TiO_2 Catalysts, ACS Catalysis, 8 (2018) 7556-7565.
[27] L. Azancot, L.F. Bobadilla, J.L. Santos, J.M. Córdoba, M.A. Centeno, J.A. Odriozola, Influence of the preparation method in the metal-support interaction and reducibility of Ni-Mg-Al based catalysts for methane steam reforming, International Journal of Hydrogen Energy, 44 (2019) 19827-19840.
[28] K.D. Dewoolkar, P.D. Vaidya, Tailored Ce- and Zr-doped Ni/hydrotalcite materials for superior sorption-enhanced steam methane reforming, International Journal of Hydrogen Energy, 42 (2017) 21762-21774.
[29] M. He, J. Zhang, Z. Shi, F. Liu, X. Li, Synthesis of hydrotalcite-like compounds from blast furnace slag: the effect of synthesis parameters on structure and crystallinity, Energy Technology 2015, Springer2015, pp. 325-331.
[30] M. Nawfal, C. Gennequin, M. Labaki, B. Nsouli, A. Aboukaïs, E. Abi-Aad, Hydrogen production by methane steam reforming over Ru supported on Ni–Mg–Al

mixed oxides prepared via hydrotalcite route, International Journal of Hydrogen Energy, 40 (2015) 1269-1277.
[31] Y. Qi, Z. Cheng, Z. Zhou, Steam reforming of methane over Ni catalysts prepared from hydrotalcite-type precursors: Catalytic activity and reaction kinetics, Chinese Journal of Chemical Engineering, 23 (2015) 76-85.
[32] E. Dahdah, J. Estephane, C. Gennequin, A. Aboukaïs, S. Aouad, E. Abi-Aad, Effect of La promotion on Ni/Mg-Al hydrotalcite derived catalysts for glycerol steam reforming, Journal of Environmental Chemical Engineering, 8 (2020) 104228.
[33] S. Basu, N.C. Pradhan, Steam reforming of acetone over NiCoMgAl mixed oxide catalysts obtained from hydrotalcite precursors, International Journal of Hydrogen Energy, 45 (2020) 18133-18143.
[34] C. Cerdá-Moreno, J.F. Da Costa-Serra, A. Chica, Co and La supported on Zn-Hydrotalcite-derived material as efficient catalyst for ethanol steam reforming, International Journal of Hydrogen Energy, 44 (2019) 12685-12692.
[35] Y.M. Kwon, H.J. Chae, M.S. Cho, Y.K. Park, H.M. Seo, S.C. Lee, J.C. Kim, Effect of a Li_2SiO_3 phase in lithium silicate-based sorbents for CO_2 capture at high temperatures, Separation and Purification Technology, 214 (2019) 104-110.
[36] J.A. Mendoza-Nieto, S. Tehuacanero-Cuapa, J. Arenas-Alatorre, H. Pfeiffer, Nickel-doped sodium zirconate catalysts for carbon dioxide storage and hydrogen production through dry methane reforming process, Applied Catalysis B: Environmental, 224 (2018) 80-87.
[37] S.C. Lee, M.J. Kim, Y.M. Kwon, H.J. Chae, M.S. Cho, Y.K. Park, H.M. Seo, J.C. Kim, Novel regenerable solid sorbents based on lithium orthosilicate for carbon dioxide capture at high temperatures, Separation and Purification Technology, 214 (2019) 120-127.
[38] F.H. Alshafei, L.T. Minardi, D. Rosales, G. Chen, Dante A. Simonetti, Improved Sorption-Enhanced Steam Methane Reforming via Calcium Oxide–Based Sorbents with Targeted Morphology, Energy Technology, 7 (2019) 1800807.
[39] A.H. Ruhaimi, M.A.A. Aziz, A.A. Jalil, Magnesium oxide-based adsorbents for carbon dioxide capture: Current progress and future opportunities, Journal of CO2 Utilization, 43 (2021) 101357.

[40] C.S. Martavaltzi, T.D. Pefkos, A.A. Lemonidou, Operational Window of Sorption Enhanced Steam Reforming of Methane over CaO−$Ca_{12}Al_{14}O_{33}$, Industrial & Engineering Chemistry Research, 50 (2011) 539-545.

[41] B. Dou, C. Wang, Y. Song, H. Chen, B. Jiang, M. Yang, Y. Xu, Solid sorbents for in-situ CO_2 removal during sorption-enhanced steam reforming process: A review, Renewable and Sustainable Energy Reviews, 53 (2016) 536-546.

[42] Q. Zhu, S. Zeng, Y. Yu, A Model to Stabilize CO_2 Uptake Capacity during Carbonation–Calcination Cycles and its Case of CaO–MgO, Environmental Science & Technology, 51 (2017) 552-559.

[43] M. Xie, Z. Zhou, Y. Qi, Z. Cheng, W. Yuan, Sorption-enhanced steam methane reforming by in situ CO_2 capture on a CaO–$Ca_9Al_6O_{18}$ sorbent, Chemical Engineering Journal, 207-208 (2012) 142-150.

[44] G. Wu, C. Zhang, S. Li, Z. Huang, S. Yan, S. Wang, X. Ma, J. Gong, Sorption enhanced steam reforming of ethanol on Ni–CaO–Al_2O_3 multifunctional catalysts derived from hydrotalcite-like compounds, Energy & Environmental Science, 5 (2012) 8942-8949.

[45] J.-N. Kim, C.H. Ko, K.B. Yi, Sorption enhanced hydrogen production using one-body CaO–$Ca_{12}Al_{14}O_{33}$–Ni composite as catalytic absorbent, International Journal of Hydrogen Energy, 38 (2013) 6072-6078.

[46] H.R. Radfarnia, M.C. Iliuta, Development of Al-stabilized CaO–nickel hybrid sorbent–catalyst for sorption-enhanced steam methane reforming, Chemical Engineering Science, 109 (2014) 212-219.

[47] K.S. Sultana, D. Chen, Enhanced hydrogen production by in situ CO_2 removal on $CaCeZrO_x$ nanocrystals, Catalysis Today, 171 (2011) 43-51.

[48] H.R. Radfarnia, M.C. Iliuta, Hydrogen production by sorption-enhanced steam methane reforming process using CaO-Zr/Ni bifunctional sorbent–catalyst, Chemical Engineering and Processing: Process Intensification, 86 (2014) 96-103.

[49] A. Di Giuliano, F. Giancaterino, C. Courson, P.U. Foscolo, K. Gallucci, Development of a Ni-CaO-mayenite combined sorbent-catalyst material for multicycle sorption enhanced steam methane reforming, Fuel, 234 (2018) 687-699.

[50] C. Wang, N. Sun, N. Zhao, W. Wei, Y. Sun, C. Sun, H. Liu, C.E. Snape, Coking and deactivation of a mesoporous Ni–CaO–ZrO_2 catalyst in dry reforming of methane: A study under different feeding compositions, Fuel, 143 (2015) 527-535.
[51] A. Di Giuliano, K. Gallucci, A. Di Carlo, S. Stendardo, C. Courson, P.U. Foscolo, Sorption enhanced steam methane reforming by Ni/CaO/mayenite combined systems: Overview of experimental results from European research project ASCENT, The Canadian Journal of Chemical Engineering, 98 (2020) 1907-1923.
[52] L. Habte, N. Shiferaw, D. Mulatu, T. Thenepalli, R. Chilakala, J.W. Ahn, Synthesis of nano-calcium oxide from waste eggshell by sol-gel method, Sustainability, 11 (2019) 3196.
[53] T. Witoon, Characterization of calcium oxide derived from waste eggshell and its application as CO2 sorbent, Ceramics International, 37 (2011) 3291-3298.
[54] N. Zhang, X. Chen, B. Chu, C. Cao, Y. Jin, Y. Cheng, Catalytic performance of Ni catalyst for steam methane reforming in a micro-channel reactor at high pressure, Chemical Engineering and Processing: Process Intensification, 118 (2017) 19-25.
[55] E. Meloni, M. Martino, V. Palma, A Short Review on Ni Based Catalysts and Related Engineering Issues for Methane Steam Reforming, Catalysts, 10 (2020).
[56] J.G.F. Madeira, E.M. Oliveira, M.V. Springer, H.L. Cabral, D.F.d.C. Barbeito, A.P.G. Souza, D.A.d.S. Moura, A.R.S. Delgado, Hydrogen production from swine manure biogas via steam reforming of methane (SRM) and water gas shift (WGS): A ecological, technical, and economic analysis, International Journal of Hydrogen Energy, (2021).
[57] O.U. Osazuwa, S.Z. Abidin, X. Fan, A.N. Amenaghawon, M.T. Azizan, An insight into the effects of synthesis methods on catalysts properties for methane reforming, Journal of Environmental Chemical Engineering, 9 (2021) 105052.
[58] A. Boyano, A.M. Blanco-Marigorta, T. Morosuk, G. Tsatsaronis, Exergoenvironmental analysis of a steam methane reforming process for hydrogen production, Energy, 36 (2011) 2202-2214.
[59] M. Broda, V. Manovic, Q. Imtiaz, A.M. Kierzkowska, E.J. Anthony, C.R. Müller, High-Purity Hydrogen via the Sorption-Enhanced Steam Methane Reforming Reaction

over a Synthetic CaO-Based Sorbent and a Ni Catalyst, Environmental Science & Technology, 47 (2013) 6007-6014.
[60] C. Agrafiotis, H. von Storch, M. Roeb, C. Sattler, Solar thermal reforming of methane feedstocks for hydrogen and syngas production—A review, Renewable and Sustainable Energy Reviews, 29 (2014) 656-682.
[61] D.P. Harrison, Sorption-Enhanced Hydrogen Production: A Review, Industrial & Engineering Chemistry Research, 47 (2008) 6486-6501.
[62] M. Taji, M. Farsi, P. Keshavarz, Real time optimization of steam reforming of methane in an industrial hydrogen plant, International Journal of Hydrogen Energy, 43 (2018) 13110-13121.
[63] J. Xiao, Y. Peng, P. Bénard, R. Chahine, Thermal effects on breakthrough curves of pressure swing adsorption for hydrogen purification, International Journal of Hydrogen Energy, 41 (2016) 8236-8245.
[64] J.R. Rostrup-Nielsen, Production of synthesis gas, Catalysis Today, 18 (1993) 305-324.
[65] J.R. Rostrup-Nielsen, J. Sehested, J.K. Nørskov, Hydrogen and synthesis gas by steam- and C02 reforming, Advances in Catalysis, Academic Press2002, pp. 65-139.
[66] J. Wei, E. Iglesia, Structural requirements and reaction pathways in methane activation and chemical conversion catalyzed by rhodium, Journal of Catalysis, 225 (2004) 116-127.
[67] J. Xu, G.F. Froment, Methane steam reforming, methanation and water-gas shift: I. Intrinsic kinetics, AIChE Journal, 35 (1989) 88-96.
[68] Z. Zhang, Z. Ou, C. Qin, J. Ran, C. Wu, Roles of alkali/alkaline earth metals in steam reforming of biomass tar for hydrogen production over perovskite supported Ni catalysts, Fuel, 257 (2019) 116032.
[69] C. Pistonesi, A. Juan, B. Irigoyen, N. Amadeo, Theoretical and experimental study of methane steam reforming reactions over nickel catalyst, Applied Surface Science, 253 (2007) 4427-4437.
[70] N.F.P. Ribeiro, R.C.R. Neto, S.F. Moya, M.M.V.M. Souza, M. Schmal, Synthesis of $NiAl_2O_4$ with high surface area as precursor of Ni nanoparticles for hydrogen production, International Journal of Hydrogen Energy, 35 (2010) 11725-11732.

[71] G.-H. Lai, J.H. Lak, D.-H. Tsai, Hydrogen Production via Low-Temperature Steam–Methane Reforming Using Ni–CeO2–Al2O3 Hybrid Nanoparticle Clusters as Catalysts, ACS Applied Energy Materials, 2 (2019) 7963-7971.

[72] H. Kim, Y.-H. Lee, H. Lee, J.-C. Seo, K. Lee, Effect of Mg Contents on Catalytic Activity and Coke Formation of Mesoporous Ni/Mg-Aluminate Spinel Catalyst for Steam Methane Reforming, Catalysts, 10 (2020).

[73] M.H. Aghaali, S. Firoozi, Enhancing the catalytic performance of Co substituted $NiAl_2O_4$ spinel by ultrasonic spray pyrolysis method for steam and dry reforming of methane, International Journal of Hydrogen Energy, 46 (2021) 357-373.

[74] N. Salhi, A. Boulahouache, C. Petit, A. Kiennemann, C. Rabia, Steam reforming of methane to syngas over $NiAl_2O_4$ spinel catalysts, International Journal of Hydrogen Energy, 36 (2011) 11433-11439.

[75] L. Zhou, Y. Guo, J. Chen, M. Sakurai, H. Kameyama, Trace precious metal Pt doped plate-type anodic alumina Ni catalysts for methane reforming reaction, Fuel, 92 (2012) 373-376.

[76] S. Damyanova, B. Pawelec, K. Arishtirova, J.L.G. Fierro, Ni-based catalysts for reforming of methane with CO_2, International Journal of Hydrogen Energy, 37 (2012) 15966-15975.

[77] S.-C. Baek, K.-W. Jun, Y.-J. Lee, J.D. Kim, D.Y. Park, K.-Y. Lee, Ru/Ni/$MgAl_2O_4$ catalysts for steam reforming of methane: effects of Ru content on self-activation property, Research on Chemical Intermediates, 38 (2012) 1225-1236.

[78] W. Liu, L. Li, X. Zhang, Z. Wang, X. Wang, H. Peng, Design of Ni-ZrO_2@SiO_2 catalyst with ultra-high sintering and coking resistance for dry reforming of methane to prepare syngas, Journal of CO2 Utilization, 27 (2018) 297-307.

[79] I. Ganesh, A review on magnesium aluminate ($MgAl_2O_4$) spinel: synthesis, processing and applications, International Materials Reviews, 58 (2013) 63-112.

[80] B. Abdullah, N.A. Abd Ghani, D.-V.N. Vo, Recent advances in dry reforming of methane over Ni-based catalysts, Journal of Cleaner Production, 162 (2017) 170-185.

[81] A.H. Khoja, M. Tahir, N.A.S. Amin, A. Javed, M.T. Mehran, Kinetic study of dry reforming of methane using hybrid DBD plasma reactor over La_2O_3 co-supported

Ni/$MgAl_2O_4$ catalyst, International Journal of Hydrogen Energy, 45 (2020) 12256-12271.

[82] S. Katheria, A. Gupta, G. Deo, D. Kunzru, Effect of calcination temperature on stability and activity of Ni/$MgAl_2O_4$ catalyst for steam reforming of methane at high pressure condition, International Journal of Hydrogen Energy, 41 (2016) 14123-14132.

[83] D. Li, M. Lu, Y. Cai, Y. Cao, Y. Zhan, L. Jiang, Synthesis of high surface area $MgAl_2O_4$ spinel as catalyst support via layered double hydroxides-containing precursor, Applied Clay Science, 132-133 (2016) 243-250.

[84] E. Cho, Y.-H. Lee, H. Kim, E.J. Jang, J.H. Kwak, K. Lee, C.H. Ko, W.L. Yoon, Ni catalysts for dry methane reforming prepared by A-site exsolution on mesoporous defect spinel magnesium aluminate, Applied Catalysis A: General, 602 (2020) 117694.

[85] F. Basile, P. Benito, G. Fornasari, A. Vaccari, Hydrotalcite-type precursors of active catalysts for hydrogen production, Applied Clay Science, 48 (2010) 250-259.

[86] A. Fonseca, E.M. Assaf, Production of the hydrogen by methane steam reforming over nickel catalysts prepared from hydrotalcite precursors, Journal of Power Sources, 142 (2005) 154-159.

[87] Y. Sekine, M. Haraguchi, M. Matsukata, E. Kikuchi, Low temperature steam reforming of methane over metal catalyst supported on $CexZr_{1-x}O_2$ in an electric field, Catalysis Today, 171 (2011) 116-125.

[88] M.A. Soria, C. Mateos-Pedrero, A. Guerrero-Ruiz, I. Rodríguez-Ramos, Thermodynamic and experimental study of combined dry and steam reforming of methane on Ru/ ZrO_2-La_2O_3 catalyst at low temperature, International Journal of Hydrogen Energy, 36 (2011) 15212-15220.

[89] Z. Bian, S. Das, M.H. Wai, P. Hongmanorom, S. Kawi, A review on bimetallic nickel-based catalysts for CO_2 reforming of methane, ChemPhysChem, 18 (2017) 3117-3134.

[90] M. Zeppieri, P.L. Villa, N. Verdone, M. Scarsella, P. De Filippis, Kinetic of methane steam reforming reaction over nickel- and rhodium-based catalysts, Applied Catalysis A: General, 387 (2010) 147-154.

[91] D. San-José-Alonso, J. Juan-Juan, M.J. Illán-Gómez, M.C. Román-Martínez, Ni, Co and bimetallic Ni–Co catalysts for the dry reforming of methane, Applied Catalysis A: General, 371 (2009) 54-59.

[92] K. Li, C. Pei, X. Li, S. Chen, X. Zhang, R. Liu, J. Gong, Dry reforming of methane over $La_2O_2CO_3$-modified Ni/Al_2O_3 catalysts with moderate metal support interaction, Applied Catalysis B: Environmental, 264 (2020) 118448.

[93] A. Kambolis, H. Matralis, A. Trovarelli, C. Papadopoulou, Ni/CeO_2-ZrO_2 catalysts for the dry reforming of methane, Applied Catalysis A: General, 377 (2010) 16-26.

[94] M.A. Nieva, M.M. Villaverde, A. Monzón, T.F. Garetto, A.J. Marchi, Steam-methane reforming at low temperature on nickel-based catalysts, Chemical Engineering Journal, 235 (2014) 158-166.

[95] U. Rodemerck, M. Schneider, D. Linke, Improved stability of Ni/SiO_2 catalysts in CO_2 and steam reforming of methane by preparation via a polymer-assisted route, Catalysis Communications, 102 (2017) 98-102.

[96] X. Yang, J. Da, H. Yu, H. Wang, Characterization and performance evaluation of Ni-based catalysts with Ce promoter for methane and hydrocarbons steam reforming process, Fuel, 179 (2016) 353-361.

[97] B. Bej, N.C. Pradhan, S. Neogi, Production of hydrogen by steam reforming of methane over alumina supported nano-NiO/SiO_2 catalyst, Catalysis Today, 207 (2013) 28-35.

[98] Y.-S. Oh, H.-S. Roh, K.-W. Jun, Y.-S. Baek, A highly active catalyst, Ni/Ce–ZrO_2/θ-Al_2O_3, for on-site H_2 generation by steam methane reforming: pretreatment effect, International Journal of Hydrogen Energy, 28 (2003) 1387-1392.

[99] T. Takeguchi, H. Watanabe, T. Murayama, H. Takahashi, W. Ueda, Quantitative Analysis of Coke Formation during Steam Reforming of Methane on a Nickel–Hydrotalcite Catalyst under Practical Operation Conditions, Chemistry Letters, 42 (2013) 124-126.

[100] E.B. Silveira, R.C. Rabelo-Neto, F.B. Noronha, Steam reforming of toluene, methane and mixtures over Ni/ZrO_2 catalysts, Catalysis Today, 289 (2017) 289-301.

[101] H.-W. Kim, K.-M. Kang, H.-Y. Kwak, J.H. Kim, Preparation of supported Ni catalysts on various metal oxides with core/shell structures and their tests for the steam reforming of methane, Chemical Engineering Journal, 168 (2011) 775-783.
[102] K. Lertwittayanon, D. Atong, P. Aungkavattana, T. Wasanapiarnpong, S. Wada, V. Sricharoenchaikul, Effect of $CaO–ZrO_2$ addition to Ni supported on γ-Al_2O_3 by sequential impregnation in steam methane reforming, International Journal of Hydrogen Energy, 35 (2010) 12277-12285.
[103] X. Guo, Y. Sun, Y. Yu, X. Zhu, C.-j. Liu, Carbon formation and steam reforming of methane on silica supported nickel catalysts, Catalysis Communications, 19 (2012) 61-65.
[104] S. Miura, Y. Umemura, Y. Shiratori, T. Kitaoka, In situ synthesis of Ni/MgO catalysts on inorganic paper-like matrix for methane steam reforming, Chemical Engineering Journal, 229 (2013) 515-521.
[105] V.M. Shinde, G. Madras, Catalytic performance of highly dispersed Ni/TiO_2 for dry and steam reforming of methane, RSC Advances, 4 (2014) 4817-4826.
[106] M.L. Andrade, L. Almeida, M. do Carmo Rangel, F. Pompeo, N. Nichio, Ni-Catalysts Supported on Gd-Doped Ceria for Solid Oxide Fuel Cells in Methane Steam Reforming, Chemical Engineering & Technology, 37 (2014) 343-348.
[107] K. Kusakabe, K.-I. Sotowa, T. Eda, Y. Iwamoto, Methane steam reforming over $Ce–ZrO_2$-supported noble metal catalysts at low temperature, Fuel Processing Technology, 86 (2004) 319-326.
[108] E.T. Kho, J. Scott, R. Amal, Ni/TiO_2 for low temperature steam reforming of methane, Chemical Engineering Science, 140 (2016) 161-170.
[109] Y. Zhang, W. Wang, Z. Wang, X. Zhou, Z. Wang, C.-J. Liu, Steam reforming of methane over Ni/SiO_2 catalyst with enhanced coke resistance at low steam to methane ratio, Catalysis Today, 256 (2015) 130-136.
[110] Z.-Y. Lim, C. Wu, W.G. Wang, K.-L. Choy, H. Yin, Porosity effect on ZrO_2 hollow shells and hydrothermal stability for catalytic steam reforming of methane, Journal of Materials Chemistry A, 4 (2016) 153-159.
[111] M. Mundhwa, C.P. Thurgood, Methane steam reforming at low steam to carbon ratios over alumina and yttria-stabilized-zirconia supported nickel-spinel catalyst:

Experimental study and optimization of microkinetic model, Fuel Processing Technology, 168 (2017) 27-39.
[112] Z. Wang, J. Ashok, Z. Pu, S. Kawi, Low temperature partial oxidation of methane via $BaBi_{0.05}Co_{0.8}Nb_{0.15}O_{3-\delta}$-Ni phyllosilicate catalytic hollow fiber membrane reactor, Chemical Engineering Journal, 315 (2017) 315-323.
[113] D.D. Athayde, D.F. Souza, A.M.A. Silva, D. Vasconcelos, E.H.M. Nunes, J.C. Diniz da Costa, W.L. Vasconcelos, Review of perovskite ceramic synthesis and membrane preparation methods, Ceramics International, 42 (2016) 6555-6571.
[114] J. Zhu, H. Li, L. Zhong, P. Xiao, X. Xu, X. Yang, Z. Zhao, J. Li, Perovskite Oxides: Preparation, Characterizations, and Applications in Heterogeneous Catalysis, ACS Catalysis, 4 (2014) 2917-2940.
[115] T. Maneerung, K. Hidajat, S. Kawi, Co-production of hydrogen and carbon nanofibers from catalytic decomposition of methane over LaNi(1−x)Mx O3−α perovskite (where M = Co, Fe and X = 0, 0.2, 0.5, 0.8, 1), International Journal of Hydrogen Energy, 40 (2015) 13399-13411.
[116] M. Abd Mutalib, F. Aziz, A.F. Ismail, W.N. Wan Salleh, N. Yusof, J. Jaafar, T. Soga, M.Z. Sahdan, N. Ahmad Ludin, Towards high performance perovskite solar cells: A review of morphological control and HTM development, Applied Materials Today, 13 (2018) 69-82.
[117] Z. Shi, A.H. Jayatissa, Perovskites-Based Solar Cells: A Review of Recent Progress, Materials and Processing Methods, Materials, 11 (2018).
[118] G. Parravano, Ferroelectric transitions and heterogenous catalysis, The Journal of Chemical Physics, 20 (1952) 342-343.
[119] T.Y. Yeo, J. Ashok, S. Kawi, Recent developments in sulphur-resilient catalytic systems for syngas production, Renewable and Sustainable Energy Reviews, 100 (2019) 52-70.
[120] U. Oemar, P.S. Ang, K. Hidajat, S. Kawi, Promotional effect of Fe on perovskite $LaNi_xFe_{1-x}O_3$ catalyst for hydrogen production via steam reforming of toluene, International Journal of Hydrogen Energy, 38 (2013) 5525-5534.

[121] K.-H. Lin, C.-B. Wang, S.-H. Chien, Catalytic performance of steam reforming of ethanol at low temperature over $LaNiO_3$ perovskite, International Journal of Hydrogen Energy, 38 (2013) 3226-3232.
[122] L. Li, B. Jiang, Z. Sun, Q. Zhang, D. Li, D. Tang, Hydrogen Production from Chemical Looping Steam Reforming of Ethanol over Perovskite-Type Oxygen Carriers with Bimetallic Co and Ni B-Site Substitution, Catalysts, 8 (2018).
[123] L. Li, B. Jiang, D. Tang, Q. Zhang, Z. Zheng, Hydrogen generation by acetic acid steam reforming over Ni-based catalysts derived from La1−xCexNiO3 perovskite, International Journal of Hydrogen Energy, 43 (2018) 6795-6803.
[124] Q. Zhang, L. Li, B. Jiang, K. Wang, D. Tang, B. Dou, An intelligent oxygen carrier of $La_{2-x}Sr_xNiO_{4-\lambda}$ for hydrogen production by chemical looping reforming of ethanol, International Journal of Hydrogen Energy, 42 (2017) 17102-17111.
[125] Z. Bian, Z. Wang, B. Jiang, P. Hongmanorom, W. Zhong, S. Kawi, A review on perovskite catalysts for reforming of methane to hydrogen production, Renewable and Sustainable Energy Reviews, 134 (2020) 110291.
[126] K. Urasaki, Y. Sekine, S. Kawabe, E. Kikuchi, M. Matsukata, Catalytic activities and coking resistance of Ni/perovskites in steam reforming of methane, Applied Catalysis A: General, 286 (2005) 23-29.
[127] S. Dama, S. Ghodke, R. Bobade, H. Gurav, S. Chilukuri, Tuning the dimensionality of layered $Sr_{n+1}Ti_{n-x}Ni_xO_{3n+1}$ perovskite structures for improved activity in syngas generation, Journal of Catalysis, 360 (2018) 27-39.
[128] X. Yin, S. Wang, B. Wang, L. Shen, Perovskite-type $LaMn_{1-x}B_xO_{3+\delta}$ (B = Fe, Co and Ni) as oxygen carriers for chemical looping steam methane reforming, Chemical Engineering Journal, (2021) 128751.
[129] K. Zhao, F. He, Z. Huang, A. Zheng, H. Li, Z. Zhao, Three-dimensionally ordered macroporous $LaFeO_3$ perovskites for chemical-looping steam reforming of methane, International Journal of Hydrogen Energy, 39 (2014) 3243-3252.
[130] M.R. Carrasco-Díaz, E. Castillejos-López, A. Cerpa-Naranjo, M.L. Rojas-Cervantes, Efficient removal of paracetamol using $LaCu_{1-x}M_xO_3$ (M=Mn, Ti) perovskites as heterogeneous Fenton-like catalysts, Chemical Engineering Journal, 304 (2016) 408-418.

[131] Q. Jiang, H. Zhang, Y. Cao, H. Hong, H. Jin, Solar hydrogen production via perovskite-based chemical-looping steam methane reforming, Energy Conversion and Management, 187 (2019) 523-536.

[132] G.R. Moradi, F. Khosravian, M. Rahmanzadeh, Effects of Partial Substitution of Ni by Cu in $LaNiO_3$ Perovskite Catalyst for Dry Methane Reforming, Chinese Journal of Catalysis, 33 (2012) 797-801.

[133] X. Zhang, Y. Su, C. Pei, Z.-J. Zhao, R. Liu, J. Gong, Chemical looping steam reforming of methane over Ce-doped perovskites, Chemical Engineering Science, 223 (2020) 115707.

[134] Y.-H. Huang, G. Liang, M. Croft, M. Lehtimäki, M. Karppinen, J.B. Goodenough, Double-Perovskite Anode Materials Sr_2MMoO_6 (M = Co, Ni) for Solid Oxide Fuel Cells, Chemistry of Materials, 21 (2009) 2319-2326.

[135] P.V. Tuza, M.M. Souza, Steam reforming of methane over catalyst derived from ordered double perovskite: effect of crystalline phase transformation, Catalysis Letters, 146 (2016) 47-53.

[136] K. Takehira, T. Shishido, M. Kondo, Partial Oxidation of CH_4 over $Ni/SrTiO_3$ Catalysts Prepared by a Solid-Phase Crystallization Method, Journal of Catalysis, 207 (2002) 307-316.

[137] X. Zhai, S. Ding, Z. Liu, Y. Jin, Y. Cheng, Catalytic performance of Ni catalysts for steam reforming of methane at high space velocity, International Journal of Hydrogen Energy, 36 (2011) 482-489.

[138] A. Mosayebi, M. Nasabi, Steam methane reforming on $LaNiO_3$ perovskite-type oxide for syngas production, activity tests, and kinetic modeling, International Journal of Energy Research, 44 (2020) 5500-5515.

[139] F. He, J. Chen, S. Liu, Z. Huang, G. Wei, G. Wang, Y. Cao, K. Zhao, $La_{1-x}Sr_xFeO_3$ perovskite-type oxides for chemical-looping steam methane reforming: Identification of the surface elements and redox cyclic performance, International Journal of Hydrogen Energy, 44 (2019) 10265-10276.

[140] H. Ding, C. Luo, X. Li, D. Cao, Q. Shen, L. Zhang, Development of BaSrCo-based perovskite for chemical-looping steam methane reforming: A study on synergistic effects of A-site elements and CeO_2 support, Fuel, 253 (2019) 311-319.

[141] H. Ding, Y. Xu, C. Luo, Q. Wang, C. Shen, J. Xu, L. Zhang, A novel composite perovskite-based material for chemical-looping steam methane reforming to hydrogen and syngas, Energy Conversion and Management, 171 (2018) 12-19.
[142] D. Mei, V.-A. Glezakou, V. Lebarbier, L. Kovarik, H. Wan, K.O. Albrecht, M. Gerber, R. Rousseau, R.A. Dagle, Highly active and stable $MgAl_2O_4$-supported Rh and Ir catalysts for methane steam reforming: A combined experimental and theoretical study, Journal of Catalysis, 316 (2014) 11-23.
[143] S.M. Lee, J.M. Won, G.J. Kim, S.H. Lee, S.S. Kim, S.C. Hong, Improving carbon tolerance of Ni-YSZ catalytic porous membrane by palladium addition for low temperature steam methane reforming, Applied Surface Science, 419 (2017) 788-794.
[144] R.B. Duarte, F. Krumeich, J.A. van Bokhoven, Structure, Activity, and Stability of Atomically Dispersed Rh in Methane Steam Reforming, ACS Catalysis, 4 (2014) 1279-1286.
[145] J.A. Farmer, C.T. Campbell, Ceria Maintains Smaller Metal Catalyst Particles by Strong Metal-Support Bonding, Science, 329 (2010) 933.
[146] T. Borowiecki, A. Denis, M. Rawski, A. Gołębiowski, K. Stołecki, J. Dmytrzyk, A. Kotarba, Studies of potassium-promoted nickel catalysts for methane steam reforming: Effect of surface potassium location, Applied Surface Science, 300 (2014) 191-200.
[147] S.S. Maluf, E.M. Assaf, Ni catalysts with Mo promoter for methane steam reforming, Fuel, 88 (2009) 1547-1553.
[148] J. Xu, L. Chen, K.F. Tan, A. Borgna, M. Saeys, Effect of boron on the stability of Ni catalysts during steam methane reforming, Journal of Catalysis, 261 (2009) 158-165.
[149] S.C. Dantas, J.C. Escritori, R.R. Soares, C.E. Hori, Effect of different promoters on $Ni/CeZrO_2$ catalyst for autothermal reforming and partial oxidation of methane, Chemical Engineering Journal, 156 (2010) 380-387.
[150] S.M. Lee, S.C. Hong, Effect of palladium addition on catalytic activity in steam methane reforming over Ni-YSZ porous membrane, International Journal of Hydrogen Energy, 39 (2014) 21037-21043.
[151] A.F. Lucrédio, E.M. Assaf, Cobalt catalysts prepared from hydrotalcite precursors and tested in methane steam reforming, Journal of Power Sources, 159 (2006) 667-672.

[152] R. Craciun, W. Daniell, H. Knözinger, The effect of CeO_2 structure on the activity of supported Pd catalysts used for methane steam reforming, Applied Catalysis A: General, 230 (2002) 153-168.
[153] L.S.F. Feio, C.E. Hori, S. Damyanova, F.B. Noronha, W.H. Cassinelli, C.M.P. Marques, J.M.C. Bueno, The effect of ceria content on the properties of $Pd/CeO_2/Al_2O_3$ catalysts for steam reforming of methane, Applied Catalysis A: General, 316 (2007) 107-116.
[154] P.S. Roy, C.S. Park, A.S.K. Raju, K. Kim, Steam-biogas reforming over a metal-foam-coated (Pd–Rh)/($CeZrO_2$–Al_2O_3) catalyst compared with pellet type alumina-supported Ru and Ni catalysts, Journal of CO2 Utilization, 12 (2015) 12-20.
[155] Y. Kathiraser, J. Ashok, S. Kawi, Synthesis and evaluation of highly dispersed SBA-15 supported Ni–Fe bimetallic catalysts for steam reforming of biomass derived tar reaction, Catalysis Science & Technology, 6 (2016) 4327-4336.
[156] Z. Wei, J. Sun, Y. Li, A.K. Datye, Y. Wang, Bimetallic catalysts for hydrogen generation, Chemical Society Reviews, 41 (2012) 7994-8008.
[157] X. You, X. Wang, Y. Ma, J. Liu, W. Liu, X. Xu, H. Peng, C. Li, W. Zhou, P. Yuan, Ni-Co/Al_2O_3 bimetallic catalysts for CH_4 steam reforming: elucidating the role of Co for improving coke resistance, ChemCatChem, 6 (2014) 3377-3386.
[158] V.K. Jaiswar, S. Katheria, G. Deo, D. Kunzru, Effect of Pt doping on activity and stability of Ni/$MgAl_2O_4$ catalyst for steam reforming of methane at ambient and high pressure condition, International Journal of Hydrogen Energy, 42 (2017) 18968-18976.
[159] J. Zhang, H. Wang, A.K. Dalai, Effects of metal content on activity and stability of Ni-Co bimetallic catalysts for CO2 reforming of CH4, Applied Catalysis A: General, 339 (2008) 121-129.
[160] A.C.W. Koh, L. Chen, W. Kee Leong, B.F.G. Johnson, T. Khimyak, J. Lin, Hydrogen or synthesis gas production via the partial oxidation of methane over supported nickel–cobalt catalysts, International Journal of Hydrogen Energy, 32 (2007) 725-730.
[161] L. Chen, Q. Zhu, R. Wu, Effect of Co–Ni ratio on the activity and stability of Co–Ni bimetallic aerogel catalyst for methane Oxy-CO2 reforming, International Journal of Hydrogen Energy, 36 (2011) 2128-2136.

[162] Y. Yu, G. Jin, Y. Wang, X. Guo, Synthesis of natural gas from CO methanation over SiC supported Ni–Co bimetallic catalysts, Catalysis Communications, 31 (2013) 5-10.

[163] J. Zhang, H. Wang, A.K. Dalai, Development of stable bimetallic catalysts for carbon dioxide reforming of methane, Journal of Catalysis, 249 (2007) 300-310.

[164] M. Wang, Z. Fu, Z. Yang, Tuning the Performance of Ni-Based Catalyst by Doping Coinage Metal on Steam Reforming of Methane and Carbon-Tolerance, Fuel Cells, 14 (2014) 251-258.

[165] D. Homsi, S. Aouad, C. Gennequin, A. Aboukaïs, E. Abi-Aad, A highly reactive and stable $Ru/Co_{6-x}Mg_xAl_2$ catalyst for hydrogen production via methane steam reforming, International Journal of Hydrogen Energy, 39 (2014) 10101-10107.

[166] J.C.S. Araújo, L.F. Oton, B. Bessa, A.B.S. Neto, A.C. Oliveira, R. Lang, L. Otubo, J.M.C. Bueno, The role of Pt loading on La_2O_3-Al_2O_3 support for methane conversion reactions via partial oxidation and steam reforming, Fuel, 254 (2019) 115681.

[167] S.S. Itkulova, S. Kussanova, Y. Boleubaev, A. Zhumakanova, Production of Hydrogen Enrich Syngas by Methane Reforming over Multicomponent Co-Pt-based Supported Catalysts.

[168] M.A. Ashraf, O. Sanz, M. Montes, S. Specchia, Insights into the effect of catalyst loading on methane steam reforming and controlling regime for metallic catalytic monoliths, International Journal of Hydrogen Energy, 43 (2018) 11778-11792.

[169] M.D. Lazar, M. Dan, M. Mihet, V. Almasan, V. Rednic, G. Borodi, Hydrogen production by low temperature methane steam reforming using Ag and Au modified alumina supported nickel catalysts, Rev. Roum. Chim, 56 (2011) 637-642.

[170] Q. Shen, Y. Jiang, F. Xia, B. Wang, X. Lv, W. Ye, G. Yang, Hydrogen production by Co-based bimetallic nano-catalysts and their performance in methane steam reforming, Petroleum Science and Technology, 38 (2020) 618-625.

[171] Y. Yan, D. Thanganadar, P.T. Clough, S. Mukherjee, K. Patchigolla, V. Manovic, E.J. Anthony, Process simulations of blue hydrogen production by upgraded sorption enhanced steam methane reforming (SE-SMR) processes, Energy Conversion and Management, 222 (2020) 113144.

[172] G. Vanga, D.M. Gattia, S. Stendardo, S. Scaccia, Novel synthesis of combined CaO-$Ca_{12}Al_{14}O_{33}$-Ni sorbent-catalyst material for sorption enhanced steam reforming processes, Ceramics International, 45 (2019) 7594-7605.
[173] T.L. LeValley, A.R. Richard, M. Fan, The progress in water gas shift and steam reforming hydrogen production technologies – A review, International Journal of Hydrogen Energy, 39 (2014) 16983-17000.
[174] B. Dou, Y. Song, C. Wang, H. Chen, M. Yang, Y. Xu, Hydrogen production by enhanced-sorption chemical looping steam reforming of glycerol in moving-bed reactors, Applied Energy, 130 (2014) 342-349.
[175] R. Soltani, M.A. Rosen, I. Dincer, Assessment of CO2 capture options from various points in steam methane reforming for hydrogen production, International Journal of Hydrogen Energy, 39 (2014) 20266-20275.
[176] M.V. Navarro, J.M. López, T. García, G. Grasa, R. Murillo, Catalyst evaluation for high-purity H_2 production by sorption-enhanced steam-methane reforming coupled to a Ca/Cu process, Journal of Power Sources, 363 (2017) 117-125.
[177] E.L.G. Oliveira, C.A. Grande, A.E. Rodrigues, Effect of catalyst activity in SMR-SERP for hydrogen production: Commercial vs. large-pore catalyst, Chemical Engineering Science, 66 (2011) 342-354.
[178] J.R. Fernández, J.M. Alarcón, J.C. Abanades, Investigation of a Fixed-Bed Reactor for the Calcination of $CaCO_3$ by the Simultaneous Reduction of CuO with a Fuel Gas, Industrial & Engineering Chemistry Research, 55 (2016) 5128-5132.
[179] W.E. Waldron, J. Hufton, S. Sircar, Production of hydrogen by cyclic sorption enhanced reaction process, American Institute of Chemical Engineers. AIChE Journal, 47 (2001) 1477.
[180] A.L. García-Lario, M. Aznar, G.S. Grasa, R. Murillo, Evaluation of process variables on the performance of Sorption Enhanced Methane Reforming, Journal of Power Sources, 285 (2015) 90-99.
[181] A.I. Lysikov, A.G. Okunev, O.V. Netskina, Study of a nickel catalyst under conditions of the SER process: Influence of RedOx cycling, International Journal of Hydrogen Energy, 38 (2013) 10354-10363.

[182] C.S. Martavaltzi, A.A. Lemonidou, Hydrogen production via sorption enhanced reforming of methane: Development of a novel hybrid material—reforming catalyst and CO_2 sorbent, Chemical Engineering Science, 65 (2010) 4134-4140.
[183] B. Arstad, J. Prostak, R. Blom, Continuous hydrogen production by sorption enhanced steam methane reforming (SE-SMR) in a circulating fluidized bed reactor: Sorbent to catalyst ratio dependencies, Chemical Engineering Journal, 189-190 (2012) 413-421.
[184] B. Dou, Y. Song, C. Wang, H. Chen, Y. Xu, Hydrogen production from catalytic steam reforming of biodiesel byproduct glycerol: Issues and challenges, Renewable and Sustainable Energy Reviews, 30 (2014) 950-960.
[185] M.R. Cesário, B.S. Barros, C. Courson, D.M.A. Melo, A. Kiennemann, Catalytic performances of Ni–CaO–mayenite in CO_2 sorption enhanced steam methane reforming, Fuel Processing Technology, 131 (2015) 247-253.
[186] S. Wang, S. Fan, L. Fan, Y. Zhao, X. Ma, Effect of Cerium Oxide Doping on the Performance of CaO-Based Sorbents during Calcium Looping Cycles, Environmental Science & Technology, 49 (2015) 5021-5027.
[187] I. Iliuta, H.R. Radfarnia, M.C. Iliuta, Hydrogen Production by Sorption-Enhanced Steam Glycerol Reforming: Sorption Kinetics and Reactor Simulation, AIChE Journal, 59 (2013) 2105-2118.
[188] Y. Khani, Z. Shariatinia, F. Bahadoran, High catalytic activity and stability of $ZnLaAlO_4$ supported Ni, Pt and Ru nanocatalysts applied in the dry, steam and combined dry-steam reforming of methane, Chemical Engineering Journal, 299 (2016) 353-366.
[189] L. Li, X. Wen, X. Fu, F. Wang, N. Zhao, F. Xiao, W. Wei, Y. Sun, MgO/Al_2O_3 Sorbent for CO_2 Capture, Energy & Fuels, 24 (2010) 5773-5780.
[190] G. Montes-Hernandez, R. Chiriac, F. Toche, F. Renard, Gas–solid carbonation of $Ca(OH)_2$ and CaO particles under non-isothermal and isothermal conditions by using a thermogravimetric analyzer: Implications for CO_2 capture, International Journal of Greenhouse Gas Control, 11 (2012) 172-180.

[191] N. Wang, Y. Feng, Y. Chen, X. Guo, Lithium-based sorbent from rice husk materials for hydrogen production via sorption-enhanced steam reforming of ethanol, Fuel, 245 (2019) 263-273.

[192] M. Zhao, X. Yang, T.L. Church, A.T. Harris, Novel $CaO–SiO_2$ Sorbent and Bifunctional $Ni/Co–CaO/SiO_2$ Complex for Selective H_2 Synthesis from Cellulose, Environmental Science & Technology, 46 (2012) 2976-2983.

[193] H. Guo, S. Wang, C. Li, Y. Zhao, Q. Sun, X. Ma, Incorporation of Zr into Calcium Oxide for CO_2 Capture by a Simple and Facile Sol–Gel Method, Industrial & Engineering Chemistry Research, 55 (2016) 7873-7879.

[194] C. Luo, Y. Zheng, J. Guo, B. Feng, Effect of sulfation on CO_2 capture of CaO-based sorbents during calcium looping cycle, Fuel, 127 (2014) 124-130.

[195] W. Liu, H. An, C. Qin, J. Yin, G. Wang, B. Feng, M. Xu, Performance Enhancement of Calcium Oxide Sorbents for Cyclic CO_2 Capture—A Review, Energy & Fuels, 26 (2012) 2751-2767.

[196] S. Wang, S. Fan, L. Fan, Y. Zhao, X. Ma, Effect of cerium oxide doping on the performance of CaO-based sorbents during calcium looping cycles, Environ Sci Technol, 49 (2015) 5021-5027.

[197] R. Koirala, K.R. Gunugunuri, S.E. Pratsinis, P.G. Smirniotis, Effect of Zirconia Doping on the Structure and Stability of CaO-Based Sorbents for CO_2 Capture during Extended Operating Cycles, The Journal of Physical Chemistry C, 115 (2011) 24804-24812.

[198] M. Broda, C.R. Müller, Sol–gel-derived, CaO-based, ZrO_2-stabilized CO_2 sorbents, Fuel, 127 (2014) 94-100.

[199] F.N. Ridha, V. Manovic, A. Macchi, E.J. Anthony, High-temperature CO_2 capture cycles for CaO-based pellets with kaolin-based binders, International Journal of Greenhouse Gas Control, 6 (2012) 164-170.

[200] Y. Wu, V. Manovic, I. He, E.J. Anthony, Modified lime-based pellet sorbents for high-temperature CO_2 capture: Reactivity and attrition behavior, Fuel, 96 (2012) 454-461.

[201] P. Gruene, A.G. Belova, T.M. Yegulalp, R.J. Farrauto, M.J. Castaldi, Dispersed Calcium Oxide as a Reversible and Efficient CO_2−Sorbent at Intermediate Temperatures, Industrial & Engineering Chemistry Research, 50 (2011) 4042-4049.
[202] S.F. Wu, Y.Q. Zhu, Behavior of $CaTiO_3$/Nano-CaO as a CO_2 Reactive Adsorbent, Industrial & Engineering Chemistry Research, 49 (2010) 2701-2706.
[203] Z. Zhou, Y. Qi, M. Xie, Z. Cheng, W. Yuan, Synthesis of CaO-based sorbents through incorporation of alumina/aluminate and their CO_2 capture performance, Chemical Engineering Science, 74 (2012) 172-180.
[204] M. Broda, A.M. Kierzkowska, D. Baudouin, Q. Imtiaz, C. Copéret, C.R. Müller, Sorbent-Enhanced Methane Reforming over a Ni–Ca-Based, Bifunctional Catalyst Sorbent, ACS Catalysis, 2 (2012) 1635-1646.
[205] R. Dębek, M. Motak, D. Duraczyska, F. Launay, M.E. Galvez, T. Grzybek, P. Da Costa, Methane dry reforming over hydrotalcite-derived Ni–Mg–Al mixed oxides: the influence of Ni content on catalytic activity, selectivity and stability, Catalysis Science & Technology, 6 (2016) 6705-6715.
[206] F. Zhou, N. Pan, H. Chen, X. Xu, C. Wang, Y. Du, Y. Guo, Z. Zeng, L. Li, Hydrogen production through steam reforming of toluene over Ce, Zr or Fe promoted Ni-Mg-Al hydrotalcite-derived catalysts at low temperature, Energy Conversion and Management, 196 (2019) 677-687.
[207] K.D. Dewoolkar, P.D. Vaidya, Improved Hydrogen Production by Sorption-Enhanced Steam Methane Reforming over Hydrotalcite- and Calcium-Based Hybrid Materials, Energy & Fuels, 29 (2015) 3870-3878.
[208] N. Chanburanasiri, A.M. Ribeiro, A.E. Rodrigues, A. Arpornwichanop, N. Laosiripojana, P. Praserthdam, S. Assabumrungrat, Hydrogen Production via Sorption Enhanced Steam Methane Reforming Process Using Ni/CaO Multifunctional Catalyst, Industrial & Engineering Chemistry Research, 50 (2011) 13662-13671.
[209] A. Antzara, E. Heracleous, D.B. Bukur, A.A. Lemonidou, Thermodynamic analysis of hydrogen production via chemical looping steam methane reforming coupled with in situ CO_2 capture, International Journal of Greenhouse Gas Control, 32 (2015) 115-128.

[210] A.L. García-Lario, M. Aznar, I. Martinez, G.S. Grasa, R. Murillo, Experimental study of the application of a NiO/$NiAl_2O^4$ catalyst and a CaO-based synthetic sorbent on the Sorption Enhanced Reforming process, International Journal of Hydrogen Energy, 40 (2015) 219-232.

[211] N. de Miguel, J. Manzanedo, P.L. Arias, Active and Stable Ni-MgO Catalyst Coated on a Metal Monolith for Methane Steam Reforming under Low Steam-to-Carbon Ratios, Chemical Engineering & Technology, 35 (2012) 2195-2203.

[212] H.-S. Roh, K.Y. Koo, J.H. Jeong, Y.T. Seo, D.J. Seo, Y.-S. Seo, W.L. Yoon, S.B. Park, Combined reforming of methane over supported Ni catalysts, Catalysis Letters, 117 (2007) 85-90.

[213] E. Ochoa-Fernández, H.K. Rusten, H.A. Jakobsen, M. Rønning, A. Holmen, D. Chen, Sorption enhanced hydrogen production by steam methane reforming using Li_2ZrO_3 as sorbent: Sorption kinetics and reactor simulation, Catalysis Today, 106 (2005) 41-46.

[214] G. Ji, M. Zhao, G. Wang, Computational fluid dynamic simulation of a sorption-enhanced palladium membrane reactor for enhancing hydrogen production from methane steam reforming, Energy, 147 (2018) 884-895.

[215] L. Lukashuk, N. Yigit, R. Rameshan, E. Kolar, D. Teschner, M. Hävecker, A. Knop-Gericke, R. Schlögl, K. Föttinger, G. Rupprechter, Operando Insights into CO Oxidation on Cobalt Oxide Catalysts by NAP-XPS, FTIR, and XRD, ACS Catalysis, 8 (2018) 8630-8641.

[216] A. Leba, R. Yıldırım, Determining most effective structural form of nickel-cobalt catalysts for dry reforming of methane, International Journal of Hydrogen Energy, 45 (2020) 4268-4283.

[217] A. Di Giuliano, F. Giancaterino, K. Gallucci, P.U. Foscolo, C. Courson, Catalytic and sorbent materials based on mayenite for sorption enhanced steam methane reforming with different packed-bed configurations, International Journal of Hydrogen Energy, 43 (2018) 21279-21289.

[218] E. Dahdah, J. Abou Rached, S. Aouad, C. Gennequin, H.L. Tidahy, J. Estephane, A. Aboukaïs, E. Abi Aad, CO_2 reforming of methane over $Ni_xMg_{6-x}Al_2$ catalysts: Effect

of lanthanum doping on catalytic activity and stability, International Journal of Hydrogen Energy, 42 (2017) 12808-12817.
[219] Q. Wang, M. Zhou, Y. Zhang, M. Liu, W. Xiong, S. Liu, Large surface area porous carbon materials synthesized by direct carbonization of banana peel and citrate salts for use as high-performance supercapacitors, Journal of Materials Science: Materials in Electronics, 29 (2018) 4294-4300.
[220] M.R. Md Radzi, M.T. Azizan, N.F.D.M. Daud, M.A. Topek, S.Z. Abidin, Aqueous phase reforming of sorbitol over Ca doped Ni/Al_2O_3 for value-added chemicals production, Materials Today: Proceedings, 5 (2018) 21728-21736.
[221] U. Sikander, M.F. Samsudin, S. Sufian, K. KuShaari, C.F. Kait, S.R. Naqvi, W.-H. Chen, Tailored hydrotalcite-based Mg-Ni-Al catalyst for hydrogen production via methane decomposition: Effect of nickel concentration and spinel-like structures, International Journal of Hydrogen Energy, 44 (2019) 14424-14433.
[222] M.A. Salam, S. Sufian, T. Murugesan, Characterization of nano-crystalline Mg–Ni–Al hydrotalcite derived mixed oxides as hydrogen adsorbent, Materials Chemistry and Physics, 142 (2013) 213-219.
[223] U. Sikander, S. Sufian, M.A. Salam, Synthesis and Structural Analysis of Double Layered Ni-Mg-Al Hydrotalcite Like Catalyst, Procedia Engineering, 148 (2016) 261-267.
[224] K. Jirátová, P. Čuba, F. Kovanda, L. Hilaire, V. Pitchon, Preparation and characterisation of activated Ni (Mn)/Mg/Al hydrotalcites for combustion catalysis, Catalysis Today, 76 (2002) 43-53.
[225] F.-X. Chiron, G.S. Patience, S. Rifflart, Hydrogen production through chemical looping using NiO/$NiAl_2O_4$ as oxygen carrier, Chemical Engineering Science, 66 (2011) 6324-6330.
[226] R. Benrabaa, A. Barama, H. Boukhlouf, J. Guerrero-Caballero, A. Rubbens, E. Bordes-Richard, A. Löfberg, R.-N. Vannier, Physico-chemical properties and syngas production via dry reforming of methane over $NiAl_2O_4$ catalyst, International Journal of Hydrogen Energy, 42 (2017) 12989-12996.

[227] J. Ren, C. Mebrahtu, R. Palkovits, Ni-based catalysts supported on Mg–Al hydrotalcites with different morphologies for CO_2 methanation: exploring the effect of metal–support interaction, Catalysis Science & Technology, 10 (2020) 1902-1913.
[228] C. García-Sancho, R. Guil-López, A. Sebastián-López, R.M. Navarro, J.L.G. Fierro, Hydrogen production by methane decomposition: A comparative study of supported and bulk ex-hydrotalcite mixed oxide catalysts with Ni, Mg and Al, International Journal of Hydrogen Energy, 43 (2018) 9607-9621.
[229] X. Kong, R. Zheng, Y. Zhu, G. Ding, Y. Zhu, Y.-W. Li, Rational design of Ni-based catalysts derived from hydrotalcite for selective hydrogenation of 5-hydroxymethylfurfural, Green Chemistry, 17 (2015) 2504-2514.
[230] L. Zhao, X. Li, C. Hao, C.L. Raston, SO_2 adsorption and transformation on calcined NiAl hydrotalcite-like compounds surfaces: An in situ FTIR and DFT study, Applied Catalysis B: Environmental, 117-118 (2012) 339-345.
[231] G. Bonura, M. Cordaro, C. Cannilla, F. Arena, F. Frusteri, The changing nature of the active site of Cu-Zn-Zr catalysts for the CO_2 hydrogenation reaction to methanol, Applied Catalysis B: Environmental, 152-153 (2014) 152-161.
[232] A. Nawar, H. Ghaedi, M. Ali, M. Zhao, N. Iqbal, R. Khan, Recycling waste-derived marble powder for CO_2 capture, Process Safety and Environmental Protection, 132 (2019) 214-225.
[233] J. Ashok, S. Kawi, Steam reforming of toluene as a biomass tar model compound over CeO_2 promoted Ni/CaO–Al_2O_3 catalytic systems, International Journal of Hydrogen Energy, 38 (2013) 13938-13949.
[234] F. Cavani, F. Trifirò, A. Vaccari, Hydrotalcite-type anionic clays: Preparation, properties and applications, Catalysis Today, 11 (1991) 173-301.
[235] G. Gliemann, K. Nakamoto: Infrared and Raman Spectra of Inorganic and Coordination Compounds. John Wiley and Sons, New York, Chichester, Brisbane, Toronto 1978. 3. Aufl., XV, 448 Seiten mit 109 Abbildungen und 95 Tabellen. Preis: $ 31,15, Berichte der Bunsengesellschaft für physikalische Chemie, 82 (1978) 1263-1263.
[236] J.T. Kloprogge, R.L. Frost, Fourier Transform Infrared and Raman Spectroscopic Study of the Local Structure of Mg-, Ni-, and Co-Hydrotalcites, Journal of Solid State Chemistry, 146 (1999) 506-515.

[237] F. Li, L. Zhang, D.G. Evans, C. Forano, X. Duan, Structure and thermal evolution of Mg–Al layered double hydroxide containing interlayer organic glyphosate anions, Thermochimica Acta, 424 (2004) 15-23.
[238] J. Das, D. Das, K.M. Parida, Preparation and characterization of Mg–Al hydrotalcite-like compounds containing cerium, Journal of Colloid and Interface Science, 301 (2006) 569-574.
[239] B. Wiyantoko, P. Kurniawati, T.E. Purbaningtias, I. Fatimah, Synthesis and Characterization of Hydrotalcite at Different Mg/Al Molar Ratios, Procedia Chemistry, 17 (2015) 21-26.
[240] M.K. Titulaer, J.B.H. Jansen, J.W. Geus, The quantity of reduced nickel in synthetic takovite: effects of preparation conditions and calcination temperature, Clays and clay minerals, 42 (1994) 249-258.
[241] N. Tangboriboon, R. Kunanuruksapong, A. Sirivat, Preparation and properties of calcium oxide from eggshells via calcination, Materials Science-Poland, 30 (2012) 313-322.
[242] L. Barelli, G. Bidini, F. Gallorini, S. Servili, Hydrogen production through sorption-enhanced steam methane reforming and membrane technology: A review, Energy, 33 (2008) 554-570.
[243] S.M. Kim, P.M. Abdala, D. Hosseini, A. Armutlulu, T. Margossian, C. Copéret, C. Müller, Bi-functional Ru/$Ca_3Al_2O_6$–CaO catalyst-CO_2 sorbent for the production of high purity hydrogen via sorption-enhanced steam methane reforming, Catalysis Science & Technology, 9 (2019) 5745-5756.
[244] C.-H. Chen, C.-T. Yu, W.-H. Chen, Improvement of steam methane reforming via in-situ CO_2 sorption over a nickel-calcium composite catalyst, International Journal of Hydrogen Energy, (2020).
[245] A. Neni, Y. Benguerba, M. Balsamo, A. Erto, B. Ernst, D. Benachour, Numerical study of sorption-enhanced methane steam reforming over Ni/Al_2O_3 catalyst in a fixed-bed reactor, International Journal of Heat and Mass Transfer, 165 (2021) 120635.
[246] X.-y. Zhao, Y.-p. Xue, C.-f. Yan, Z.-d. Wang, C.-q. Guo, S.-l. Huang, Sorbent assisted catalyst of Ni-CaO-La_2O_3 for sorption enhanced steam reforming of bio-oil with

acetic acid as the model compound, Chemical Engineering and Processing: Process Intensification, 119 (2017) 106-112.
[247] P.T. Clough, M.E. Boot-Handford, L. Zheng, Z. Zhang, P.S. Fennell, Hydrogen production by sorption enhanced steam reforming (SESR) of biomass in a fluidised-bed reactor using combined multifunctional particles, Materials, 11 (2018) 859.
[248] P. Pecharaumporn, S. Wongsakulphasatch, T. Glinrun, A. Maneedaeng, Z. Hassan, S. Assabumrungrat, Synthetic CaO-based sorbent for high-temperature CO_2 capture in sorption-enhanced hydrogen production, International Journal of Hydrogen Energy, 44 (2019) 20663-20677.
[249] X. Wang, Y. He, T. Xu, B. Xiao, S. Liu, Z. Hu, J. Li, CO_2 sorption-enhanced steam reforming of phenol using Ni–M/CaO–$Ca_{12}Al_{14}O_{33}$ (M = Cu, Co, and Ce) as catalytic sorbents, Chemical Engineering Journal, 393 (2020) 124769.
[250] S.Z. Abbas, V. Dupont, T. Mahmud, Modelling of H_2 production via sorption enhanced steam methane reforming at reduced pressures for small scale applications, International Journal of Hydrogen Energy, 44 (2019) 1505-1513.
[251] H.-S. Roh, K.-W. Jun, Carbon Dioxide Reforming of Methane over Ni Catalysts Supported on Al2O3 Modified with La_2O_3, MgO, and CaO, Catalysis Surveys from Asia, 12 (2008) 239-252.
[252] R. Dębek, M. Motak, M.E. Galvez, T. Grzybek, P. Da Costa, Influence of Ce/Zr molar ratio on catalytic performance of hydrotalcite-derived catalysts at low temperature CO_2 methane reforming, International Journal of Hydrogen Energy, 42 (2017) 23556-23567.
[253] C. Dang, H. Li, G. Yang, Y. Cao, H. Wang, F. Peng, S. Wang, H. Yu, High-purity hydrogen production by sorption-enhanced steam reforming of iso-octane over a Pd-promoted Ni-Ca-Al-O bi-functional catalyst, Fuel, 293 (2021) 120430.
[254] D. Li, R. Li, M. Lu, X. Lin, Y. Zhan, L. Jiang, Carbon dioxide reforming of methane over Ru catalysts supported on Mg-Al oxides: A highly dispersed and stable Ru/Mg(Al)O catalyst, Applied Catalysis B: Environmental, 200 (2017) 566-577.